FZR
FORSCHUNGSZENTRUM ROSSENDORF

Institute for Safety Research

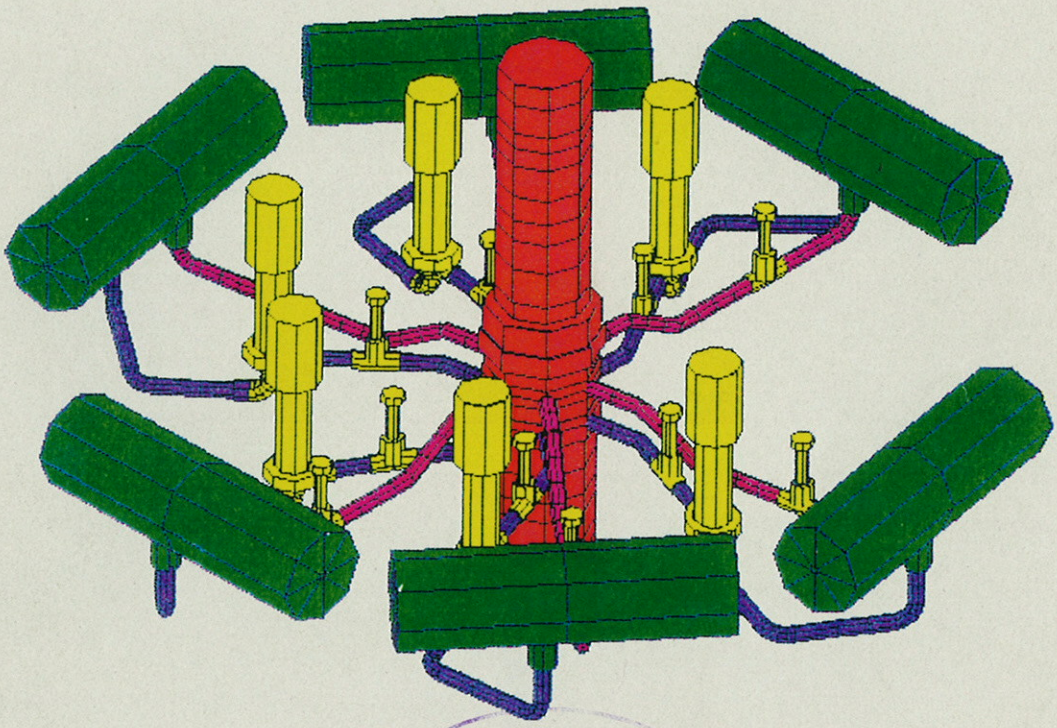

Annual Report 1995

Forschungszentrum Rossendorf e. V.
Institut für Sicherheitsforschung

Annual Report 1995

Editors:
F.-P. Weiß, U. Rindelhardt

FZR-152
September 1996

Front page:
Finite element sketch for modelling the structural dynamics and vibration behaviour of a VVER-440 pressurized reactor

For further information on the research projects described in the present annual report, please address the director or one of the authors at the institute.

Postal address:

Postfach 51 01 19
D-01314 Dresden
Germany

Telecommunication:

Tel.: +49 351 260 3480
Fax: +49 351 260 3440
E-mail weissfp@fz-rossendorf.de

CONTENTS

Preface

Generals:

The operation or even the existence of most technical infrastructures is connected with hazards to the environment and to human beings.

In the nuclear industry, these hazards emerge from the handling of radioactive material, while in process industries they are related to burnable, explosive, or toxic substances.

The scientific work at the Institute for Safety Research (IFS) covers a wide range of safety related investigations, including:

- safety assessment of existing and future plants by analyzing hypothetical accidents,
- estimation of safety margins and residual lifetimes by studying materials degradation and materials ageing due to operational loads,
- improvement of operational safety by developing model and pattern recognition based methods for early failure detection,
- risk assessment and risk management of conventional waste deposits by hazard ranking with expert systems and by decision support.

During 1995, efforts were specifically undertaken to deepen the methodical character of IFS research, i. e. to focus model and code development upon basic phenomena related to accidental sequences and technical diagnostics. The efforts were further directed to measuring techniques and monitoring procedures that can be applied as well in nuclear as in process industries.

In particular, the IFS works on the following research tasks, which in general split into several projects:

* investigation of thermo-fluiddynamic single effects
* thermalhydraulics and neutron kinetics for accident analysis
* materials safety
* simulation of radiation and particle transport
* mechanical integrity of technical systems and process monitoring
* hazard ranking and risk management for waste deposits
* magneto-hydrodynamics of conductive fluids
* renewable energies

The attached graphs give an overview about sources and deployment of funding on the different research tasks. The external funding through research grants and contracts with the industry considerably increased the available manpower. In 1995 about 50% of the staff was externally financed. As a rule, this part of the personnel worked on special applications and modifications of methods and tools. This e. g. concerns the qualification of thermalhydraulics, neutron kinetics, and mechanical accident analysis codes for VVER specific applications. It further concerns fluence calculations of the VVER reactor pressure vessels, modeling of the primary circuit vibration behaviour and the development and installation of an

Distribution of funding sources

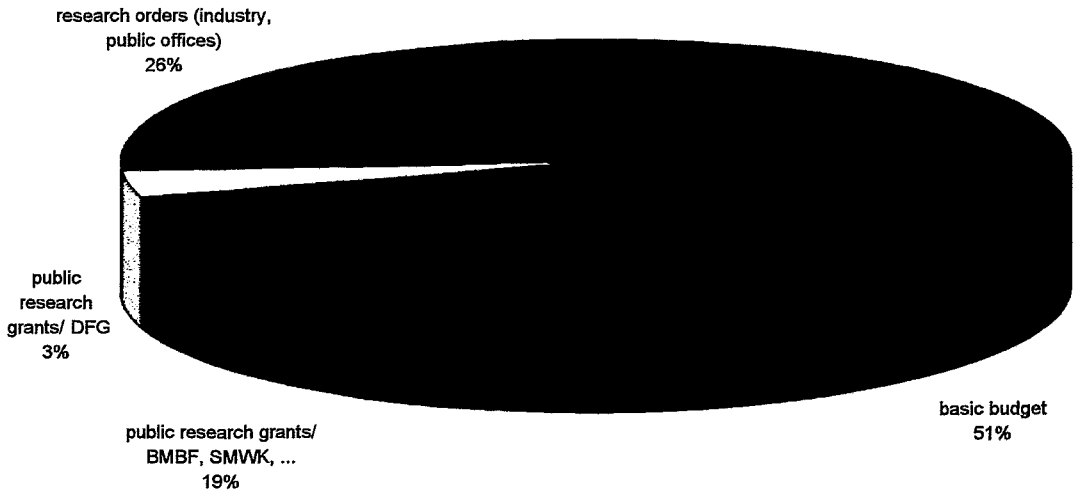

Deployment of funding on the various tasks/projects

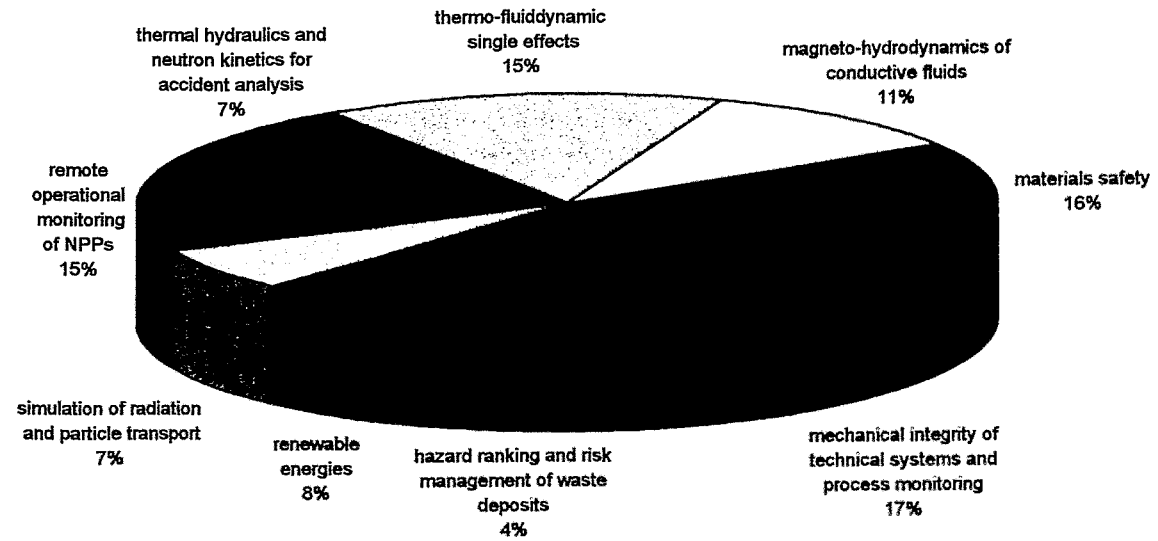

operational monitoring system as a pilot project at the Saporoshye NPP in Ukraine.

The relations with the Dresden Technical University (TUD) were drastically substantiated. TUD and IFS closely work together in the framework of an "Innovationskolleg" of DFG about the magneto-fluiddynamics of conductive fluids. Five of 11 total projects with that college were located at Rossendorf. In this way, the DFG will support the Research Center Rossendorf with $2.3 \cdot 10^6$ DM over the next three years.

Moreover, the IFS succeeded in sustainably strengthening relations with the European Union by accomplishing the study on "Identification of Topics for Cooperation between the European Community and Eastern European Contries in the Field of Nuclear Reactor Safety, Radioactive Waste and Site Restoration". This study is one of the guide lines along which common safety research project with Eastern institutions can be arranged.

Important Results:

Thermofluiddynamics/neutron kinetics
A laboratory set-up for basic experimental work in transient two phase flows could be finished. Operation with air and water was started in December 1995. Steam water operation is envisaged for spring 1996.

Based on the validated version of the neutron kinetics code DYN3D for hexagonal fuel elements which are typical for VVER reactors, a version for squared fuel element cross sections is now available. This version has passed several benchmark calculations on BWR (Boiling Water Reactors) and PWR (Pressurized Water Reactors) scenarios.

Materials safety
Sponsored by DFG, X-ray small angle scattering with a micro-beam has for the first time been applied to scan the deformation field ahead of a crack tip. This analysis unambigouosly reveals deformation induced structural changes. The nature of these changes is not yet completely clarified. However, the expected creation of micro-voids could not be confirmed.

Vibration modelling/analysis of mechanical aspects of accident scenarios
Structural dynamic modelling of the pressure vessel and internals for a BWR was started. Emphasis is particularly put on the load-deflection behaviour of the core shroud and of the RPV. These components are modeled as shell and volume elements to calculate the mechanical stress distrubution due to pressure and temperature transients during emergency core cooling.

A validated model for the simulation of vibrations of VVER-440 reactors is now available for routine application.

Particle and radiation transport

A Monte-Carlo-programme for the simulation of the one-dimensional transport of high energetic "heavy" ions in heterogeneous human tissue was developed. This tool is primarily used to estimate the dose contribution of light fragments in ion cancer therapy. The energy straggling of the primary particles and the energy distributions of the light fragments could be calculated for special phantoms constituted from different layers. The dose increase in the far reaching tail by the fragments could clearly be shown.

Risk assessment of waste deposits/decision analysis

Decision analytical methods have proven to be applicable in the selection of an appropriate remediation technique for conventional waste deposits. The multi person decision model (system of decision criteria, specific attributes for the deposit, risk behaviour of the involved institutions and persons) has been quantified for a deposit in Saxony (Bergen/Lausitz). The involved environmental offices, the regional authorities, and the firms offering remediation technologies accepted the decision analytical approach and partially even regarded it helpful.

Selected Reports

STUDIES OF LIQUID-GASEOUS TWO-PHASE SYSTEMS BY POSITRON EMITTING RADIOTRACERS

F. Hensel

1. Introduction

The imaging technique of Positron Emission Tomography PET originates from nuclear medicine. It is mainly applied as an in vivo non invasive tool by which metabolic activities can be investigated. Typical PET positron emitters like ^{11}C, ^{13}N, ^{15}O and ^{18}F can substitute naturally occurring isotopes in a wide variety of organic compounds. Besides the medical imaging, industrial and engineering applications are known. Examples are the investigation of chemical processes e.g. catalysis [2] and water flow monitoring in an oil reservoir rock [3]. Even for problems related to transport and mixing in foams or flows with high gas fractions, PET seems to be an appropriate experimental technique.

PET is based on a coincidence detection technique. If a positron and an electron annihilate, two 511 keV photons are emitted into opposite directions. So the place of annihilation can be located along the line joining two detectors with coincident signals. Image reconstruction methods allow the determination of the spatial tracer distribution from a set of event projections. Several effects are limiting the accuracy [6]. In the case discussed here the distance between the emission and the annihilation point of the positron is very important. In water, typical values for these stopping ranges are about 2 mm [6]. Typical densities of the interesting two phase systems are about 10% of the density of water under normal conditions. This causes much higher ranges in some of the planned applications, where the positron range becomes the most important limiting effect.

The feasibility studies on radiotracer applications for two-phase flow systems started in 1994. The main goal was to observe mixing and flow processes with sufficient spatial and time resolution. The first experiments were performed using a locally fixed ^{45}Ti positron source. The results of a numerical simulation of the positron ranges were checked against density measurements of two-phase media which are based on the density dependence of positron ranges. Kinematic transport measurements were carried out in two-phase flows with the isotope ^{18}F in a liquid tracer. A double head spherical PET-scanner was used, which was originally developed for treatment plan verification of 3D conformal radiation therapy [1].

2. Density Measurement

The density measurement technique is just based on the density (ρ) dependence of the positron range *r*. In [7] the following equation can be found, which based on the assumption of a continuous slowing down of the positrons (i.e. the use of a stopping power):

$$r(E_0, \rho) = \frac{R(E_0)}{\rho} \qquad (1)$$

R is a material dependent quantity varying with the starting energy E_0 of the positron. Thus positron range distributions can be used to determine the density of a medium.

This type of density measurement combines high density sensitivity of the positrons with low absorption of the annihilation radiation. This allows detector mounting outside the possibly aggressive medium. So, with a pair of detectors placed on opposite walls of a pipe, the spatial annihilation distribution inside the pipe can be measured (Fig. 1).

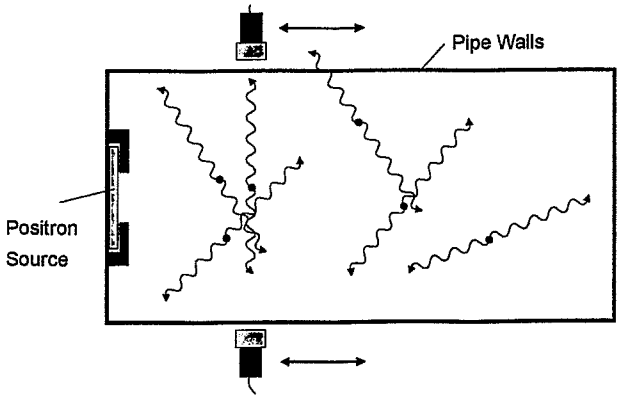

Fig. 1: Sketch of the density measurement technique

Monte-Carlo simulations were performed to check the feasibility and to determine the optimum density range that could be covered. The calculations were carried out for dry steam and for solid foams, made of polyurethane or polystyrene, respectively. Though the solid foams are inhomogeneous media, in the calculations they were approximated by homogeneous densities.

The annihilation distribution steeply descends at source distances up to 150mm. If the density increases, the mean positron range for a given energy decreases and more positron annihilations occur closer to the positron source. The estimated ranges can be measured by commonly used BGO detector systems for γ-radiation. Results for polystyrene foams are shown in Fig. 4 below.

The simulation results were checked in a series of experiments with polyurethane and polystyrene foam blocks of 25cm*25cm*40cm. The densities ranged between 15kg/m^3 and 38kg/m^3. The experimental setup is shown in Fig. 2. The positron source and the

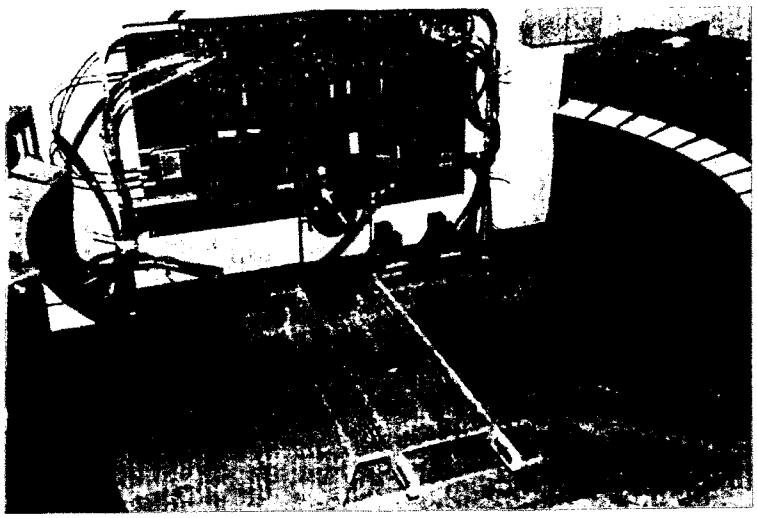

Fig. 2: Experimental Assembly for Density Measurements

foam block holder can be seen in the mid of the picture. Most of the positrons are emitted directly into the foam block, all other annihilate inside the source holder material.

The experimental data were also used to assess the feasibility of the technique when using a simpler detector arrangement. So, no three-dimensional reconstruction was made. A sketch of the simplified geometry is given in Fig. 3. It consists of pairs of opposite detector columns. The allowed coincidences are symbolized as straight lines. The width of the detector columns can be varied in steps of 6.75 mm, the single crystal size.

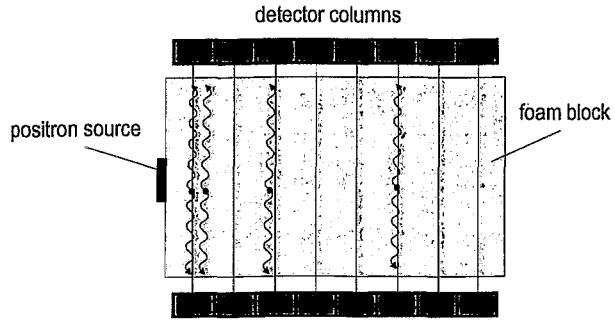

Fig. 3: Simplified Detector: Columns with direct coincidences only, top view

Fig. 4 shows the coincidence rates for that arrangement. For the given case the column width is one crystal. Fifteen columns have been used. The curves obtained in the experiments show the same behavior like the calculated ones. A detailed evaluation, including an error estimation and an optimization for the simplified detector assembly is currently under progress.

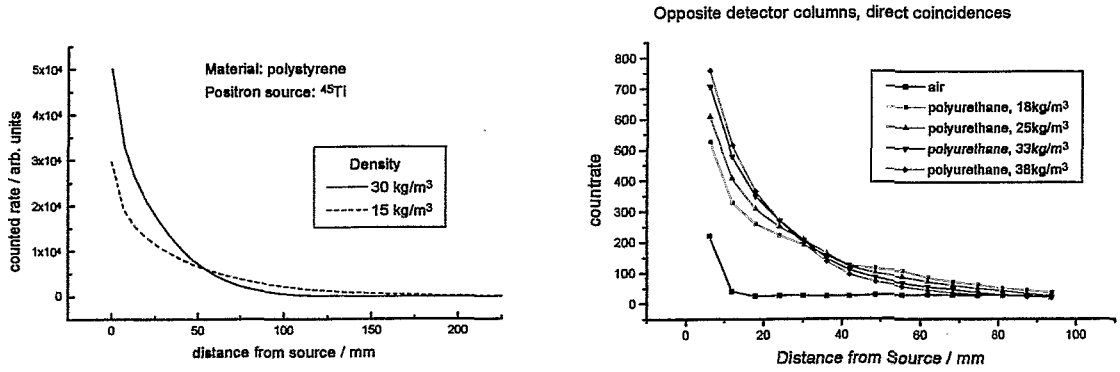

Fig. 4: Coincidence rates obtained for the simplified detector arrangement, calculation (left) and experiment with ^{45}Ti source (right)

3. Tracer Transport Measurements

Typical applications might be the investigation of turbulent transport processes and the distribution of solved substances in liquids and foams. Appropriate marking substances really occurring in the investigated system (e.g. surfactants, detergents) should be used. However, the positron ranges provoke resolution limitations particularly in low density media. A point source of positrons causes annihilations in a certain area around the

source. For distributed positron sources, this leads to a "smearing" of the measured tracer concentration.

In a first experiment, the transport of a tracer in a turbulent bubbly flow generated in a tank (Fig. 5) was studied. The tracer injector allows a low momentum injection of about 0.8 ml of the tracer liquid. Ink injection tests are possible, too. The liquid phase was distilled water with additives of isopropanol and NaCl. Pressurized air was injected. NaF (^{18}F) was used as tracer because of its half-life of 1.83h and a low maximum positron energy (0.63MeV) causing a small positron range. This enables a better resolution. Further, NaF behaves very similar to NaCl and is therefore suited to study the developing distribution spreading of NaCl in the bubbly flow.

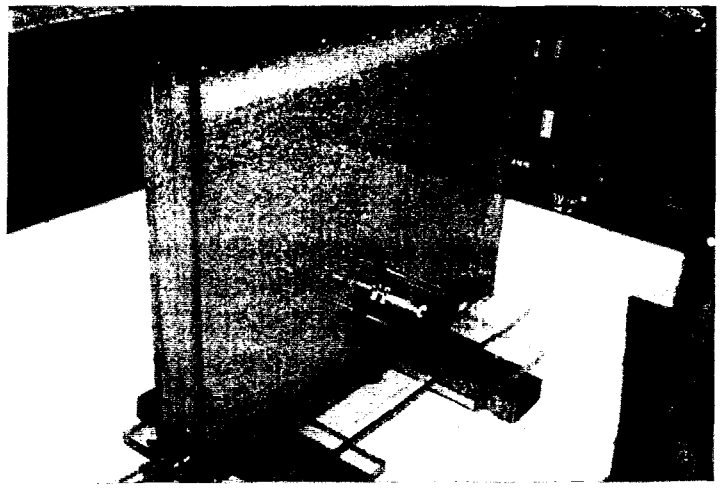

Fig. 5: Experimental setup for tracer spreading investigations

For certain time intervals, a midplane backprojection of the eventlines was carried out. The resulting distributions prove that even activities of only about 1-5MBq can supply quantitative insights into the spreading process. Fig. 6 shows typical normalized tracer concentration distributions. In each 500 ms time interval about 50.000 events have been processed. Similar experiments were made for mixing processes inside a vertical tube.

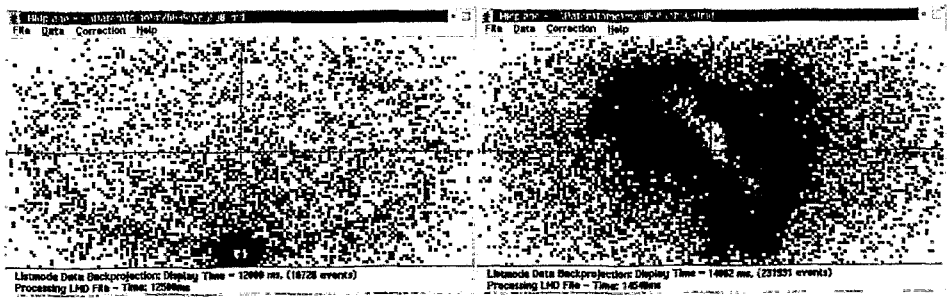

Fig. 6: Instantaneous midplane concentrations of the tracer in the bubbly medium (before injection and 2 seconds after tracer injection)

Another experiment dealt with the drainage of a surfactant stabilized foam. The foam was generated by shaking a tracer containing liquid inside a plastic bottle. Tracer concentration distributions are given in Fig. 7. The summation time interval here was 1.5s. The summation for the first distribution starts with the beginning of the dry out, the next picture is taken 7.5s later. For the evaluation of this experiment, a detailed knowledge of

range effects is needed, because the decreasing local foam density affects the positron range. Nevertheless, the obtained course of space dependent concentration changes qualitatively confirms the assumed behavior.

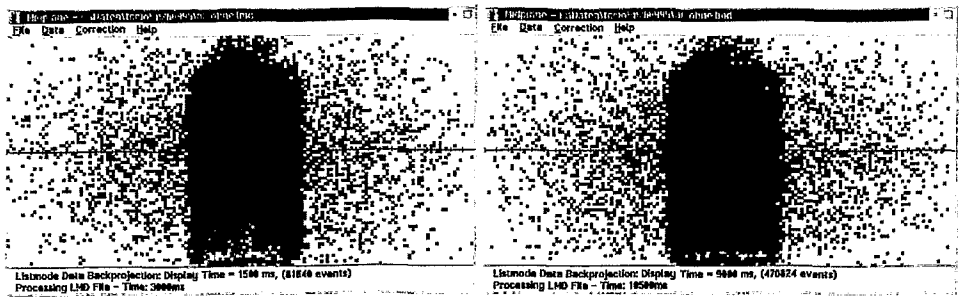

Fig. 7: Midplane concentrations of the tracer in the foam Drainage (immediately after shaking and 7.5s later)

4. Conclusions

The feasibility of a density measuring technique based on PET could be shown. Future efforts are directed to detector optimization to develop an easy to handle low cost experimental assembly. It should contain an encapsulated positron source and 2-4 pairs of detectors to cover a wide density range.

Liquid positron emitting tracers were successfully applied to monitor transport processes in bubbly flows. At present PET is still restricted to slow processes, due to the necessary summation or integration of event data to calculate a spatial distribution with sufficient statistical accuracy. A full 3-dimensional reconstruction still requires much more data. However, if the experiments are restricted to geometries where the distribution dependence for one direction is of minor importance, a simple and time sparing midplane backprojection can be applied. So the time intervals and the needed radioactive inventory can be reduced. Time resolutions of about 0.5s can be achieved. For an exact determination of a concentration distribution algorithms are required, which can take into account effects like positron range and false coincidences generated by scattering and random events.

Transport processes in bubbly flows and foams seem to be appropriate subjects for PET tracer techniques. Generally PET isotopes are available in a wide range of half-lives and elements, thus tracers can be tailored for very different technical investigations.

References

[1] W. Enghardt et al: Annual Report 1994, FZR-78 (1995) 135

[2] G. Jonkers et al: Surface catalysis studied by in situ positron emission, Nature 1992, 355, 63

[3] E.A. van den Bergen et al: Industrial Applications of positron emission computed tomography. Nucl. Geophys. Vol. 3, No. 4 (1989), 407-418

[4] J. Pawelke: Ph.D. Thesis, FZR-97 (1995)

[5] J. Pawelke, L. Byars, W. Enghardt et al: The investigation of different cameras for in-beam PET imaging. Phys. Med. Biol. 41 (1996) 279-296

[6] D.W. Townsend, M. Defrise: Image Reconstruction Methods in Positron Tomography, CERN 93-02 (1993)

[7] Stopping Powers for Electrons and Positrons. ICRU Report 37, Bethesda (1984), ISBN 0-913394-31-9

DEPRESSURIZATION OF FOAMING LIQUIDS

H. Steinkamp

1. Introduction

In chemical reactors the temperature can increase by the runaway of an exothermal chemical reaction or by external heating. This causes a pressure rise within the reactor and may under unfavourable conditions result in uncontrolled release of toxic, burnable and explosive substances. In order to prevent the damage of the equipment, the reactor is equipped with a safety valve. It has to be guaranteed, that the pressure inside the reactor remains in an admissible range. A retention system is installed to collect the vented fluids. Experimental investigations are carried out to study the influence of foaming liquids on the hydrodynamic processes during emergency depressurization. Foam production has a significant effect on the two-phase mixture inside the reactor, because it leads to an increase of the gas hold-up. The present work deals with the influence of different low-molecular-weight surfactants on the foam production and the resulting entrainment of the liquid phase into the vent-line.

2. Experimental set up

In order to investigate the mass discharge of gas and liquid a small-scale test facility was set up. This small scale blow-down system is shown in Fig. 1. Main part is a model of the chemical reactor. It has an inner diameter of 110mm and a height of 380mm. The 8mm safety valve is simulated by a magnetic valve located in the vent-line on top of the reactor. The released fluids are lead through the vent line into the cyclone to separate the vented two-phase mixture. The vessels are made of acrylglas to observe the fluid dynamic process optically during depressurization. During the experiments the pressure inside the reactor and the temperature of the reactants are measured. In order to determine the void fraction of the two-phase mixture the pressure difference is measured in three axial sections of the reactor. The volume flow of the discharged liquid is measured by weighting the mass collected in the separator. The ejected gas flow rate is measured with a flow metre.

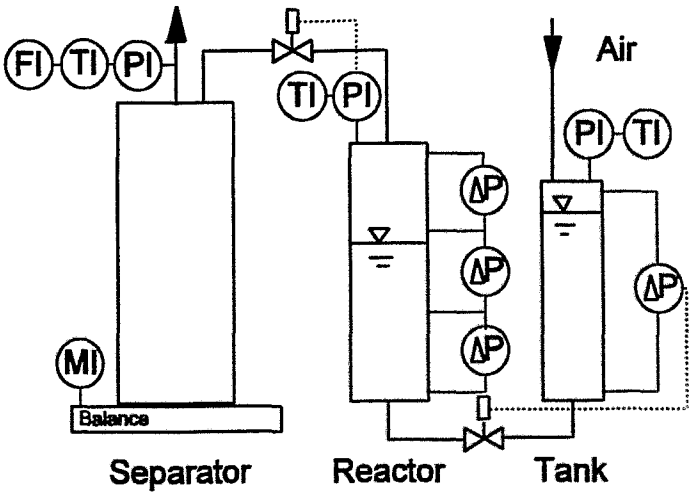

Fig 1: Small scale blow-down system

The reaction of sodium carbonate and sulphuric acid was chosen as a model of a gas producing runaway reaction. A 10%-sodium carbonate solution inside the reactor is mixed with the 20%-acid out of the tank and carbondioxid is produced. The kinetic of the reaction is controlled by the injected volume flow rate of acid. In order to investigate the influence of foam production during depressurization different alcohols are added to the sodium carbonate in the reactor.

3. Experimental results

For the case of carbonate solution without surface active additives, the volumetric gas fraction inside the reactor is shown in Fig. 2. At the beginning of the experiment the reactor is 60% filled with sodium carbonate solution. So the void fraction in the bottom section is 0% and 100% in the top section. In the middle section the calculated void fraction is nearly 30%, because this section is approximately 70% full of liquid. By injecting the acid into the reactor the liquid level increases, indicated by a decrease of the average gas fraction in the middle section. Gas generation starts and after nearly 30s a significant level swell is observed. Simultaneously, the gas fraction in the bottom and the middle sections increases. The mixture level rises up reaching the top of the vessel. In the result, two-phase flow enters the relief device. During the period of two-phase discharge, the gas fraction in top region of the vessel is 50%. A characteristic axial profile of the gas fraction is observed.

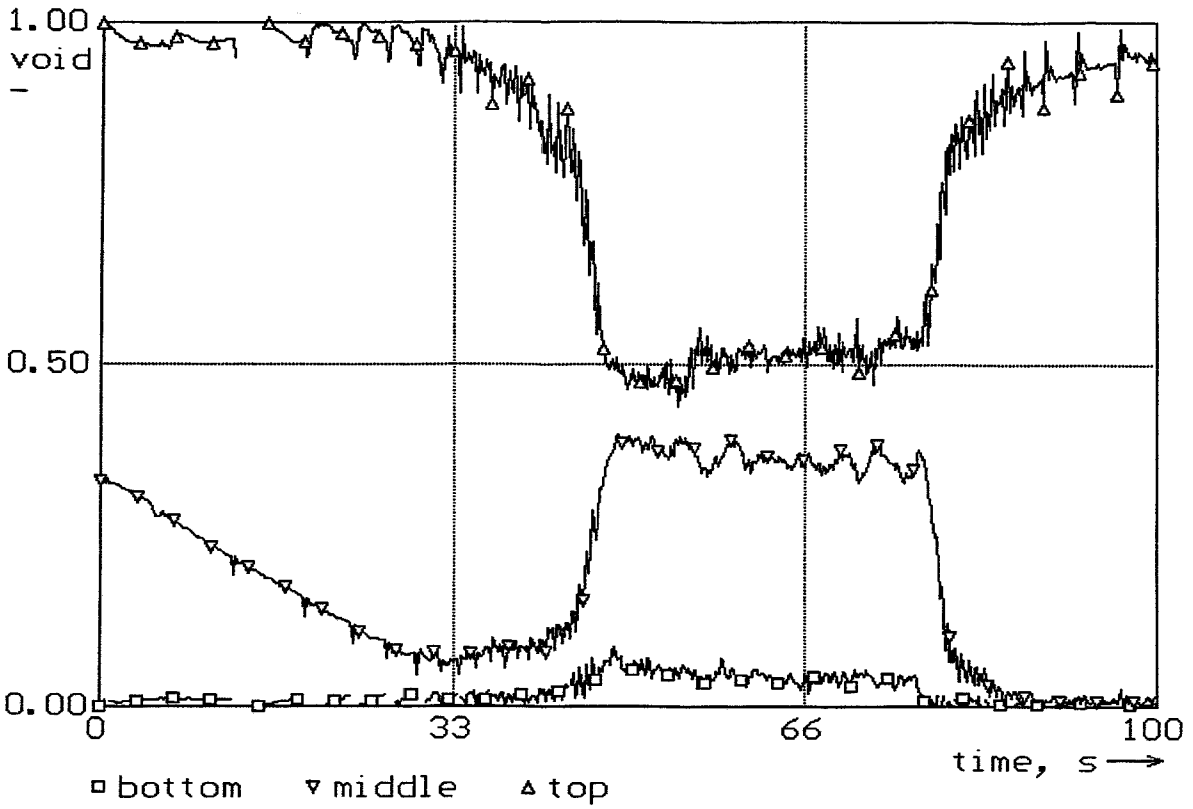

Fig. 2: Void fraction in the reactor for pure carbonate solution

The reaction runs with approximately constant speed during the next 30s. When the acid reservoir is expired, the reaction calms down.

Analogous experiments were performed with different additives. Fig. 3 shows the expulsed mass of liquid as a function of time for different low-molecular-weight alcohols, which were applied in a concentration of 1%. The additives decrease the surface tension. By this reason, gradients of the surfactant concentration in the liquid lamellae between approaching bubbles lead to an inhibition of bubble coalescence, caused by Marangony effects. The consequence is an increased foam production and in the result, a growing liquid entrainment. The generated foam is not very stable, nevertheless the effect on the process

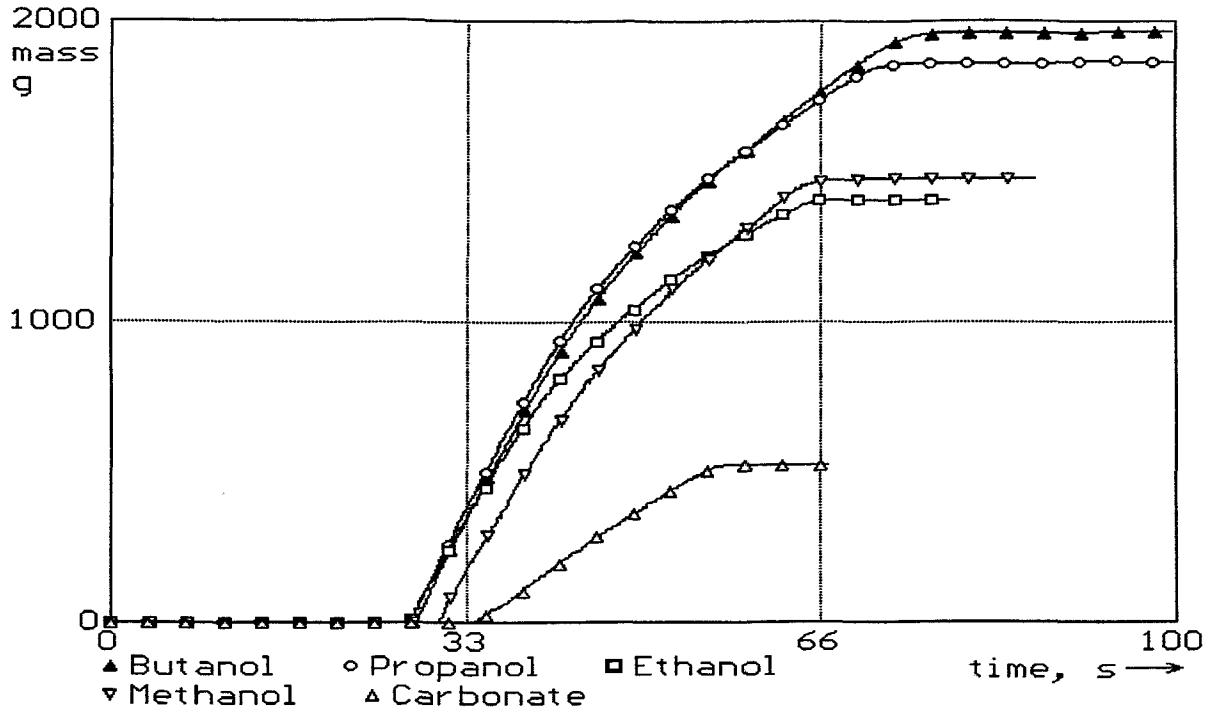

Fig. 3: Discharged mass during depressurization for different liquids (applied concentration of the alcohols: 1%)

is significant, because the characteristic time constants of the depressurisation process are of the same range as the decay time of the foam. Among the investigated alcohols, Butanol has the major effect on the foam generation and the liquid discharge. In comparison to pure carbonate solution, the mass of the expulsed liquid can increase nearly for times.

4. Conclusions

The experiments have shown that low concentrations of additives have a strong effect on the liquid entrainment during depressurization, even if the present substances are not high performance surfactants, but alcohols of low molecular weight. The results suggest that the majority of multi-component systems occurring in practice may contain compounds of more or less surface activity, which can provoke a significant increase of the entrainment of liquid into the pressure relief system. On the other hand, experimental investigations of the venting process are almost every time carried out with pure liquids. Design calculations performed on the basis of these experimental data can lead to an underestimation of the entrainment. For this reason, the work will be continued in direction to include the foam behaviour into the theoretical models of the depressurization process. The goal is the creation of a computer code applicable for a realistic simulation of the venting process in the presence of surface active compounds. The presented results underline the significance of this work.

SIMULATION OF TRANSIENT NATURAL CONVECTION IN SIDE WALL HEATED STORAGE TANKS

A. Aszódi[1], P. Liewers[2], H.-M. Prasser

1. Introduction

Storage tanks are in widespread use in industry. The stored fluids are often dangerous (toxic, inflammable, radioactive, etc.). The effect of external heating on such fluids stored in tanks (for instance due to a fire) is a central question in safety analysis [3]. Several experiments were performed with water filled open tanks using different geometries in order to study the natural convection induced by heating [1]. The experiments proved that the convection pattern and the heating up is completely different for the two cases: 1. Heating from the bottom and 2. Heating through the side walls.

If the power of bottom heating is big enough, mixing is very good in the tank because an unstable density stratification develops causing irregular turbulent circulation [4]. The heated water rises over the whole cross-section of the tank and mixes with the cold water. When boiling starts, steam bubbles rise from the tank bottom but collapse in the upper region where the fluid is still subcooled. Bigger loss of volume begins when the bulk reaches the saturation temperature. If the tank is heated from the side walls, heating-up occurs in an entirely different way as illustrated in Fig. 1. Thermocouples labelled 'a' were fixed closely to the wall. Thermocouples 'b' were located at a distance of 1 cm from the wall. As later experiments have further shown, practically there is no radial temperature gradient in the bulk. The temperature gradient is restricted to the some mm thick convection layer at the wall.

It is to be seen in Fig. 1 that the heating from the side walls leads to large temperature differences over the height of the vessel. A boundary layer develops at the heated wall where warm water flows up. The temperature faster increases at the top of the vessel than at the bottom. A stable horizontal temperature stratification develops with a vertical temperature difference of up to 50 °C. Since the temperature early reaches values near the boiling point at the surface, the loss of water by evaporation early becomes significant, too. Steam bubbles can rise to the water surface in the warm boundary layer already during subcooled boiling. Therefore the loss of the water starts very soon and is more intensive. Moreover characteristic temperature jumps are observed. The temperature jumps occur later and the lifts are higher as the distance from the surface increases. However, in all cases after the jump the temperature is approximately 1 to 1.5 °C lower than the saturation temperature. Another characteristic fast change is the beginning of boiling in the entire volume which starts approximately at 1600 s. At this moment the saturation temperature is simultaneously reached in the whole water volume. This volumetric boiling causes a constant gradient of water loss (see also Fig. 1).

---

[1] Technical University of Budapest
[2] Nuclear Analytics and Engineering Rossendorf Inc.

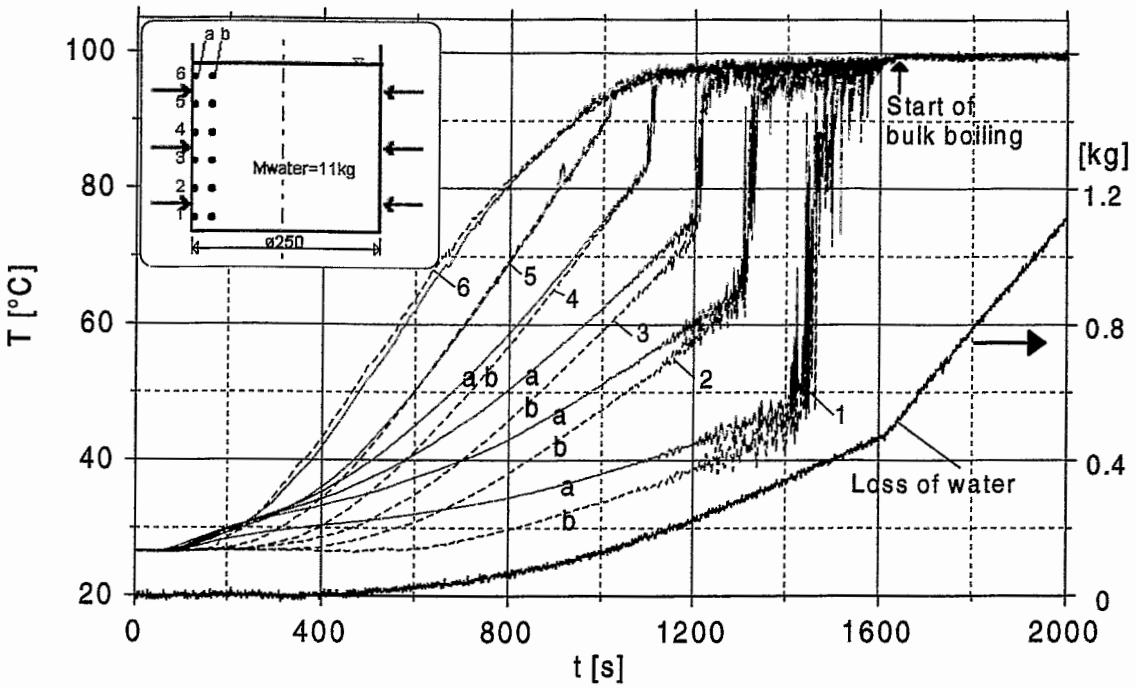

Fig. 1: Experimental mockup and results of the experiment with the vessel heated by side walls (Liewers et al. [1])

2. The 2D model

In order to clarify the physical nature of heating-up and evaporation in the vessel a two-dimensional mathematical model was developed [2]. The flow in the vessel was approximated by a two-dimensional flow in rectangular Cartesian coordinates. It was assumed that neither varying temperature nor gas fraction influence the density of the liquid in the mass conservation equation and in the inertial term of the momentum equation. The changing density was taken into account only in the volume force term in the momentum equation (Boussinesq-approximation). This approximation restricts model application to low gas fractions. But the simplification leads to simpler calculation of the velocity field of the liquid phase. When instantaneous temperature and gas fraction distributions are given, the volume force term can be determined explicitly and the motion of the liquid can be further calculated independently from the gaseous phase.

For the gaseous phase a constant bubble rise velocity was assumed. The vector of the gas velocity ($\vec{v}_g$) results from the liquid velocity by adding a constant value (w_g^+) to the vertical velocity component.

$$v_{g,x} = v_{f,x}$$
$$v_{g,y} = v_{f,y} + w_g^+ \qquad (1)$$

In this constant drift approach the momentum of the gaseous phase is neglected and there is no need to solve a second momentum equation. So, the model consists of four main equations: the energy conservation equation for the two-phase mixture, the momentum and mass conservation equation for the fluid and the mass conservation equation for the gaseous phase.

The energy conservation equation is

$$\frac{\partial T}{\partial t}+v_x\frac{\partial T}{\partial x}+v_y\frac{\partial T}{\partial y}=a\cdot\Delta T+\frac{q_v}{\rho_0\cdot c_p}\,, \tag{2}$$

where

$$a=\lambda_T/(\rho_0\cdot c_p) \tag{3}$$

is the thermal diffusivity of water, λ_T is the thermal conductivity, and q_v is the volumetrical heat source power.

The transport of the gaseous phase is described by the corresponding mass conservation equation:

$$\frac{\partial\varphi}{\partial t}+v_x\frac{\partial\varphi}{\partial x}+\left(v_y+w_g^+\right)\frac{\partial\varphi}{\partial y}=D_\varphi\cdot\Delta\varphi+q_\varphi\,, \tag{4}$$

where

$$\varphi=\frac{V_g}{V_g+V_f} \tag{5}$$

is the relative steam content and D_φ is the gas diffusion coefficient (empirical parameter). Based on the work [5] a constant bubble rise velocity of $w_g^+=0.2\,\mathrm{m/s}$ was chosen. The phase transition due to evaporation and condensation was modelled assuming thermodynamical equilibrium. The mass source of steam (q_φ) was computed from the superheating or subcooling of water.

The momentum conservation equation for the fluid was solved in the form of a vorticity transport equation. According to the above mentioned Boussinesq-approximation density, heat conductivity, specific heat capacity and viscosity were replaced by constant values related to the reference temperature.

The vorticity transport equation is

$$\frac{\partial\omega}{\partial t}+v_x\frac{\partial\omega}{\partial x}+v_y\frac{\partial\omega}{\partial y}=\frac{\mu_T}{\rho_0}\Delta\omega-\frac{1}{\rho_0}g_y\frac{\partial\rho}{\partial x}, \tag{6}$$

where

$$\omega=-(rot\,\vec{v})_z=\frac{\partial v_x}{\partial y}-\frac{\partial v_y}{\partial x} \tag{7}$$

is the vorticity intensity, μ_T is the dynamical viscosity, and g_y is the constant gravitational acceleration.

The density of the medium in the volume force term can be computed as follows:

$$\rho=\varphi\cdot\rho_g+(1-\varphi)\cdot\rho_f\,, \tag{8}$$

where ρ_g is the density of saturated steam (p=1 bar) and ρ_f is the density of water. ρ_g is constant, ρ_f is a function of temperature.

The continuity equation, when using the stream function (Ψ) with

$$v_x=\frac{\partial\Psi}{\partial y}\ \text{and}\ v_y=-\frac{\partial\Psi}{\partial x}. \tag{9}$$

and disregarding the gaseous phase, takes the form of a Poisson equation

$$\Delta\Psi = \omega . \qquad (10)$$

The differential equation system (2), (4), (6), and (10) was solved by using the finite difference method for a rectangular flow area of 0.25 * 0.25 m. The time function of heat power transmitted to the water (known from the experiments) was taken into account, too. The analysis of the characteristic Rayleigh-numbers has shown the flow to be weakly turbulent. Therefore, a constant scalar turbulent viscosity

$$\mu_T = C_{\mu,Tu} \cdot \mu_{laminar} \qquad (11)$$

and a turbulent heat conductivity

$$\lambda_T = C_{\lambda,Tu} \cdot \lambda_{laminar} \qquad (12)$$

were introduced to approximate for turbulence. The dimensionless parameters $C_{\mu,Tu}$ and $C_{\lambda,Tu}$ were determined empirically. There are three reasons for using this very simplified assumption: (1) commonly used k-ε turbulence models are not available for two-phase flows, (2) in the case of single-phase flow, k-ε turbulence models produce a very strong attenuation of unsteady macroscopic vortices, because they were originally developed for steady state calculations. Test calculations with CFD-codes, based on k-ε models, have shown that the characteristic insteady flow pattern of a bottom-heated vessel cannot be satisfyingly reproduced. (3) When using a k-ε turbulence model it is necessary to solve two additional transport equations. This makes the numerical solution more complicated and requires more CPU time.

3. The simulation results

The simulation results are shown in Fig. 2 to 8. For computation, the flow area was divided into 32 by 32 cells. After fitting D_φ, $C_{\mu,Tu}$ and $C_{\lambda,Tu}$, the simulation has reproduced the characteristic phenomena observed in the experiments (see Fig. 2). There is remarkable agreement with the experiments especially for the temperature jumps in the middle of vessel. Based on the model results, the physical phenomena can be explained as follows.

The water close to the wall is heated quickly and flows up due to buoyancy (see Fig. 3). This warm water forms a horizontal layer at the water surface. The resulting stratification is very stable because, the density is less at the top of the vessel than at the bottom. Therefore, mixing can hardly occur. The boundary layer is practically totally separated from the bulk of the water. As time goes on, more and more water flows upwards in the boundary layer, and the stratification also occupies the lower regions (see Fig. 4).

The first significant change happens after 1000 s, when boiling starts near the wall in the top region. The density of steam is approximately 1000 times less than the density of water, therefore a small quantity of steam can induce a much higher buoyancy. Thus velocities become larger, too. At this time, the maximal velocity is 0.03 m/s in the tank. This is one order of magnitude higher than for single-phase circulation. When the temperature gets close to 100 °C at the top of the vessel, the temperature of this layer cannot increase further, and hence a uniform temperature distribution develops in the top layers (Fig. 5). In this area then boiling with net production of steam occurs close to the wall (see Fig. 6) what induces a strong circulation in the upper part of the vessel.

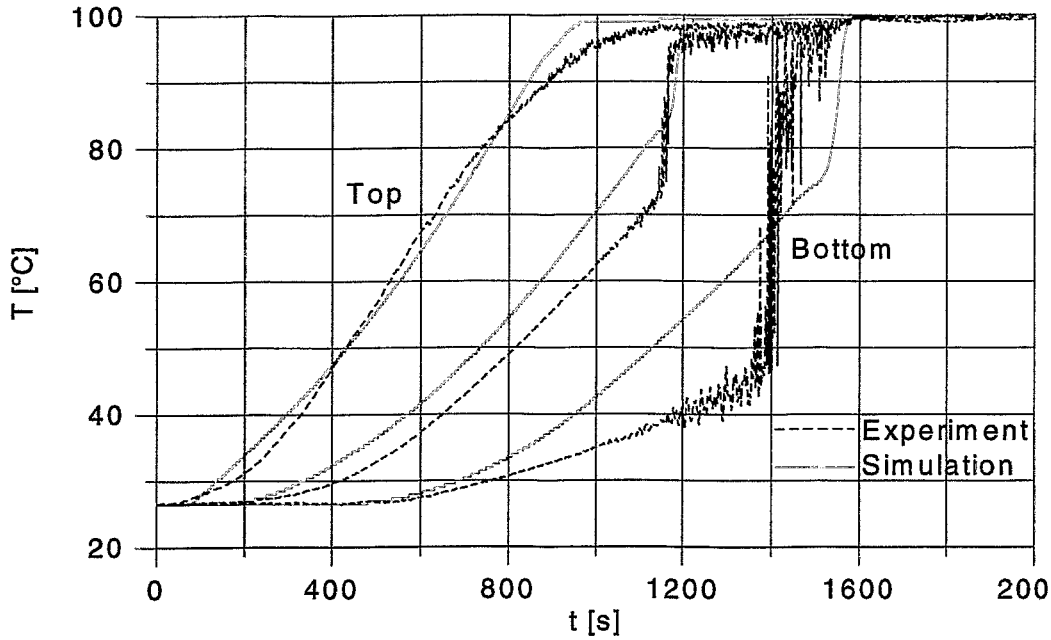

Fig. 2: Calculated and measured temperature courses at different heights in the tank

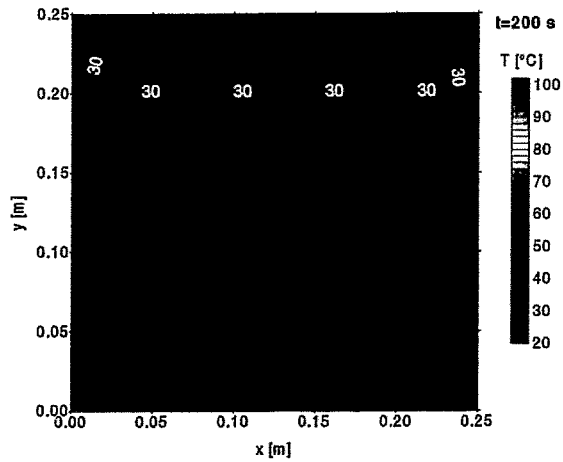

Fig. 3: Temperature field *t*=200 s

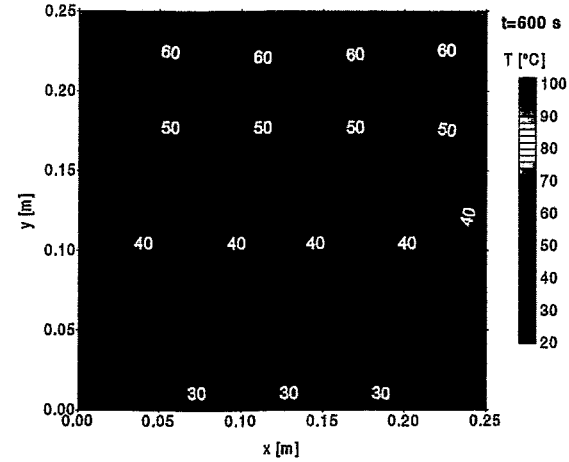

Fig. 4: Temperature field *t*=600 s

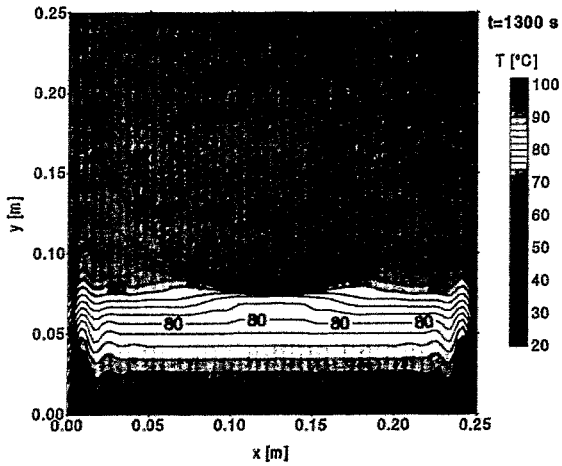

Fig. 5: Temperature field *t*=1300 s

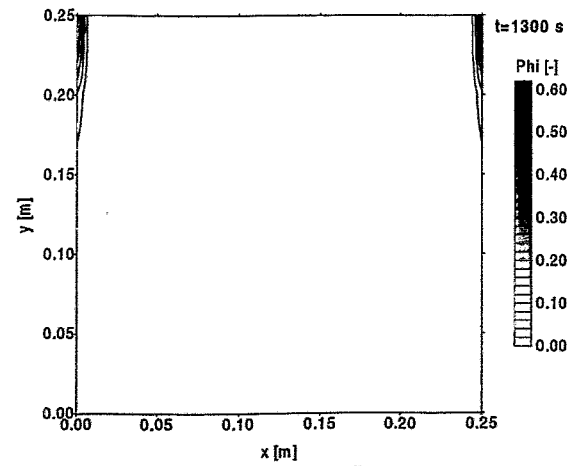

Fig. 6: Steam content field *t*=1300 s

It can be seen well in Fig. 5 that a separating line can be drawn across the middle of the vessel at a height of 8 cm: above this line the temperature is close to the saturation temperature, while there is a steep negative temperature gradient downwards. When this separating line reaches the thermocouples one after the other, temperature jumps are observed as shown in Fig. 2. The maximal velocity also increases close to the wall because of the increasing steam content of the water. After 1628 s, the whole vessel inventory approaches the saturation temperature and steam is generated along the whole length of the wall (see Fig. 7). At this time, the maximal velocity is 0.18 m/s. When the velocity of the downward flow becomes greater than the velocity of the bubble rise in the centre of the vessel, most of the produced steam is entrained into the bulk of the liquid. The enthalpy of steam bubbles provokes saturation in the whole vessel. The quick onset of volumetric boiling (Fig. 8) can be noticed through the fact that the measuring points reach the saturation temperature at the same time (compare Fig. 1 and 2).

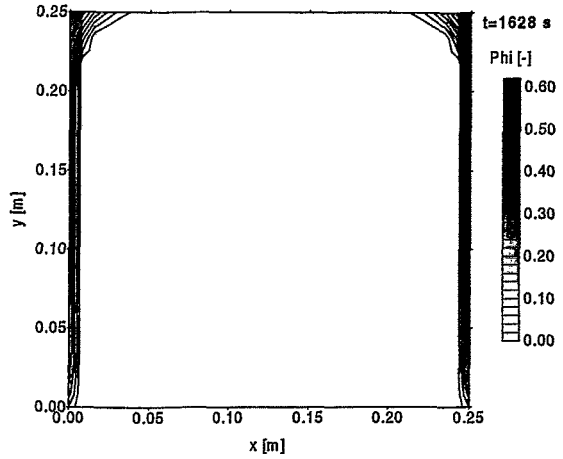

Fig. 7: Steam content field t=1628 s

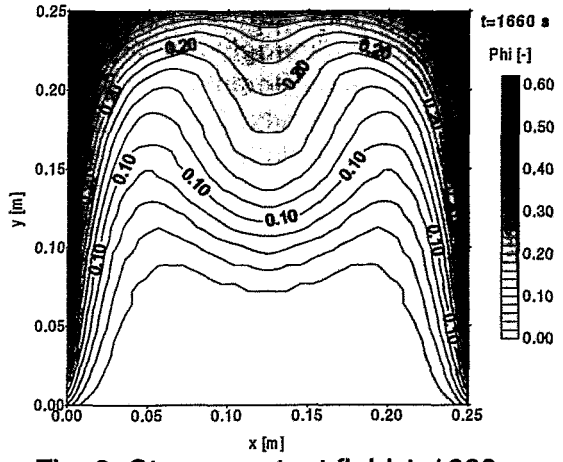

Fig. 8: Steam content field t=1660 s

4. Conclusions

The goal of this work was physically to explain the characteristic phenomena that have been observed in experiments made with side-wall heated storage tanks. A two dimensional mathematical model was developed to describe natural convection within the tank. The specific features of side wall heating - which yields a considerably non-uniform temperature distribution in the tank - were clarified. By using the model, it is possible to identify the temperature stratification as the cause of temperature jumps observed in the experiments. The quick transition from slight subcooling to volumetric boiling was also reproduced correctly by the model. It can be concluded that the governing physical phenomena are: buoyancy forces of the steam bubbles exerted on the fluid motion and the convective transport of the bubbles. This result corresponds well with the result of theoretical analysis made by Grolmes and Epstein [3].

The model contains three essential parameters namely the coefficients of turbulent viscosity ($C_{\mu,Tu}$), turbulent heat conductivity ($C_{\lambda,Tu}$) and diffusion of the gaseous phase (D_φ), which had to be fitted. The overall characteristics of the entire process were described well by the model. Particularly, the used approximations did not distort the model's capability of describing the important features of the fluid behaviour. So, an important advantage of the model lies in its simplicity. Further research work is

necessary to implement advanced turbulence models and to develop a comfortable users interface, which e.g. allows an easy variation of the treated geometry. Possibly this research will be founded on one of the available CFD-codes.

This paper represents the results of a common research work of coworkers of the Nuclear Analytics and Engineering Rossendorf, Research Center Rossendorf, and the Technical University of Budapest which was partly funded by the SMWK (Sächsisches Ministerium für Wissenschaft und Kunst).

References

[1] A. Aszódi, H.D. Giera, J. Herzig, P. Liewers: „Modelluntersuchungen zum Gefahrenpotential eines Lagers flüssiger radioaktiver Stoffe", Annual Meeting on Nuclear Technology 1995, Nürnberg, 16.-18. May 1995, proceedings ISSN 0720-9207 pp. 165-168.

[2] A. Aszódi: „Numerische Simulation der Aufheizung eines wassergefüllten Topfes über den Gefäßmantel", VKTA Rossendorf, November 1994

[3] M. A. Grolmes, M. Epstein: „Vapor-Liquid Disengagement in Atmospheric Liquid Storage Vessels Subjected to External Heat Source, Plant/Operations Progress", Vol. 4, No. 4 (1985) pp. 200-205.

[4] H. Oertel jr.: „Thermal instabilities", in J. Zierep and H. Oertel Jr. (ed.), Convective Transport and Instability Phenomena, G. Braun Verlag, Karlsruhe, 1982, pp. 3-24.

[5] A. Sokolichin, S. Becker, G. Eigenberger: „Modellierung und numerische Simulation von G/L-Blasen-Stroemungen", Chem.-Ing-Tech. 66 (1994) Nr. 4, pp. 505-510.

Nomenclature

t	[s]	time
T	[°C]	temperature
x	[m]	coordinates in horizontal direction
y	[m]	coordinates in vertical direction
v	[m/s]	velocity
w_g^+	[m/s]	constant bubble rise velocity
ω	[1/s]	vorticity intensity
Ψ	[m²/s]	stream function
φ	[-]	relative gas content
ρ	[kg/m³]	density
μ	[kg/m/s]	dynamical viscosity
λ	[W/m/K]	thermal conductivity
c_p	[J/kg/K]	specifical heat capacity
a	[m²/s]	thermal diffusivity of fluid
q_v	[W/m³]	volumetrical heat source power
g	[m/s²]	gravitational acceleration
Δ		Laplace-operator in Cartesian coordinates $\Delta = \frac{\partial^2}{\partial x^2} + \frac{\partial^2}{\partial y^2}$

INVESTIGATIONS OF AN EXTERNAL HEATED STORAGE VESSEL BY MEANS OF CFX-4 CALCULATIONS

A. Aszódi*, E. Krepper

1. Introduction

Storage tanks for fluids are widely used industrial facilities. As a consequence of an external fire, the heat-up of the inventory may lead to the evaporation of the liquid and to release of significant quantities of dangerous gases into the environment. Experimental investigations have shown that the liquid inventory behaves very differently depending on the mode of heating [1]. Bottom heating leads to an irregular thermoconvective motion of the liquid, which causes good mixing, so that saturation is reached at all places inside the tank approximately at the same time. The maximum enthalpy of the liquid always remains close to the average value. If the vessel is heated from the side, a stable temperature stratification is observed leading to large temperature gradients. Evaporation can start much earlier than the average temperature reaches saturation. In order to clarify the physical nature of the details of the heating-up and the evaporation process in simple geometrical boundary conditions a two-dimensional mathematical model was developed, which includes also evaporation and two-phase flow [2]. For more complicated configurations to investigate possible measures for better mixing of the fluid in the case of side wall heating the CFD-code CFX-4 was applied.

2. Modelling of side wall heating by CFX-calculations

As a first step to find a comparison to the results gained by the 2D-model [2], the same arrangement using the CFD-code CFX-4 was calculated. During these investigations only the first period of the experiment in single phase mode was modelled. The vessel was represented by a two dimensional Cartesian grid. Only half of the volume was considered, using the option of a symmetrical plane. Corresponding to Rayleigh-Numbers of $4 \cdot 10^9 ... 2 \cdot 10^{10}$, the application of the „Low Reynolds K-Epsilon Model" has proven to yield the best results. Fig. 1 shows a good agreement of the CFX-calculations with the experiment and the results of the 2D-model.

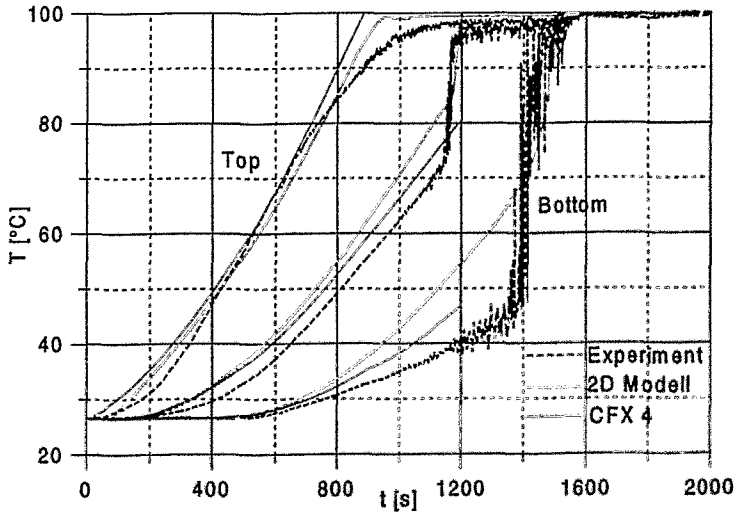

Fig. 1: Measured and calculated temperature courses for the vessel with side wall heating

* Technical University of Budapest

3. Insertion of baffle plates

To avoid fast temperature increase at the fluid surface in the case of side wall heating, a better mixing of the fluid has to be established. This could be achieved by insertion of baffle plates inside the vessel. To investigate the influence of this passive safety measure, additional calculations were performed. The own 2D-model [2] is not suitable for the description of complex arrangements.

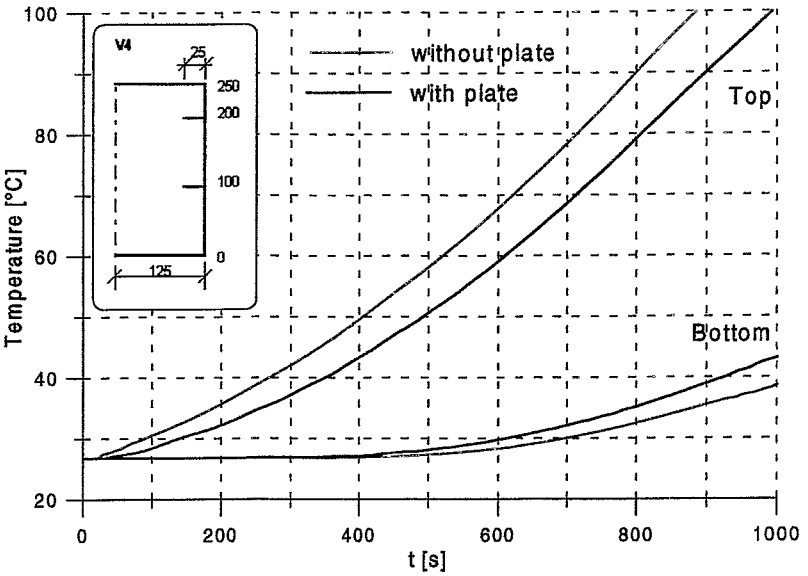

Fig. 2: Influence of a baffle plate on the temperature course in the case of side wall heating (see Fig. 3 and 4)

The effect of two baffle plates on the temperature transient is shown in Fig. 2. The arrival of saturation temperature on the top is postponed by more then 100 seconds. The influence on the temperature and on the velocity field is shown in Fig. 3 for the top without plates and in Fig. 4 with buffle plates.

The influence of the baffle plates may probably be increased by further optimization of the arrangement. Additional CFX-calculations modelling the 3-dimensional case and two phase flow are planned.

The calculations have shown, that passive constructive measures, like inserted plates, are capable, to disturb the stratification and to avoid enhanced heating of the fluid surface.

References

[1] A. Aszódi, H.-D. Giera, J. Herzig, P. Liewers
Modelluntersuchungen zum Gefahrenpotential eines Lagers flüsiger radioaktiver Stoffe
Jahrestagung Kerntechnik 1995

[2] A. Aszódi, P. Liewers, H.-M. Prasser
Simulation of transient natural convektion in side wall heated storage tanks
Jahresbericht 1995 des Instituts für Sicherheitsforschung

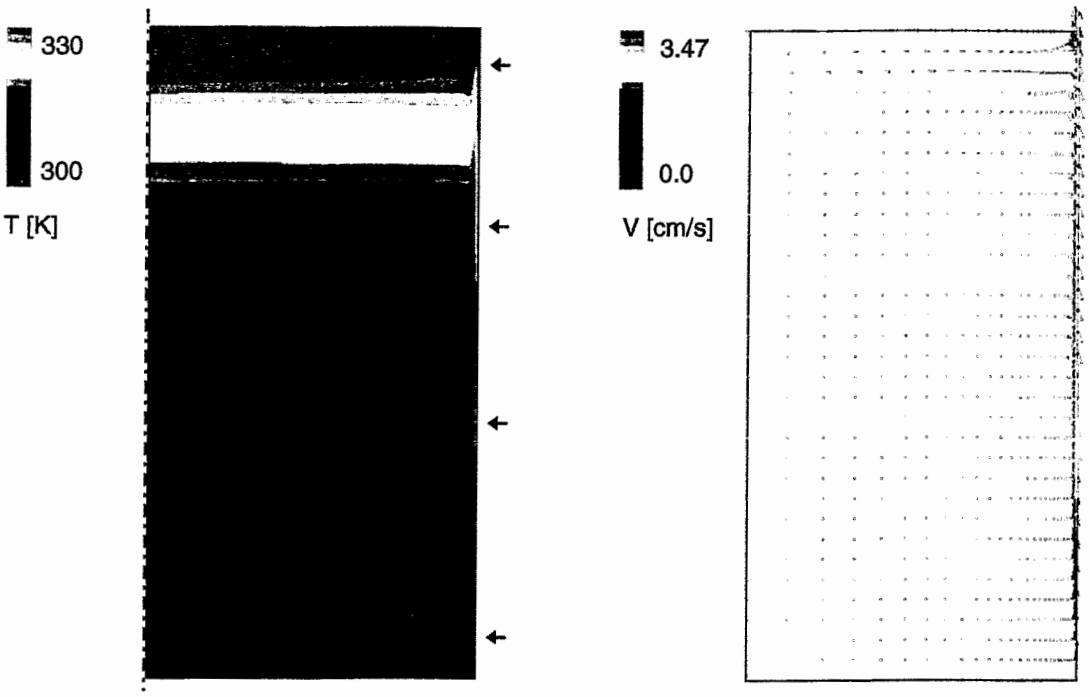

Fig. 3: Field of temperatures and velocities in a side wall heated top after 515 sec (CFX-calculation) (Symmetric plane on left side, heat from right side)

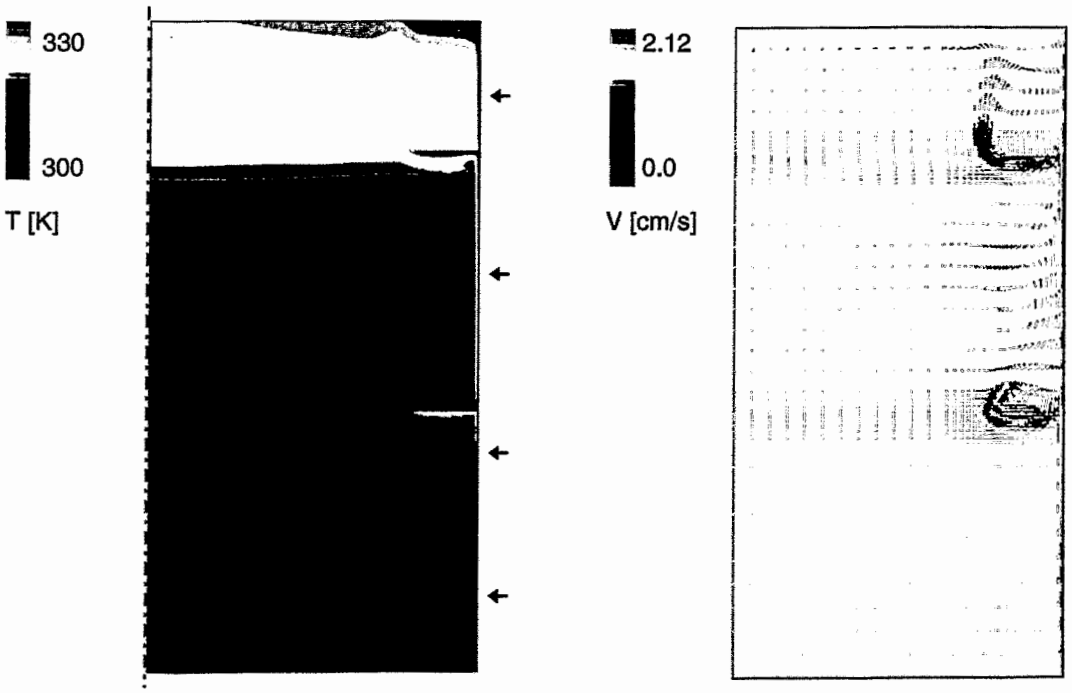

Fig. 4: Field of temperatures and velocities in a side wall heated top with two inserted buffle plates after 528 sec (CFX-calculation)

UPGRADING AND APPLICATION OF THE 3D CORE MODEL DYN3D

U. Grundmann, U. Rohde

1. Introduction

The 3-dimensional core model DYN3D developed in the Research Center Rossendorf can be applied for steady state and transient analysis of VVER-type reactor cores [1]. It consists of three main parts:

- neutronic model based on a nodal method
- thermal hydraulics of coolant flow and fuel rod model
- cross section calculation based on a given library

The general flow chart of DYN3D can be seen in Fig. 1 showing also the basic models of the code. Analysing a transient, safety parameters as DNB ratio or maximum fuel temperatures can be estimated for defined hot channels connected with channels of maximum power release by using hot channel factors.

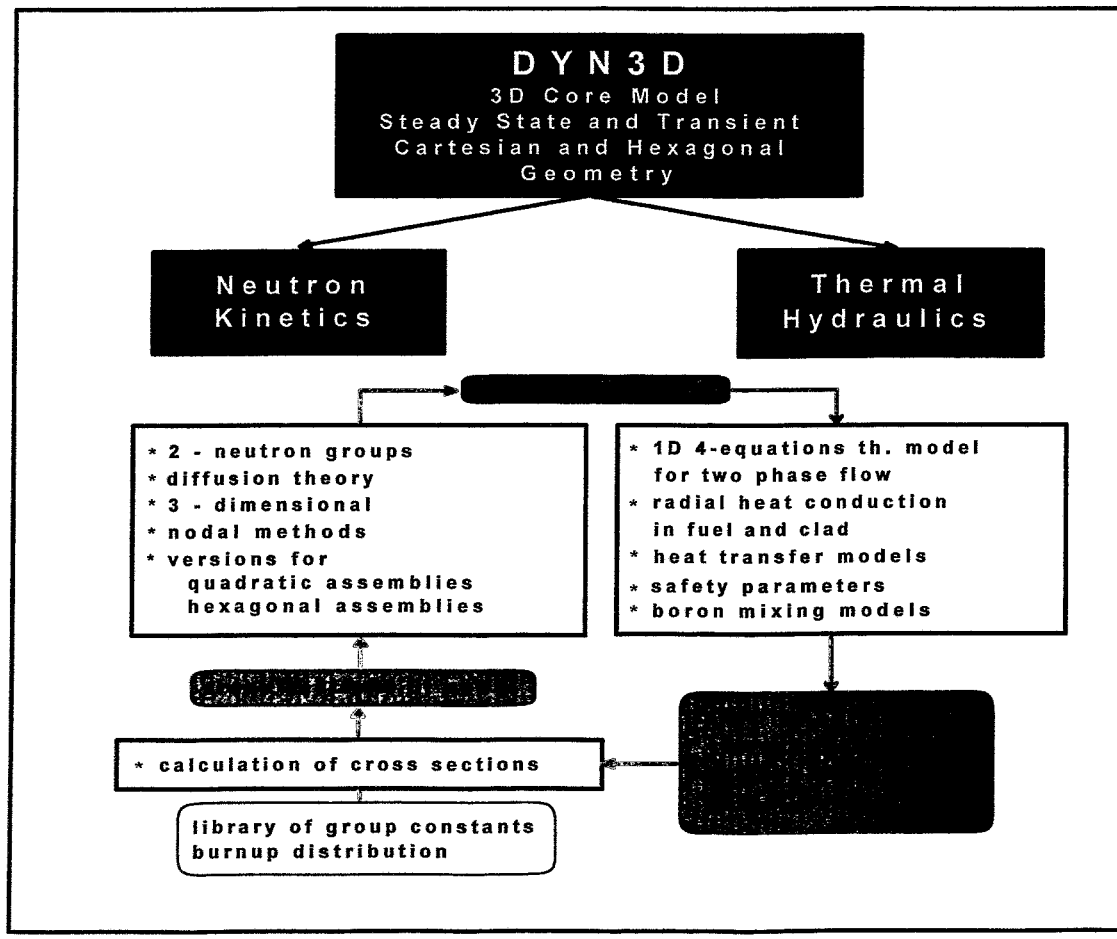

Fig. 1: General flow chart of DYN3D

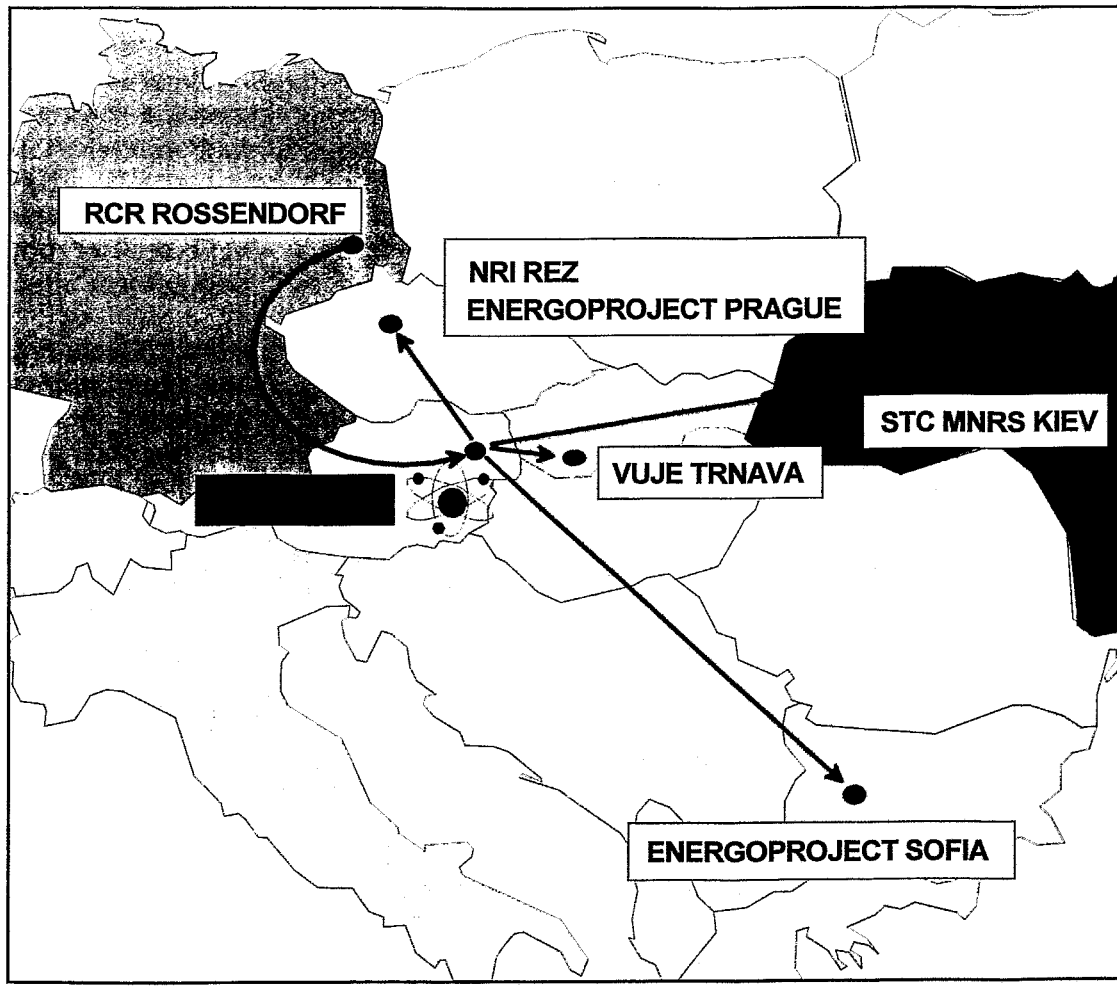

Fig. 2: Transfer of DYN3D to organizations in the frame of IAEA regional project

DYN3D was transferred to several eastern European countries in the frame of the regional project "Safety Assessment of VVER-440 Reactors" of the International Atomic Energy Agency (IAEA). At present, DYN3D is used at NRI Rez and Energoproject Prague (Czech Republic), VUJE Trnava (Slovak Republic) and the Scientific Technological Center of the Ministry for Nuclear and Radiation Safety (STC MNRS) for solving safety relevant problems of VVER-reactors, see Fig. 2.

To analyse transients being initiated by perturbations in the cooling loops (deboration, steam line break) DYN3D was coupled with the system code ATHLET developed by Gesellschaft fuer Anlagen - und Reaktorsicherheit (GRS) [2].

2. Upgrading of DYN3D

The VVER pressurised water reactors consist of hexagonal fuel assemblies. The original DYN3D core model could not be used for western reactors loaded with quadratic fuel assemblies. To be able to analyse transients in these reactors too, a new option of DYN3D for Cartesian geometry was developed [3]. On the basis of international benchmarks, this option was verified for application to PWR and BWR. Due to the unified code structure of both versions for hexagonal and quadratic geometry, the coupling of the Cartesian DYN3D version with ATHLET can be accomplished easily.

3. Validation

DYN3D has been verified by comparisons of results with experimental data and by benchmarks. As there are no experiments available for accident scenarios, the comparisons with other codes and benchmarking are important steps of code validation. Comparisons with different codes for hexagonal fuel assemblies were carried out in the frame of Working Group D "VVER Safety Analysis" of the Atomic Energy Research (AER) association, a forum for co-operation in the field of VVER reactor physics research.

The first two comparisons of the implemented neutronic models were based on given cross sections data. The ejection of a peripheral rod in a VVER-440 with successive scram was considered in the first benchmark. The second problem was similar to the first one, but the ejected control rod worth was 2ß (ß is the part of delayed neutrons) which results in a sharp and high power peak connected with large deformations of flux. The Doppler effect as the main feedback effect for this type of transients was the only feedback. It can be concluded from this benchmark that the differences in total power release and maximum fuel temperature are mainly caused by the different models for the description of the black absorbers in the codes. Therefore the cross sections and the rod worth were given in the 3rd benchmark for comparing the models of coolant flow and fuel rod on the basis of given thermophysical properties. The initiating event was the same as in the second benchmark. The super prompt critical power excursion starting from hot zero power leads to a strong increase of maximum fuel temperatures [4]. Results of five different research institutes calculated with four different code systems were compared:

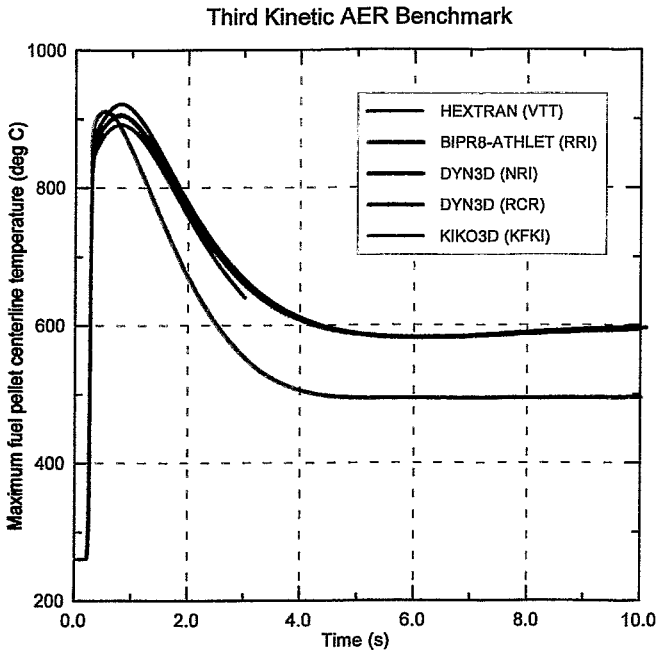

Fig. 3: Comparison of maximum fuel centerline temperatures

- KFKI AEKI Budapest (KIKO3D)
- NRI Rez (DYN3D)
- RCR Rossendorf (DYN3D)
- RRC Kurtchatov Institute, Moscow (BIPR8-ATHLET)
- VVT Helsinki (HEXTRAN)

The comparison of the behaviour of maximum fuel temperature in Fig. 3 shows a good agreement in the range of temperature increase. A possible explanation of the deviations of BIPR8-ATHLET results after the temperature maximum might be the different heat transfer model selected for this application in the ATHLET code.

The NEACRP LWR Benchmarks were defined for validation of codes developed for quadratic fuel assemblies [5]. Different rod ejection's in PWR's at hot zero power (HZP)

and full power (FP) are considered for comparison of 3-dimensional codes. On the basis of published results [6] the calculations were carried out with the Cartesian version of DYN3D. Fig. 4 shows good agreement of the power curve with the reference solution for the most interesting case, namely the ejection of a peripheral rod in a standard PWR at HZP. The strong space dependency of power shape at power maximum can be seen in Fig. 5. The comparisons described in more detail in [3] demonstrate that the results are in good agreement with the reference solution.

4. Code Application

The code DYN3D was applied to investigate transients in VVER-440 reactors. At HZP the ejection of the most reactive rod of the inserted control rod banks K4, K5 and K6 during start up measurements was calculated, showing that the safety limits are not exceeded [7].

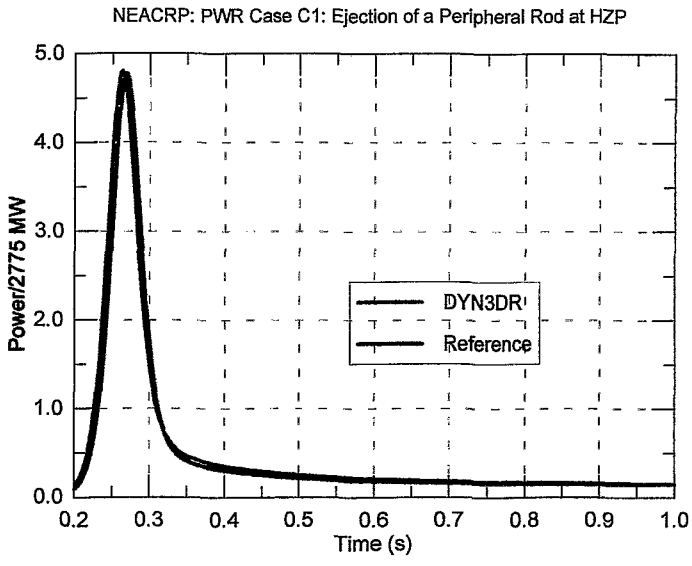

Fig. 4: Comparison of nuclear power with the reference solution in [7].

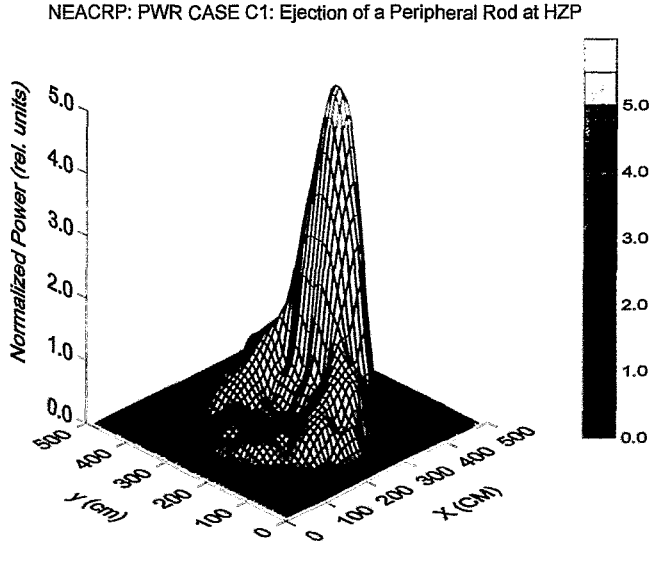

Fig. 5: Normalized assembly power distribution at power maximum

The transient initiated by a plug of diluted boron in one loop entering the core was studied for different assumptions about the mixing in the lower plenum. The three cases of no mixing, realistic mixing according to the implemented model and homogeneous mixing were investigated. It was shown that no mixing is the most serious case leading to violation of the safety limits [8]. In practice, the assumption that the water of one loop is not mixed with the water of the others is too conservative. Assessing the safety with regard to these types of transients the validation of the mixing model is needed for more realistic calculations.

The code DYN3D was used in the NRI Rez for studying similar transients [9]. Considering the safety parameters, for example the maximum fuel temperature, the same tendency was observed as in the own calculations, that is an overestimation of temperature using no mixing and an underestimation by assuming ideal mixing of boron in the lower plenum.

Series of calculations with DYN3D were carried out in the organisations which obtained the code through the IAEA regional project.

For example, DYN3D was used for supporting one-dimensional calculations with the code REPA1D licensed in the Czech Republic for the simulation of reactivity initiated accidents [10]. Especially the use of Doppler weighting factors for analyses of strong space-time effects has to be justified by 3-dimensional calculations. The one-dimensional results using Doppler weighting factors lower than 2.5 gives conservative results compared with 3-dimensional DYN3D calculations.

Using DYN3D a spectrum of rod ejection accidents for the Bohunice V-2 plant was performed by the Nuclear Power Plant Research Institute (VUJE) Trnava (Slovak Republic) in close co-operation with the IAEA [11].

The code DYN3D was transferred to STC MNRS Kiev for supporting the safety assessments of VVER-reactors in Ukraine. A first step was the implementation of the code in the STC MNRS and the qualification of Ukrainian experts in handling the code. Several parameters as critical boron concentration and control rod worth measured during the startup phase of a VVER-1000 power plant were compared with the calculated results. Transients as ejection of a single control rod, withdrawal of control rod bank and coast down of one coolant pump in a VVER-1000 were analysed by the Ukrainian experts. Comparisons with own calculations show a good agreement [12]. Applying the code DYN3D and the coupled code system DYN3D-ATHLET for safety assessment a further co-operation is necessary .

5. Summary

A new option of the code DYN3D for fuel assemblies with Cartesian geometry was developed. Validation work for the hexagonal as well as the Cartesian version was done by comparisons with results of other codes and benchmark solutions. DYN3D is used in different organisations of countries utilising VVER-reactors.

References

[1] U. Grundmann and U. Rohde
"DYN3D/M2 - a Code for Calculation of Reactivity Transients in Cores with Hexagonal Geometry".
Report FZR 93 - 01

[2] U. Grundmann, D. Lucas, S. Mittag and U. Rohde
"Weiterentwicklung und Verifikation eines dreidimensionalen Kernmodells für Reaktoren vom Typ WWER und seine Ankopplung an den Störfallcode ATHLET".
Report FZR-84

[3] U. Grundmann
"The Code DYN3DR for Steady State and Transient Analyses of Light Water Reactor Cores with Cartesian Geometry"
Report FZR-114

[4] R. Kyrki-Rajamäki, E. Kaloinen
"Results of the Third Three-Dimensional Hexagonal Dynamic AER Benchmark Problem Including Thermohydraulics Calculations in the Core and a Hot Channel".
Proceedings of 5th Symposium of AER, Dobogokö, Hungary, 1995

[5] H. Finnemann, A. Galati
"NEACRP 3-D LWR Core Transient Benchmark"
Report NEACRP-L-335, Rome, 1992

[6] H. Finnemann, H. Bauer, A. Galati and R. Martinelli
"Results of LWR Core Transient Benchmarks",
Report NEA/NSC/DOC(93) 25, OECD NEA, 1993

[7] U. Grundmann, U. Rohde
"3-dimensional Analysis of an Absorber Rod Ejection Accident in the Reactor WWER-440 by the code DYN3D/M2"
Proceedings of 1st Symposium of AER, Rez, Czech Republic, 1991

[8] U. Grundmann, U. Rohde
"Investigations on a Boron Dilution Accident for a VVER-440 Type Reactor by the Help of the Code DYN3D"
Proceedings of Topical Meeting on "Advances in Reactor Physics",
Knoxville (USA), 1994

[9] J. Hadek
"Information on Preliminary Calculations of Transients in VVER-440 Reactors Caused by a Suddenly Dilution of Boron Acid Concentration in the Coolant"
Meeting of AER Working Group D, Helsinki, 1995

[10] I. Tinka
"Space-Time Kinetics Support for Point Kinetics Calculations"
Proceedings of 4th Symposium of AER, Sozopol, Bulgaria, 1994

[11] "Guidlines for Accident Analysis of WWER Nuclear Power Plants"
Report IAEA-EBP-WWER-01, IAEA Vienna, 1995

[12] U. Rohde, U. Grundmann
" Qualifizierung ukrainischer Experten auf dem Gebiet reaktorphysikalischer Berechnungen und Einschätzungen"
Abschlußbericht zum Vorhaben des SR 2075/5 des BMU, Rossendorf 1996

NATURAL CIRCULATION EXPERIMENTS AT THE ISB-VVER INTEGRAL TEST FACILITY

E. Krepper

1. Introduction

From the thermalhydraulic point of view, the main safety related differences of Russian VVER-reactors compared to typical western PWR's are the lower geodetic height differences in the primary circuit because of the horizontal steam generators. This influences the core cooling capability at natural circulation conditions, which is the most important heat transport mechanism during accident situations.

The ISB-VVER is a 1/3000 volume scaled test facility for VVER-1000 thermalhydraulics, located in Elektrogorsk, near Moscow. From October 1992, to present, many transient and loss of coolant tests have been performed.

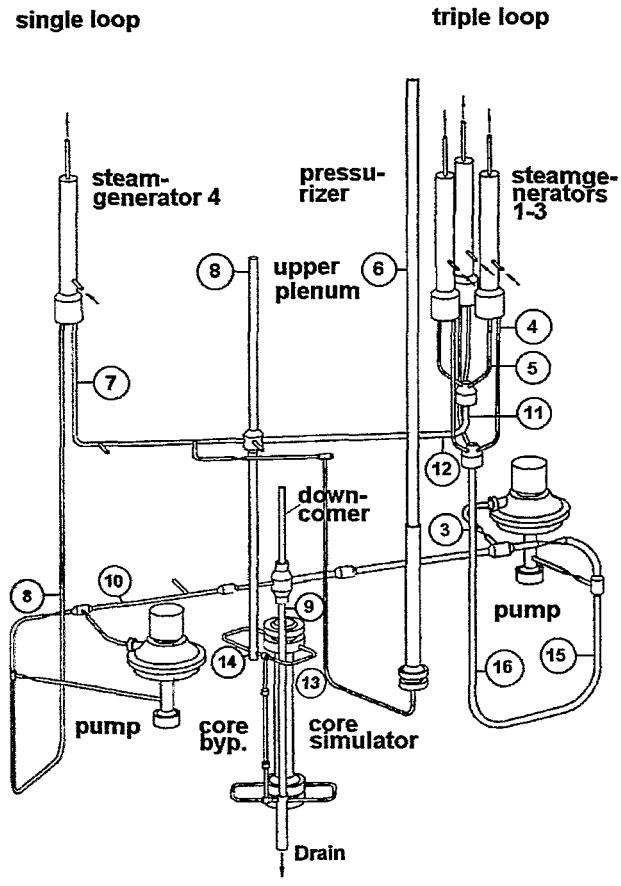

Fig. 1: Schema of the ISB-VVER facility and locations of the conductivity probes

In 1995, natural circulation experiments were conducted, which were scientifically accompanied by the Institute for Safety Research of Research Center Rossendorf (RCR). Using the thermalhydraulic code ATHLET of GRS, pretest calculations were performed, to define and tune the boundary conditions of the test. In March 1995 the first tests were performed. Analyzing the first results, the test regime was slightly modified and it was decided, to perform a second test with 200 kW, in addition to the test with 100 kW power of the core simulator. In August, 1995, the final experiments were conducted. During all tests the facility was, in addition to the standard instrumentation, equipped with needle shaped conductivity probes for measuring the void fraction. These probes were developed and manufactured by RCR.

2. Basic Test Phenomena

The experiment was particularly aimed at the investigation of phenomena, which play a role during the later phases of small break loss of coolant accidents (SBLOCA), when natural circulation is the only mechanism for decay heat removal. To simulate the leak, defined amounts of coolant were drained from the lowest point of the facility at defined times. The power of the core simulator corresponded to a scaled down decay heat (100 kW). Controlled stationary conditions were held at the steam generator secondary sides. The initial conditions are given in Table 1. The electric fuel rod heating was stopped when the cladding temperature started to increase. The above described SBLOCA scenario provides safety relevant phenomena like single and two phase natural circulation, boiler condenser mode, natural circulation instabilities and cold leg loop seal clearing.

Similar experiments were carried out in 1989 at the Hungarian PMK-facility and 1992 at PACTEL in Finland (ISP-33). Both facilities simulate VVER-440 thermalhydraulics.

3. Pretest Calculations

The pretest-calculations were to determine suitable boundary conditions to ensure the occurrence of all phenomena and to reveal possible problems that might come up in the experiment.

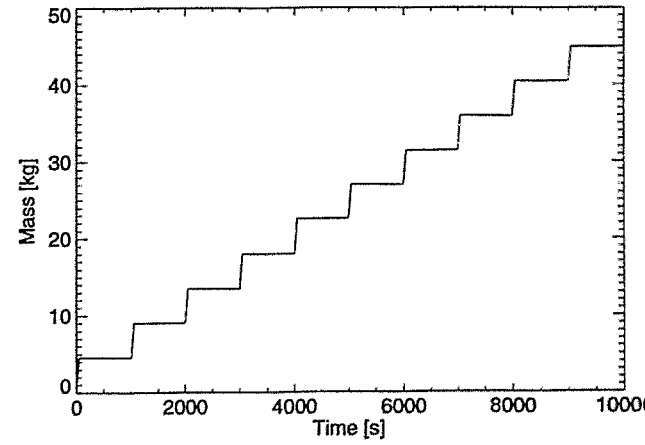

Fig. 2: Integral drained coolant mass

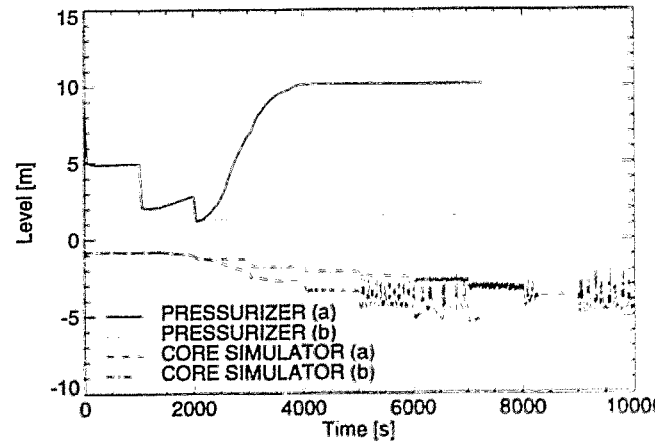

Fig. 3: Collapsed levels (pretest calculations)
(a) connected pressurizer
(b) isolated pressurizer

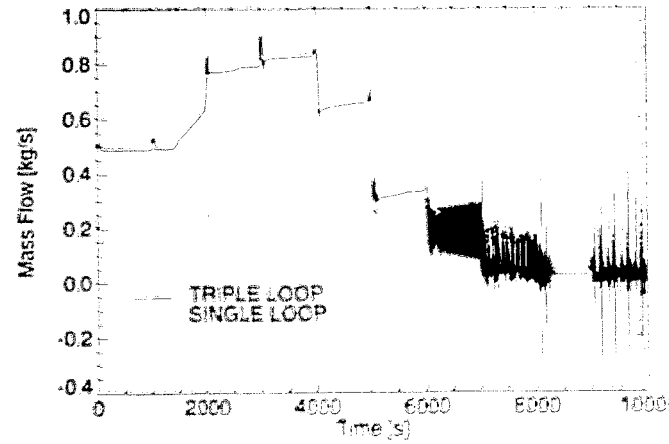

Fig. 4: Mass flows with isolated pressurizer (pretest calculation)

During the ISP-33 experiment at the PACTEL-facility, the coolant inventory was reduced by about 10% at each drain step. The rod cladding temperature increased after the 7th drain step, when the coolant inventory was reduced to about 30% of the initial value. The related pretest calculations already indicated, that the cladding temperature would increase with 50% coolant inventory. Therefore, it was decided for ISB, to reduce the initial coolant inventory of about 90 kg by 5% i.e. by 4.5 kg in each drain step (see Fig.2).

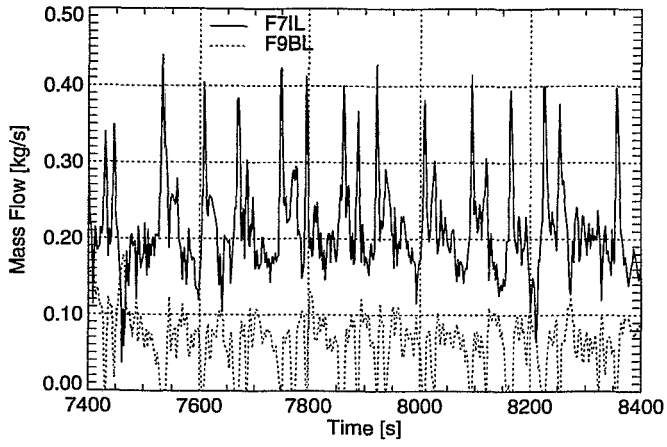

Fig. 5: Mass flows in the triple loop (F7IL) and in the single loop (F9BL) at 100 kW (experiment)

The pretest calculations provided refilling of the pressurizer due to the pressurizer heat losses and connected condensation. As a result, the level in the core simulator will decrease faster and the cladding temperature increase will occur earlier (see case a) of Fig. 3). Therefore it was proposed to isolate the pressurizer after its depletion (case b) of Fig. 3).

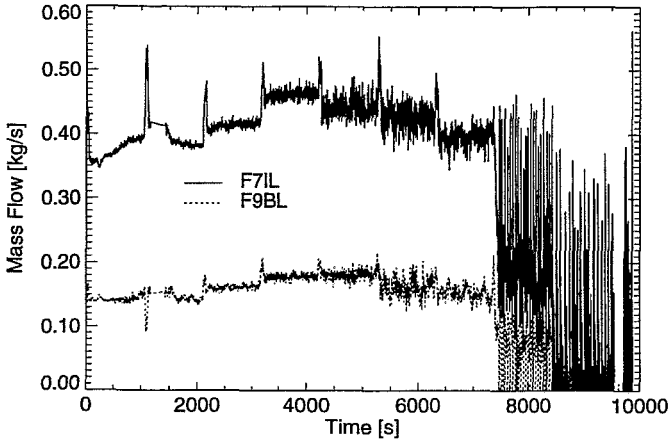

Fig. 6: Mass flows in the triple loop (F7IL) and in the single loop (F9BL) at 200 kW (experiment)

At the first experiments in March 1995 difficulties arose concerning the control of secondary pressure. Nevertheless, using the results of these experiments, a better adjustment of the initial conditions in the calculations was possible. It was found, that at the low power level of 100 kW the natural circulation instabilities did not appear in the calculations. Therefore it was proposed to carry out a second additional natural circulation experiment at 200 kW, to ensure, that the natural circulation instabilities would happen during the experiment.

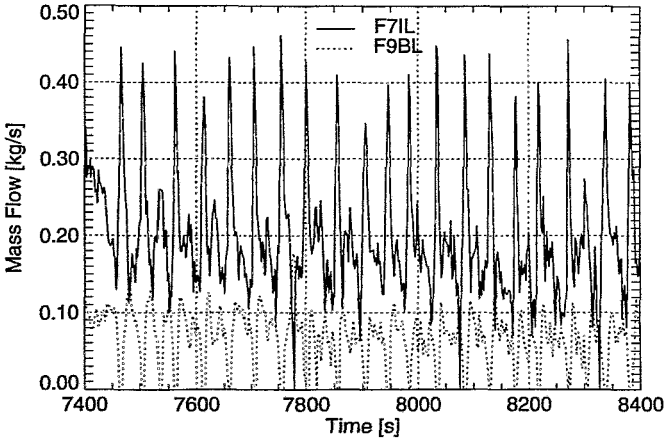

Fig. 7: Detail of Figure 6

4. The Experiments

The experiments performed in August 1995 confirmed the pretest calculations. At 100 kW core simulator power, irregular instabilities of the mass flows were found (see Fig. 5), whereas in the second experiment at 200 kW these instabilities were quite regular with a time period of about 65 seconds (see Figs. 6 and 7). This corresponds to the time for one complete circulation through the loop. These oscillations were caused by density wave instabilities and could even be found in the calculations. The instabilities which were observed one drain step later, at about 9000 sec, could be shown by the calculations to be caused by clearing and refilling of the pump seal in the single loop. (see Fig. 8).

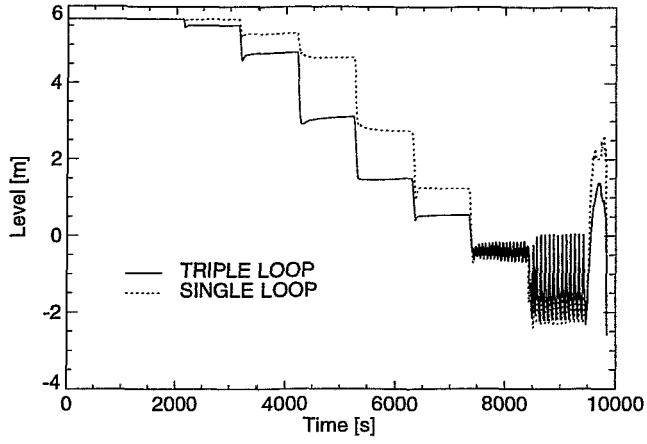

Fig. 8: Collapsed levels in the cold legs at 200 kW (posttest calculations)

There are plans to qualify the ISB test facility by replacing the vertical steam generators with horizontal ones. Then, performing the same experiments, the possibility arises to directly investigate the influence of the steam generator type upon the thermalhydraulic behaviour of PWR's.

		Nominal conditions	Exp. 1	Exp. 2
Power	[kW]	960.0	100.0	200.0
Pressure	[MPa]	15.75	15.75	15.75
Temperature upper plenum	[°C]	320	320	342
Temperature downcomer	[°C]	280	280	284
Mass flow triple loop	[kg/s]	4.24	0.26	0.36
Mass flow single loop	[kg/s]	1.44	0.10	0.14

Tab. 1: Initial conditions of the ISB-facility at nominal conditions and at the two natural circulation experiments

A SPECIMEN RECONSTITUTION TECHNIQUE TO IMPROVE THE AVAILABILITY OF TEST MATERIAL FROM OPERATING PLANTS

H.-W. Viehrig and J. Böhmert

1. Introduction

Specimen reconstruction, i.e the welding of half pieces of already tested specimens renders possible to use that material for testing purposes twice [1,2]. This helps partially to overcome the lack of test specimens from plants or nuclear installations which already have been in operation and so permits to improve the statistical accuracy of the measured mechanical properties. In view of the efforts to extend reactor pressure vessels (RPV) lifetime it is desirable directly to measure the RPV materials toughness by using fracture mechanical parameters. Presently, the residual lifetime is assessed via measuring the embrittlement induced shift of the ductile-to-brittle transition temperature of Charpy-V specimens in the framework of so called surveillance programmes. These surveillance programmes do not include fracture mechanical specimens. Therefore, a specimen reconstitution technique is developed to obtain single-edge notched bend (SENB) specimens for fracture mechanical tests from broken halves of Charpy specimens [3,4]. The reconstitution technique has to fulfill the following demands:

- standard specimen geometry,
- tests results like the original standard specimens, and
- the loaded material of the insert piece must not be influenced by the welding and machining procedure.

The main concern in surveillance specimen preparation by welding is the risk of thermally annealing the irradiated material. Hence, the maximum temperature has to be below the irradiation temperature (300°C).

2. Reconstitution Technique

The production of a reconstituted specimen includes 3 steps:

1. Cutting off the fractured surface from a broken half of Charpy-V specimen to get an insert piece.
2. Welding of end blocks to the insert piece to get a slug.
3. Machining of the slug to get the reconstituted Charpy size SENB specimen.

The insert pieces are welded by using a stud arc welding technique. Fig. 1 schematically demonstrates the stud arc welding technique. The quality of the welding joint was sufficient when using a welding engineering as proposed by the producer of the stud welding appliance. Unfortunately the heat input of 15 kWs leads to a temperature profile with a temperature maximum below 300°C only within the 6 mm centre section of the 25 mm insert piece and even higher than 300°C in the whole range of a 20 mm insert piece (Fig.2 and 3). Hence, a short time welding technology producing only a heat input of 3,8 kWs was developed. Then, the maximum temperature does not reach the permissible

limit of 300°C in a sufficiently large centre section of both the 20 and 25 mm insert pieces (Fig. 3).

An electric discharge cutting machine is an accurate numerically controlled tool, which produces a final surface and dimensional quality of the specimens as required in the standards. The electric discharge cutting machine is used to remove the oversized studs and weld seams from the welded slug and to machine the V-grooves, side grooves and internal clip-gauge seats in the Charpy size SENB specimen.

3. Assessment and Validation of Specimen Reconstitution Technique

Fig. 4 and 5a show the macrograph of the welding joints for standard and short time welding engineering (Fig. 1). The insert piece is a DIN 10 CrMo 9 10 heat resistant structural steel with a bainitic structure while the studs are of DIN St37 steel with a ferritic-perlitic structure. The big heat input using standard welding engineering produces large melting baths on the front sides of the insert piece. Hence, there are welding joints with big bulges and large heat affected zones (2-2.5 mm length). The lower heat input of the short time welding engineering avoids these bulges of melted material (Fig. 5a) and the heat affected zones identified in the microsection shown in Fig. 5b are small (0.4 mm). These metallographic results confirm the measured hardness profiles of the 25 mm insert pieces shown in Fig. 6 and 7. The width of the molten and heat affected zones increases with the heat input (Fig. 6). In case of short time welding engineering (Fig. 7) there is an unaffected zone of 20 mm within the centre of the 25 mm insert piece.

Fig. 8 shows the measured adsorbed energy-temperature values for standard and reconstituted Charpy-V specimens of a reactor pressure vessel steel ASTM A533 B Class 1. The Charpy-V transition curves are hyperbolic tangent fittings. The dynamic yield strength versus test temperature of both specimen types are presented in Fig. 9. In spite of statistical scattering in the measured values the following conclusions can be drawn:

- The standard and reconstituted Charpy-V specimens are identical in adsorbed energy, lateral extension and fracture appearance - transition temperature - curves and dynamic strength-temperature - curves.

- There is practically no difference between specimens welded with the standard and short time welding engineering.

- In case of Charpy impact testing the quality of the welding joint is not so important. Small welding defects like inclusions, blowholes and edges can be neglected. No fracture and deformation of a welding joint was observed during impact loading.

4. Summary

Specimen reconstitution techniques offer the possibility to reach improved statistics of the measured material parameters when only small amounts of material are available. The essential tools for specimen reconstitution are a stud welding appliance and an electric wire discharge machine. In order to keep the maximum temperature below 300°C during stud welding a special short time welding engineering was developed. The validity of the

Figures

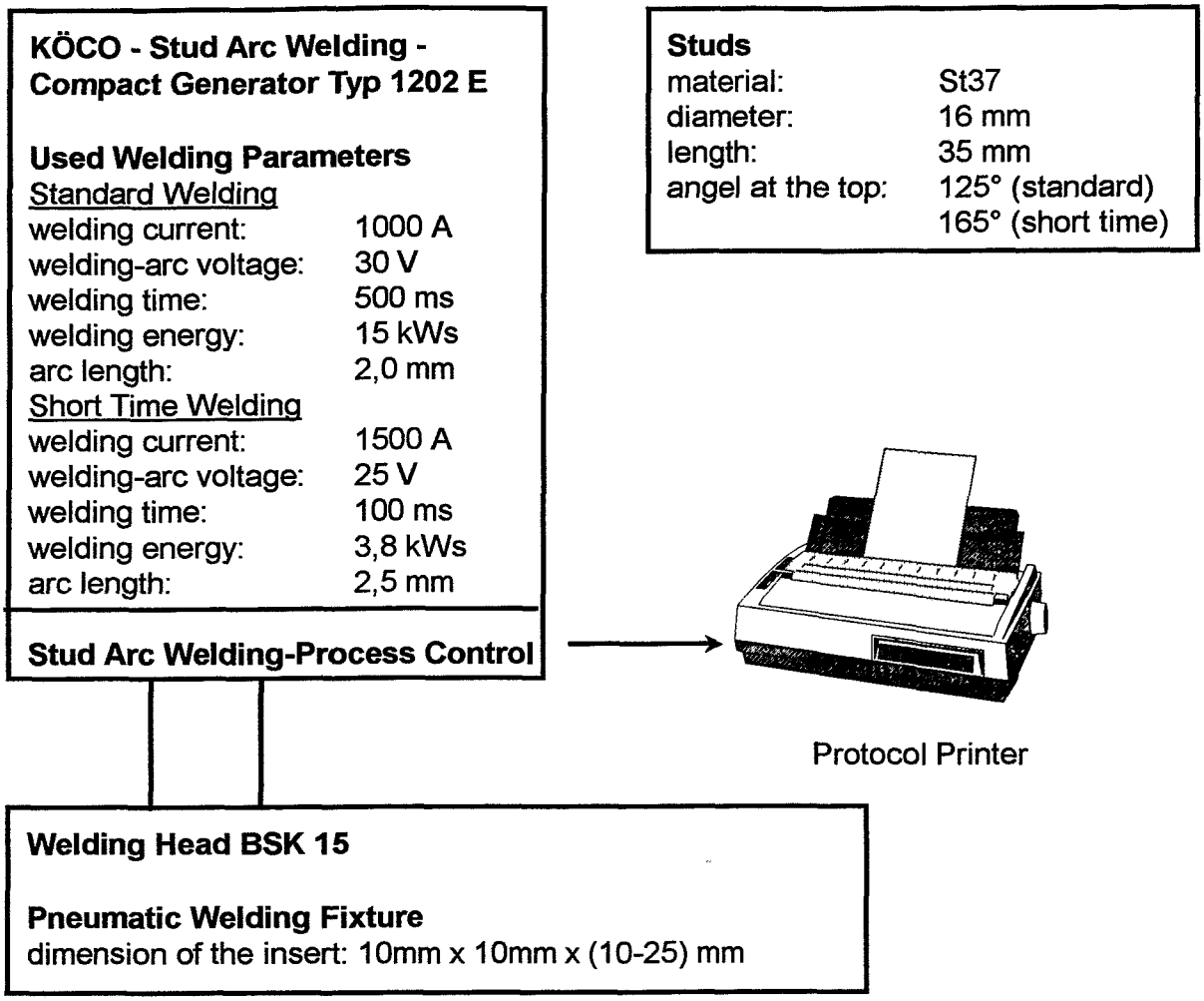

Fig. 1: Block diagram of the stud arc welding appliance

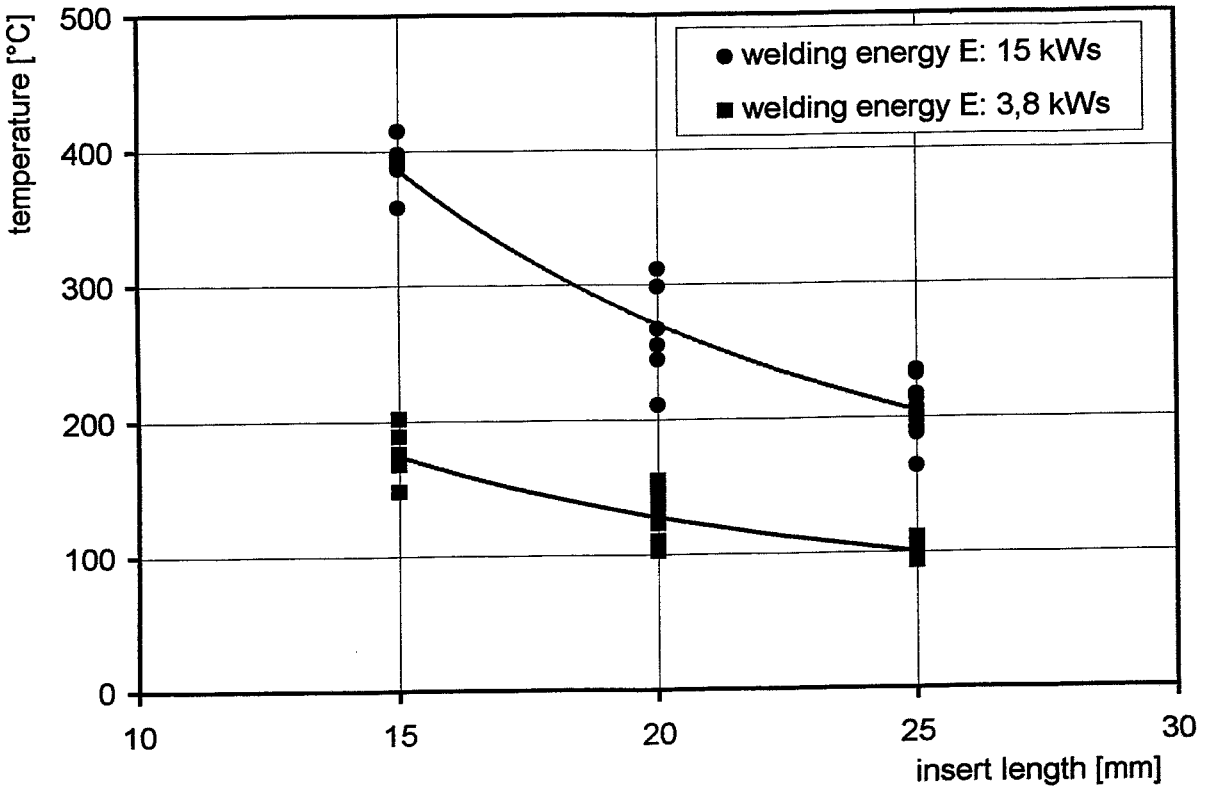

Fig. 2: Temperature maximum at the centre of the insert piece versus the insert length

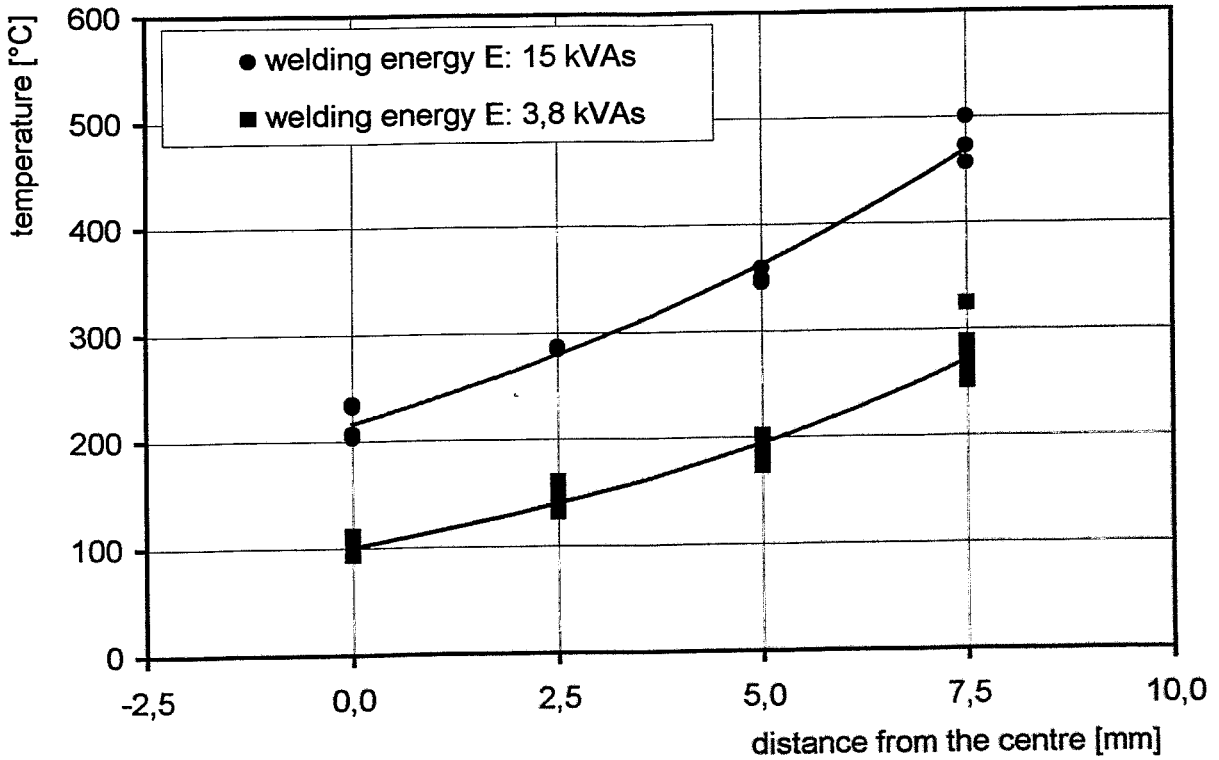

Fig. 3: Temperature maximum versus the distance from the centre of a 25 mm insert piece

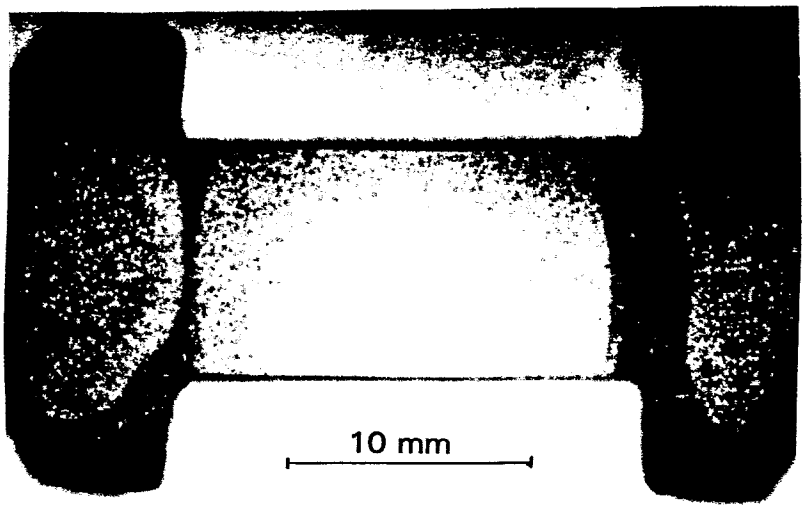

Fig. 4:
macrograph of the welding joints and the insert piece
- standard welding engineering (500 ms, 15k Ws)
- insert piece: 10 CrMo9 10
- studs: St37

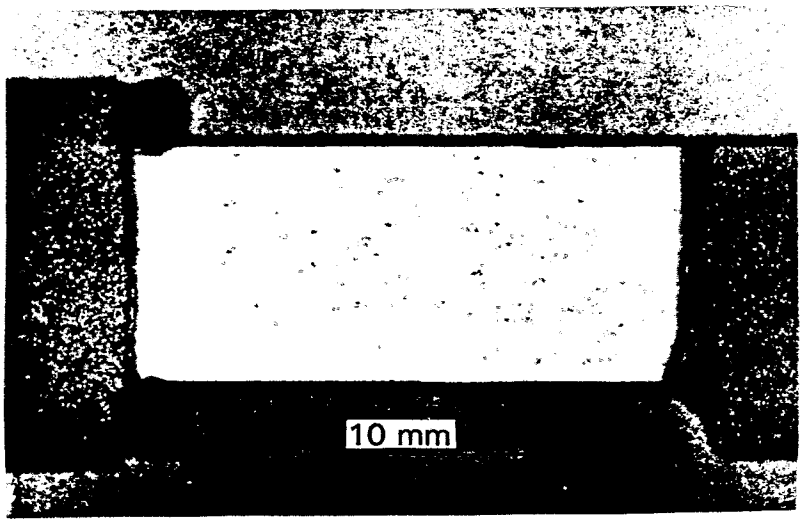

Fig. 5a:
macrograph of the welding joints and the insert piece
- short time welding engineering (100 ms, 3.8 kWs)
- insert piece: 10 CrMo 9 10
- studs: St37

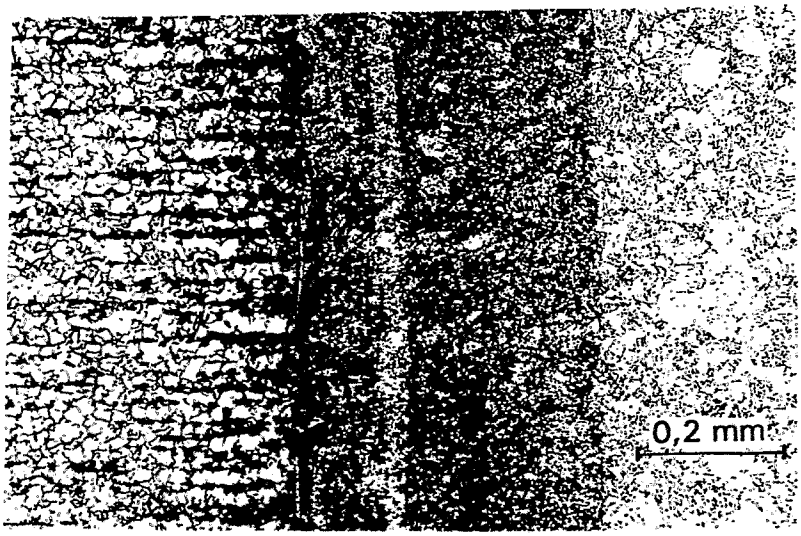

Fig. 5b:
microsection of one welding joint shown in Fig. 5a

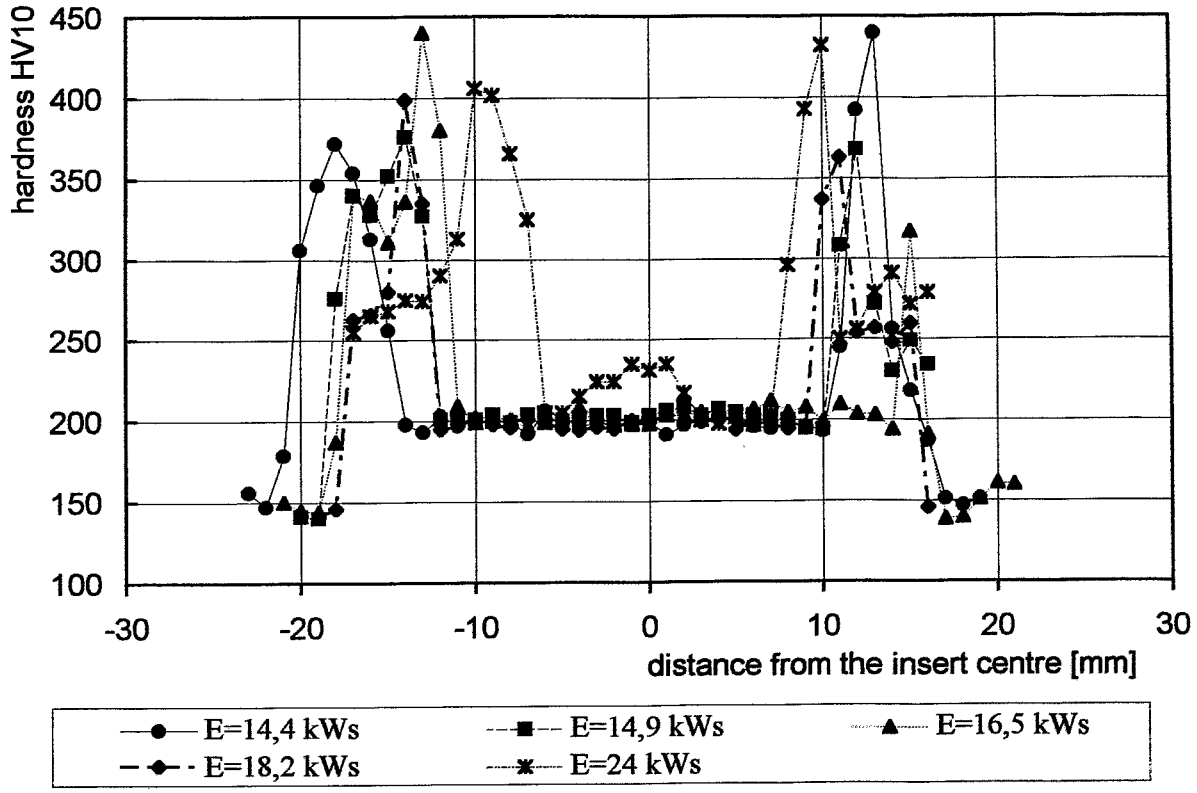

Fig 6: Hardness HV10 versus the distance from the centre of 25 mm insert pieces for different welding energies (welding time >= 500 ms)

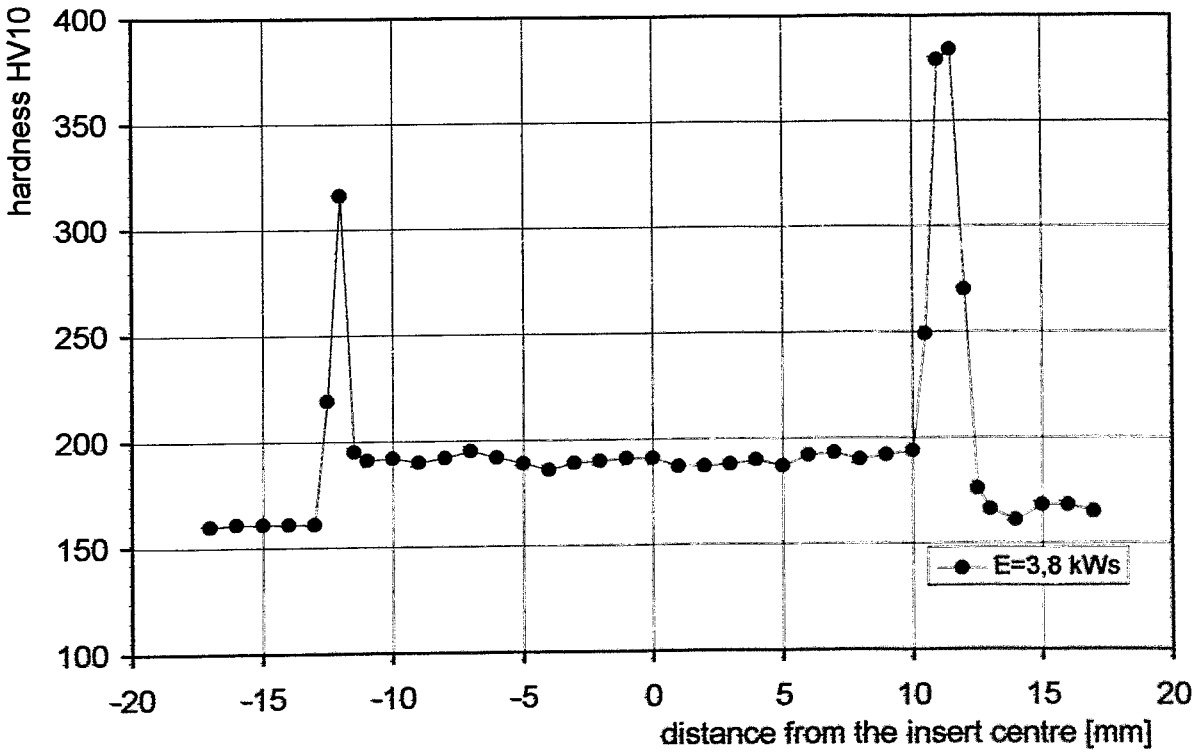

Fig. 7 Hardness HV10 versus the distance from the centre of a 25 mm insert piece for short time welding engineering

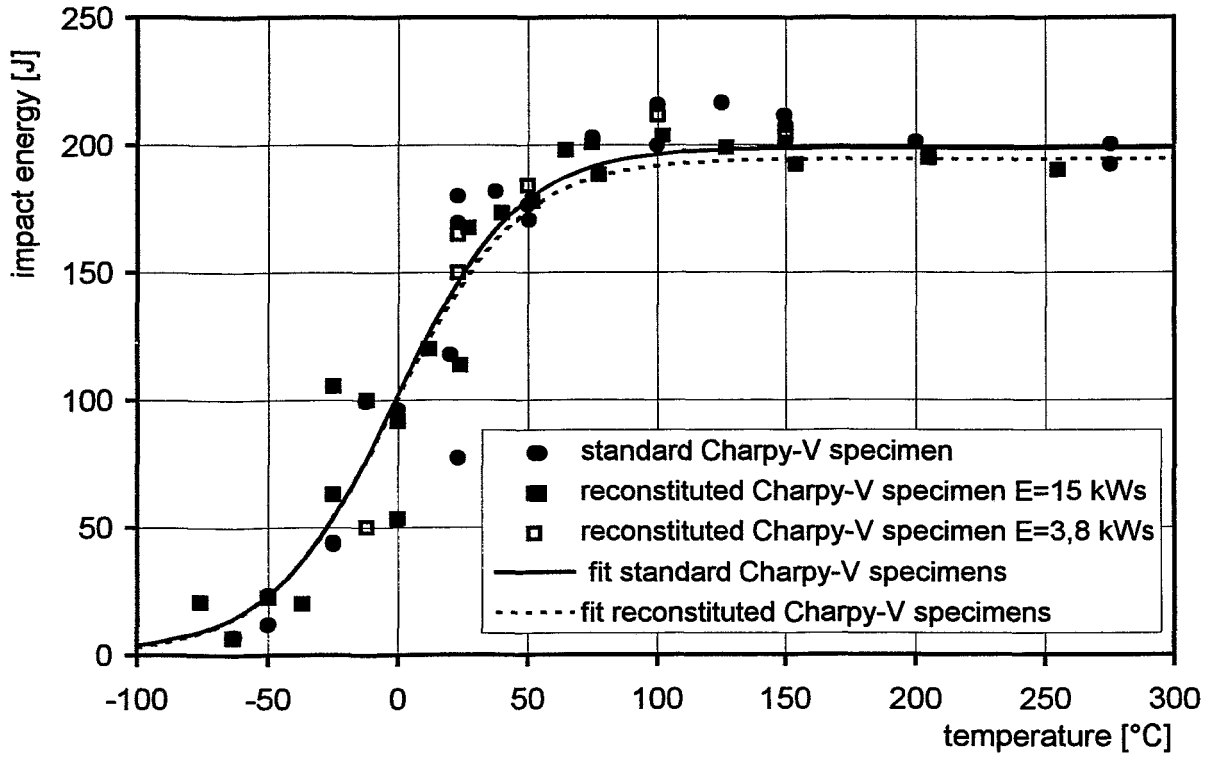

Fig. 8: Charpy-V impact energy transtion curves of standard Charpy-V and reconstituted specimens (RPV steel ASTM A533 B Cl. 1), orientation L-T

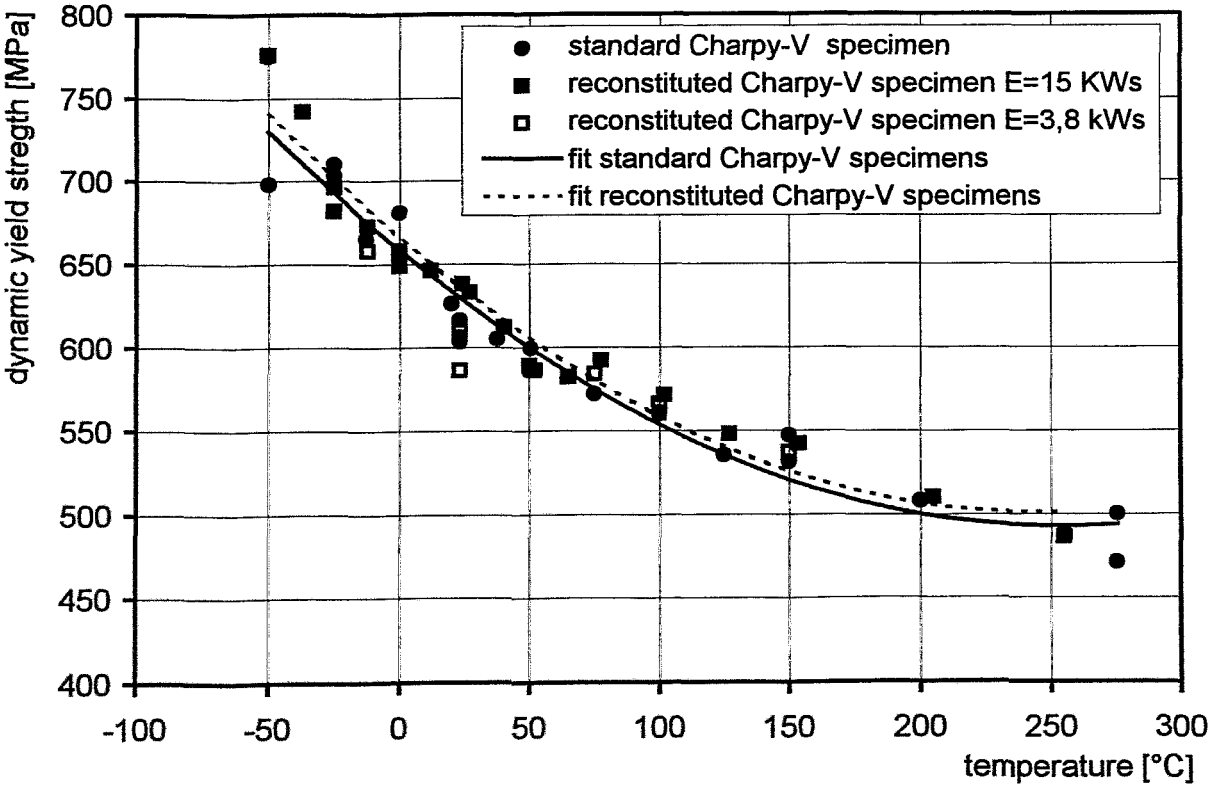

Fig. 9: Dynamic yield strength versus temperature of standard Charpy-V and reconstituted specimens (RPV steel ASTM A533 B Cl. 1), orientation L-T

applied reconstitution techniques was analysed by Charpy-V impact testing of standard and reconstituted Charpy-V specimens. The fitted transition curves of adsorbed energy, lateral extension and fracture appearance values from both types of specimen agree very well.

The production of SENB specimens for fracture mechanical testing by using the partial unloading compliance technique imposes higher demands on the quality of the welding joint. Welding defects and the material of the end blocks influence as well the calculated crack length. The next steps in view of the application of reconstituted Charpy size SENB specimens for fracture mechanical testing are to improve the quality of the welding joints and to investigate the influence of the end block material on the calculated crack length.

References

[1] E. Klausnitzer, "Detailed Investigations on Reconstituted Charpy Specimens with Insert Length down to 10 mm", Workshop on Experience with Testing Reconstituted Charpy Specimens, San Diego, CA, USA, 1991

[2] E van Walle, A. Fabry, T. van Ransbeeck, J.-L. Puzzolante, W. Vandermeulen, J. Van de Velde,E. Klausnitzer, and M. Gerscha, "The Reconstitution of Small Remnant Parts of Charpy-V Specimens", presented at SMIRT 11, PCS 2, Tapai, Taiwan, 1991

[3] M. Valo and R. Ahlstrand, "Application of Reconstitution Welding Technique for Studying Base Metal of Novovoronesh Unit-1 Trepan Sample", paper presented at ASTM International Symposium on Small Specimen Test Techniques and Their Application to Nuclear Reactor Vessel Thermal Annealing and Plant Life Extension, New Orleans, Louisiana, USA, 29-31 January 1992

[4] F. De Backer and F. Gutierrez-Solana, "Influence of the Configuration of Reconstituted Specimens on Fracture Toughness Characterisation of Pressure Vessel Steels", paper presented at the ECF11 Conference, Poitiers-Futuroscope, France, 3-6 September 1996, Proc. Ed. by J. Petit, Volume III, pp. 1965-1970

The project this report is based on was funded by the BMBF (Bundesministerium für Bildung , Wissenschaft, Forschung und Technologie) and registered with No. 1500919). The authors are responsible for the scientific content of the report.

CORRELATIONS BETWEEN THE CHARPY V-NOTCH IMPACT ENERGY AND FRACTURE MECHANICS PARAMETERS

J. Böhmert, U. Bergmann, H.-W. Viehrig

1. Introduction

The fracture toughness is the critical material parameter for the safety assessment of the reactor pressure vessel. Usually these values are only available for the unirradiated initial state. The measurement of the fracture toughness based on ASTM standard E399 requires specimen sizes that can hardly be put into practice for irradiated materials. Apart from the development of methods to measure valid fracture mechanics parameters by using small specimens, which can be irradiated, well-verified correlations between mechanic-technological properties and fracture mechanics parameters provide a useful approach to the safety assessment of aged reactor pressure vessels. As the ageing of the reactor pressure vessel material is monitored by a surveillance programme using Charpy V-notch impact specimens it is expedient to utilize the data obtained from these tests.

The paper evaluates correlations between fracture mechanics parameters, which are derived from the J-integral concept, and the upper shelf energy. For this a wide range of different reactor pressure vessel steels and reference materials was investigated.

2. Material

Specimens of the Russian reactor pressure vessel steels 15Kh2MFA, 15Kh2NMFA, 18Kh2MFA, 10KhNMAA (weld metal) and the ASTM- type steels A533B Class1, A508 Class3, weld metal 508 were investigated. As reference materials the low-carbon 1% cromium-1% molybdenum steel 10CrMo9.10 and the high strength steel StE460 were employed. Details about chemical composition, heat treatment, orientation, and depth position are given in [1].

3. Testing methods

Fracture mechanics parameters were measured by the single specimen compliance technique [1]. The tests were performed on a servohydraulic tester MTS 810/TESTSTAR in a temperature range of -150 to 200°C using 3-point bending specimens in Charpy geometry (10mm x 10mm x 55mm) and 0.5 CT specimens. Before testing, all specimens were fatigue precracked and 20% side-grooved. In order to determine the crack initiation toughness the stretch zone was manually marked on the electron microscopic photographs and measured with an image processing system.

Charpy impact bend tests were performed on an instrumented pendulum impact machine according to DIN 50115 with an initial energy of 300J and an initial velocity of 5.5 m/s.

4. Results

The enumerated methods provided crack resistance curves in dependence on the temperature and the material. Fig. 1 shows the crack resistance curves for 3 of the tested materials at room temperature. The so-called crack initiation toughness is a fracture mechanics parameter, which is regarded as geometry-independent. This parameter describes the resistance of the material against the start of a steadily growing crack. An acceptable approach is based on the J integral at given limits of crack growth. For instance, the ESIS recommendation EGF P1-92 suggests the J integral at 0.2mm of total crack growth ($J_{0.2}$). However, the derivation of a J integral at finished crack blunting (J_i) provides a parameter, which is physically founded, but it is more difficult to measure and needs higher efforts. The corresponding point on the crack resistance curve can be found from measurements of the critical stretch zone width.

In Fig. 2 the dependence of parameters J_i and $J_{0.2}$ on the temperature is shown for a heat of the Russian reactor pressure vessel steel 15Kh2MFA. J_C is the value at the initiation point for the case of instable crack growth.

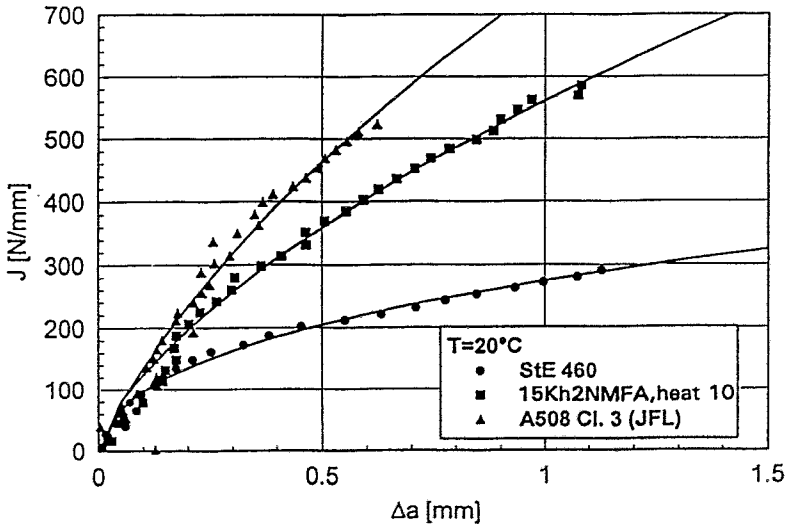

Fig. 1
Crack resistance curve of steel types StE460, 15Kh2MFA and A508 Cl. 3 at room temperature

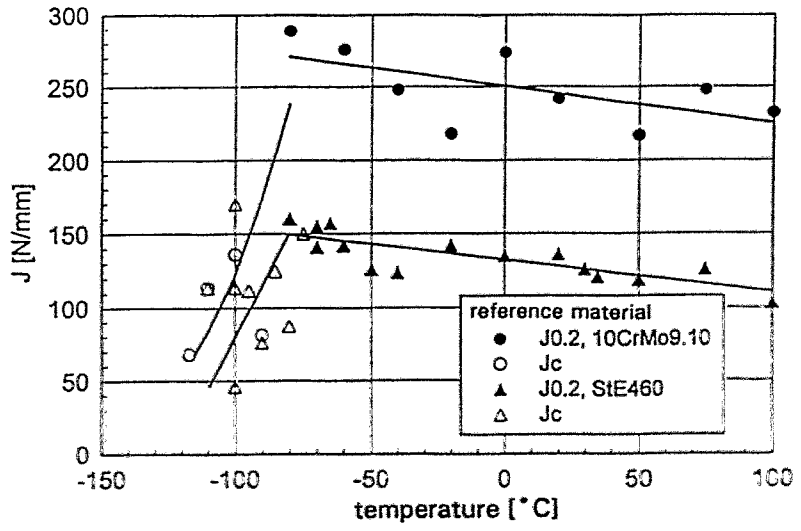

Fig. 2
J integral at crack initiation vers. temperature for 15Kh2MFA reactor pressure vessel steel

The tested materials cover a relatively wide range of toughness. The technical crack initiation toughness $J_{0.2}$ ranges between 134 N/mm and 242 N/mm within the upper shelf region and the impact energy varies from 85 J to 250 J. Thus, there is a usable data base for evaluating correlations.

There are different approaches to correlate the fracture mechanics parameters and the impact energy. They fall in two categories:

- 2dimensional correlations between impact energy and crack initiation toughness
- reconstruction of a crack resistance curve from the impact energy.

As the simplest case a linear relation between impact energy and toughness is assumed. Fig. 3 gives the regression line and the scatterband for this kind of correlation. In a first approximation the linear approach can be accepted both for $J_{0.2}$ and J_i. The correlation is, however, weak for J_i. Several steels show well-distinguished values of the impact energy in spite of identical crack initiation toughness. These steels possess differently steep crack resistance curves.

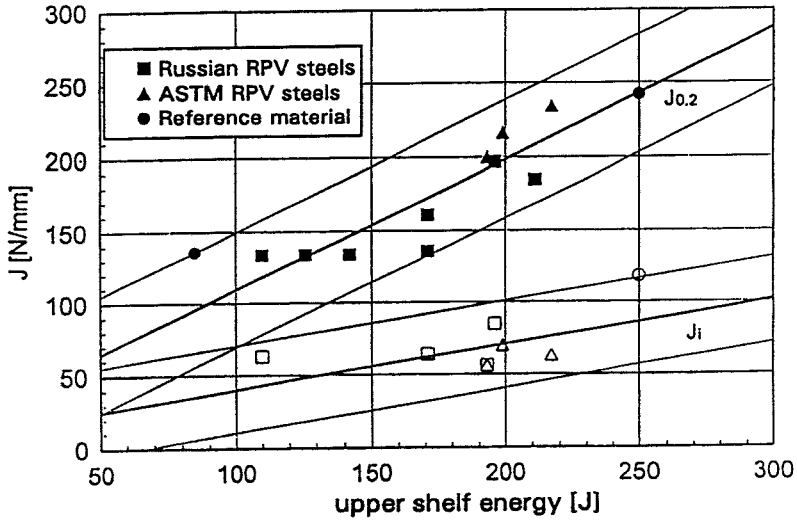

Fig. 3 Correlation between crack initiation toughness and Charpy V-notch impact energy

Based on extensive data sets, Roos /2/ recommends a 3rd order polynom regression model to improve the consideration of the minor influence of low impact energies as depicted in Fig. 3. With

$$J_{0.2} = 114.8 + 7.247 \circ 10^{-4} A_V^2 + 6.077 \circ 10^{-6} A_V^3 \quad (1)$$

and

$$J_i = 60.331 - 0.00176 \circ A_V^2 + 1.0211 \circ 10^{-5} A_V^3 \quad (2)$$

the correlation shown in Fig. 4 is obtained. A_V is the upper shelf energy. The correlations allow to estimate $J_{0.2}$ or J_i with a relative error (2σ-level) of $<20\%$ or $<35\%$, respectively. In general, a 2dimensional approximation for the correlation between crack initiation toughness and impact energy is not satisfying. Experimental results indicate that a stable crack growth of 1 mm consumes not more than about 40% of the Charpy V-notch impact energy. Therefore, an unambiguous correlation

between both parameters can only be expected when the energy consumption for crack initiation and crack growth is controlled by the same material parameter. Obviously, the presented results (Fig.1) do not confirm this assumption.

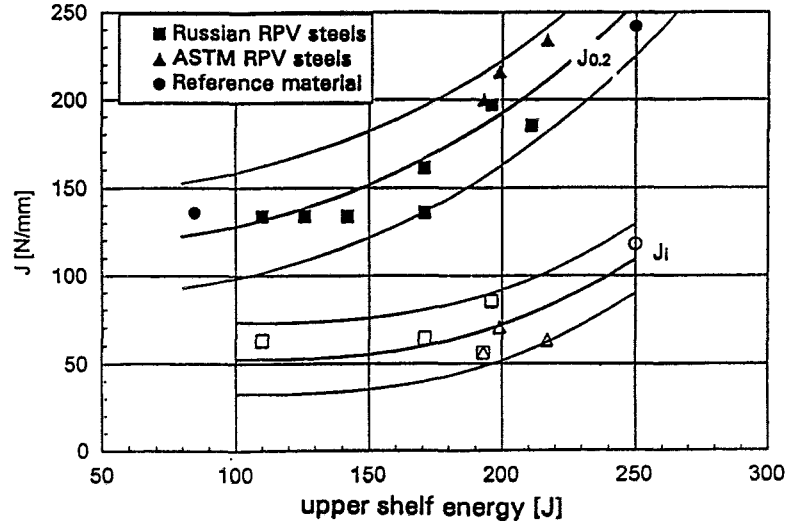

Fig. 4
Correlation between crack initiation toughness and Charpy V-notch impact energy using a nonlinear approach according to [2]

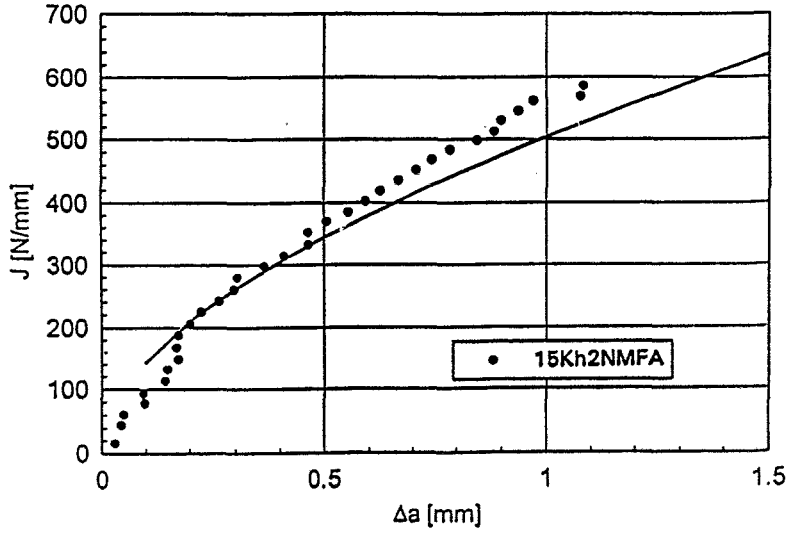

Fig. 5
Comparison of the measured crack resistance curve with the curve calculated according to Aurich[3] for 15Kh2MFA

Aurich [3] and Dougan [4] try another concept. As the impact energy comprises portions of energy from the total damage process during the smashing of the specimen, it is expected that the total crack resistance curve can be reproduced. In [3] an approximation is described to calculate the crack resistance curves of ISO-V 3-point bend specimens and CT specimens by means of the upper shelf energy. This approximation is based on a 3-parameter relation between the consumed energy U and the crack growth Δa. Using empirical results the relation is connected with the parameter "impact energy". With the formalism given in [3] the measured curves correspond to the calculated curves within the range of validity of this approximation of $\Delta a = 0.1 \ldots 1$ mm (see Fig.5).

Dougan [4] applies a 2-parameter approach

$$J = C \, \Delta a^n \qquad (3)$$

with the constants C and n empirically calculated from the impact energy and the flow stress. With Δa = 0.2mm or = 0.05mm (= median value of the stretch zone width) $J_{0.2}$ or J_i, respectively, can be calculated. The comparison with the experimentally measured data is presented in Fig. 6. The Dougan's approach provides a similar course of the correlation between crack initiation toughness and impact energy like the approach according to [2]. However, the experimental trends can only very roughly be described.

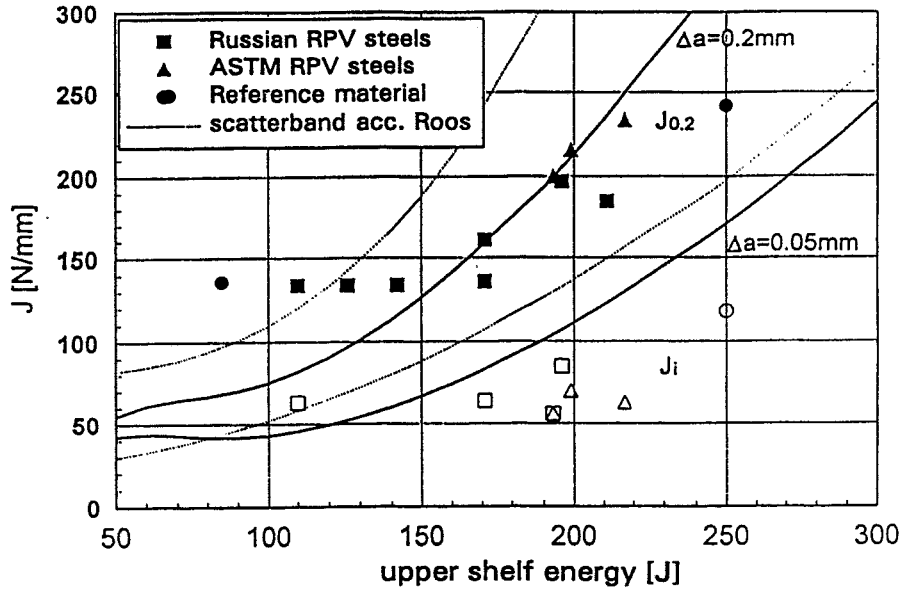

Fig. 6 Comparison of the crack initiation toughness with the J integral calculated from the Charpy V-notch impact energy according to Dougan [4]

5. Conclusion

Investigations of correlations between different material parameters are an acceptable way to complete the data base for safety assessment. Above all fracture mechanics parameter can only be obtained by extensive tests and high material consumption. For irradiated material such parameters are rarely obtainable. To solve the problem the crack initiation toughness or the crack resistance can be estimated by the Charpy V-notch impact energy. Some approaches of this kind were examined by using the available data material. The method of Aurich [3] determining crack resistance curves in the range of Δa = 0.1 to 1mm was especially successful. Simple 2dimensional correlations are only partially useful and in a small range of the parameters. However, the extrapolation of such correlations to material types or states for which they were not measured is always problematic. That is just the case if they are applied for irradiated reactor pressure vessel steel. Only an improved micromechanical understanding of the processes involved in crack initiation and growth might possibly generate qualified correlations and could enable extrapolations beyond the immediate data range in which the correlation was established. Moreover, a micromechanical understanding creates the possibility to use additional and more sophisticatedly determined material parameters for new correlative relations.

References

/1/ U.Bergmann, J.Böhmert, H.-W.Viehrig
"Bestimmung bruchmechanischer Kennwerte an Reaktordruckbehälterstählen mit der Einproben-Compliance-Methode und Korrelationen zur Kerbschlagarbeit"
FZR-81, März 1995

/2/ E. Roos
"Grundlagen und notwendige Voraussetzungen zur Anwendung der Rißwiderstandskurve in der Sicherheitsanalyse angerissener Bauteil"
Fortschrittsberichte VDI, Reihe 18 Nr. 122, VDI-Verlag, Düsseldorf, 1993

/3/ D. Aurich
"Analyse und Weiterentwicklung bruchmechanischer Versagenskonzepte"
Forschungsbericht 174, Bundesanstalt für Materialforschung und -prüfung, Berlin, 1990

/4/ J.R. Dougan
"Relationships between Charpy-V-Notch Impact Energy and Fracture Toughness"
NUREG/CR-2362, ORNL/TM-7921, 1982

SMALL ANGLE SCATTERING EXPERIMENTS TO CHARACTERIZE THE MICROSTRUCTURAL DAMAGE BY DUCTILE FAILURE PROCESS

J. Böhmert, M. Grosse

1. General concept

The commonly observed mechanism of ductile fracture progresses through the stages

- void nucleation
- void growth and
- void coalescence.

However, dense dislocation structures can be initiated before and so already predamage the material. For understanding the ductile fracture process and for predicting the material behaviour with micromechanical models appropriate microstructural quantities must be defined and experimentally measured in their dependence on the conditions of deformation.

As a rule, such parameters are measured by using the classical methods of metallography. Although these methods have successfully been applied to investige the fracture mechanism in many materials they are connected with some significant disadvantages: they are destructive, provide results only from an arbitrarily selected 2dimensional section, and do not give information on the early stages of the damage process. Therefore, it seems to be worth using advanced methods. Such a promising method could be small angle scattering. Small non-periodic structure defects scatter an incidenting electromagnetic wave with an intensity which depends on topological and chemical parameters of these structural defects. The method is volume-integrating. Besides, it can potentially function without destroying the specimen and in situ. Above all it is especially appropriate for investigating of defects in the size range between 1 and 100 nm and thus for detecting early damage stages. Finally, it allows to gain new kinds of parameters like fractal dimensions which could not be determined with the conventional methods. The method has already been used to investigate the creep damage in [1], the microstructural changes by fatigue loading [1,2], and e.g. the dislocation structure of deformed single crystals [3]. This paper describes first attempts to apply the method to inhomogeneous deformation states ahead of the tip of a bending-loaded crack or in the necking range of a tensile-loaded specimen.

2. Experimental

As small angle scattering devices are highly specialized equipment and normally do not cover a wide range of scattering vectors Q, several scattering installations with different resolution and working range for Q were utilized to certainly provide the wanted information. They comprised both small angle X-ray scattering and neutron scattering but conventional X-ray diffraction devices as well. Neutron interaction with matter is generally low. Thus, a large probe volume can be investigated. Local differences within the microstructure, however, are not detectable. For that strongly focused X-ray beams with high intensity are

appropriate like the MICROFOCUS beamline at the European Synchrotron Radiation Facility. An important parameter of the experimental equipment is the measuring range of the scattering vector Q because it is approximately proportional to the reciprocal length of scattering structure defects. Typically Q is in the interval between $10^{-4}...10^{-3}$/nm for double-crystal diffractometers and $10^{-2}...10^{-0}$/nm for the Synchrotron facilities. That allows to analyse microstructural defects of about 1 μm when using double-crystal diffractometers and sizes between 1 and 100 nm with dedicated small angle scattering facilities. A summary of the used experimental installations is given in Tab.1.

Table 1 Summary of experiment data

Test-No.	Beam/Source	Device	Objective	Experimental Condition	Material
1	X-ray synchrotron HASYLAB	JUSIFA	Damage structure in necking zone after tensile loading	Q-range: $10^{-2}...10^{-0}$/nm Beam size: 0,5 mm x 1 mm λ = 0.155 nm	AlMgSi, aged
2a	Neutron source BENSC	SV 12 double-crystal diffractometer	Damage structure in necking zone after tensile loading	Q-range: $10^{-4}...3 \cdot 10^{-2}$/nm Beam size: 3 mm x 6 mm λ = 0.48 nm	AlMgSi, aged
2b				Q-range: $10^{-4}...3 \cdot 10^{-2}$/nm Beam size: 3 mm x 4 mm, 20 mm x 12 mm λ = 0.48 nm	Al
3	X-ray tube	double-crystal diffractometer	Damage structure in necking zone after tensile loading	Q-range: $10^{-4}...10^{-3}$/nm Beam size: 1 mm x 2 mm λ = 0.154 nm	like test 1
4	X-ray synchrotron ESRF	MICROFOCUS ID13	Micro-beam-scanning ahead of a crack tip after bending loading	Q-range: $10^{-2}...10^{-0}$/nm Beam size: 15 μm x 150 μm Scan step: 200 μm 50 μm λ = 0.095 nm	AlMgSi, over-aged Al
5	X-ray synchrotron ESRF	MICROFOCUS ID13 + Bragg-Fresnell-Lense	Micro-beam-scanning ahead of a crack tip after bending loading	Q-range: $2 \cdot 10^{-2}...8 \cdot 10^{-1}$/nm Beam size: 2 μm x 2 μm Scan step: 5 μm λ = 0.125 nm	AlMg3, Ti

Tensile specimens or precracked bending specimens in Charpy-V geometry were machined from commercial Al 99.5, Al alloys or Titan and loaded in a tensile or 3 point bend test. X-ray scattering samples were cut parallel to the tensile direction or to the bending direction, respectively. The samples were thinned by mechanical grinding and chemical etching to a thickness of about 220 μm. For neutron scattering several tensile specimens were assembled to a sample of 50 mm x 20 mm x 9 mm.

3. Results

Except the experiments with the X-ray double-crystal diffractometer, there are special small angle scattering features within the range of high deformation, i.e. in the necking zone after tensile testing or near the crack tip after bending. Typical 2 dimensional X-ray scattering patterns near and far the crack tip are shown in Fig. 1. Outside the plastic zone strong streaks often appear. These streaks could be caused by the diffraction of grain boundaries. Inside the plastic zone only

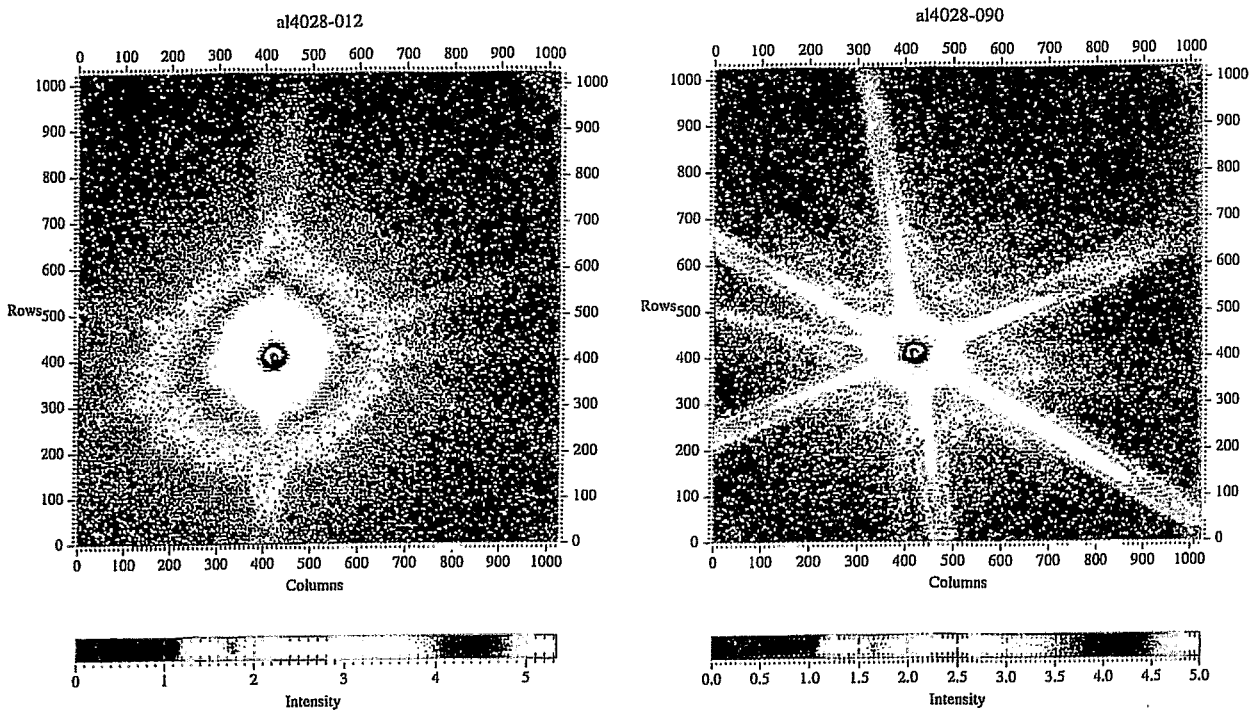

Fig. 1 Small angle X-ray scattering pattern near (left) and far (right) the crack tip
Al 99.5, bent, 150 μm x 15 μm beam size, X-ray energy: 12 keV

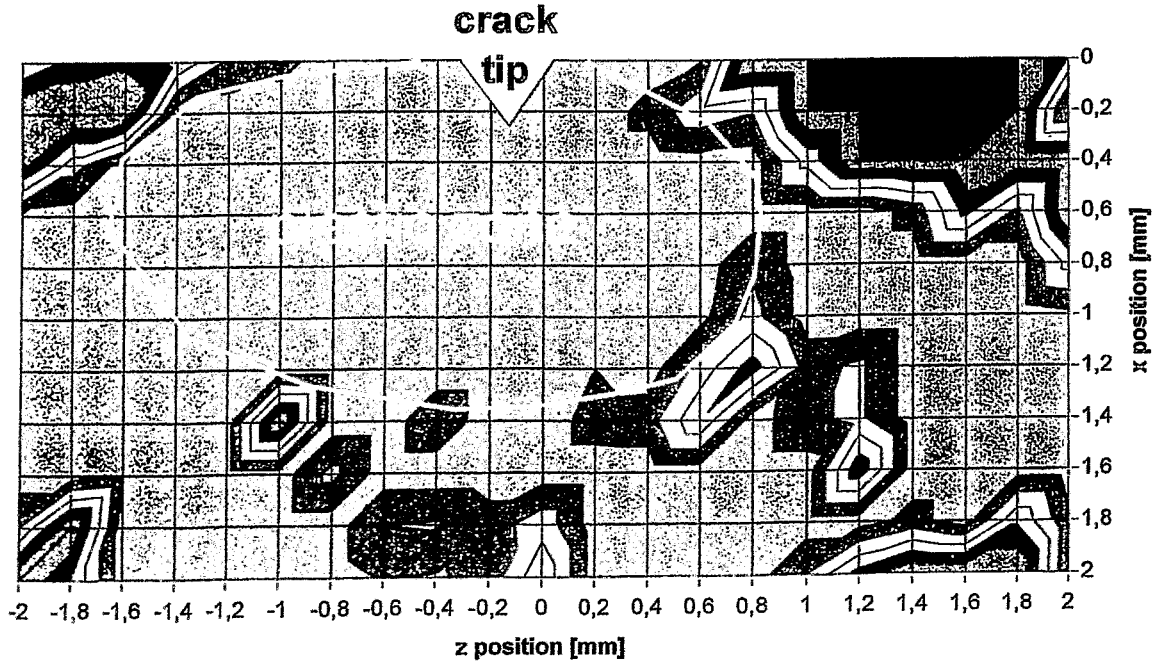

Fig. 2 2d-distribution of the total length of the scattering streaks
Al 99.5, bent

residues of streaks can be seen as the grain structure is at least partially destroyed due to the strong deformation. In some cases, one streak, which is very intensive and always oriented in the same direction, can be still observed near the crack tip. The connection between this streak phenomenon and the plastic deformation can be recognized from Fig. 2 where for every measuring point the sum of the lengths of all streaks of the 2-dimensional scattering patterns (related to an arbitrarily selected intensity) is mapped. The local distribution of the total length of the streaks approximately corresponds to the plastic zone.
The change of the total scattering intensity I (without consideration of the intensity of streaks) for different positions along a line in crack growth direction can be seen in Fig. 3. The scattering intensity decreases with increasing distance from the crack tip. Both the Guinier plot (ln I versus Q^2)and the Porod plot (log I versus log Q) do not confirm the assumption that the defects are geometrically defined particles (voids). The well-defined linear course in log-log-plot hints at a power law behaviour. Hierarchical substructures with fractal dimensions or dislocation arrangements scatter according to a power law. The exponent is between -2.7 and -3.5 for pure Al and increases with the distance from the crack tip. For AlMgSi the exponent is -3 or higher and does not show a dependence on the distance. For dislocation pile-ups an exponent of approximately -3 is expected [3]. The plastic deformation of the AlMgSi specimen is not so strong as the deformation of the Al specimen. Summarizingly one can conclude that the scattering effects are rather caused by dislocation structures than by voids or micropores.

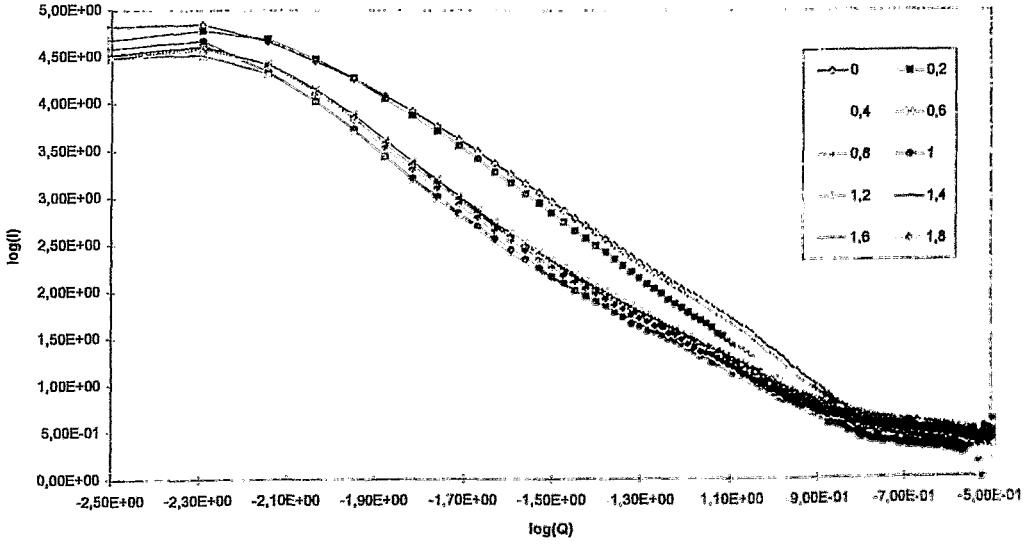

Fig. 3
Small angle X-ray scattering intensity versus scattering vector Q for different distances from the crack tip (values correspond to distance in mm)
Al 99.5, bent

As regards the fine distribution close to the crack tip similar results can be obtained in experiments with the 2 μm beam at the ESRF/MICROFOCUS-Beamline.

Fig. 4 presents results of the neutron small angle scattering experiment. The locations a, b and c are within the necking zone, b is the location with the largest reduction of the cross section. The curves d and e show the scattering intensity outside of the necking zone. In every case, in the Q-range between 10^{-4} and 10^{-3} nm^{-1}, the slopes of the curves log I versus lg Q exhibit a bimodal linear

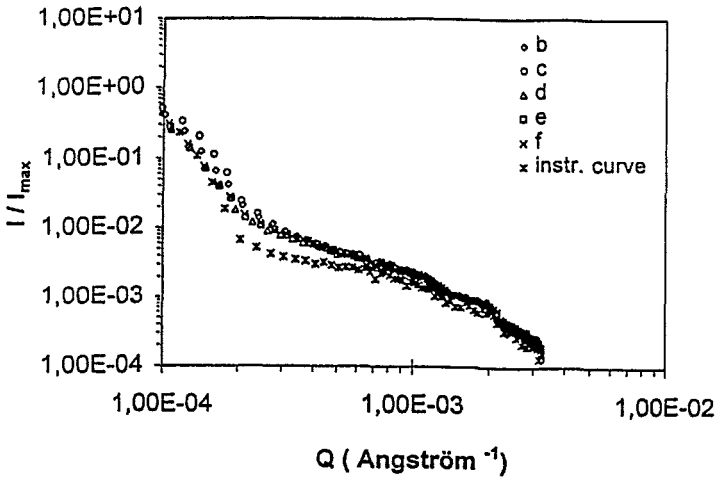

Fig. 4 Small angle neutron scattering intensity versus scattering vector Q for different positions in the necking zone
Al 99.5, tensile-loaded

dependency. Small differences between scattering intensities of the various locations can only be found for smaller values of Q. This suggests that the scattering effects might be preferentially caused by precipitates. A deformation-induced scattering effect occurs for scattering defects with a radius of gyration of approximately 500...650 nm. That could be the expected voids. The evidence of void-induced small angle neutron scattering is not really convincing. There are two possible reasons for it. First, the number of small voids of dimensions between 100...1000 nm is very low. Secondly, the experiment averages over a too large volume to be able to recognize differences in the void formation.

4. Conclusion

Small angle X-ray and neutron scattering methods offer the capability to investigate the microstructural changes through strong deformation. The scattering pattern results from the superposition of different effects such as precipitates, grain boundaries, dislocations, and voids. The interpretation of experimental findings turns out to be difficult. For the investigated alloy systems the assumption of a ductile fracture mechanism based on competitive growth of very small microvoids could not be confirmed. Instead of that, a damage mechanism related to the formation of dislocation structures is more evident. The experiments will be continued with simplier structured material and by using additional metallographic methods.

References

[1] H. Walter, P. Pizzi: Small Angle Neutron Scattering for Nondestructive Testing, Chapter 10 in: Research Techniques in Nondestructive Testing 4 (1980), p. 3411

[2] F. Häußler, J. Schaber et al.: SANS Studies as a Contribution to Structural Characterization of Industrial Materials, in BENSC Experimental Reports 1995

[3] A.K. Seeger, J. Appl. Phys. 30 (1959) 30, 629

CALCULATION OF THE NEUTRON YIELD IN A MIRROR BASED PLASMA NEUTRON SOURCE

H. Kumpf, K. Noack

1. Introduction

The contents of the present contribution is exposed in more detail in the FZR-report [1]. It should be viewed as a part of the efforts made commonly by the Budker Institute Novosibirsk and FZR for examining the feasibility of an intense 14-MeV neutron source based on the Novosibirsk concept of an open trap. Recently the whole subject has been presented in a broader context in [2].

The special topic of the paper is the calculation of the 14 MeV neutron yield and its spatial distribution in such a neutron source admitting only inevitable approximations. This is done by a direct simulation of the orbits of the tritium and deuterium ions originating from the injected neutral t and d beams in the magnetic field of the device. The method adopted for the solution of the equations of motion is the well known guiding centre approximation (g.c.a.), adapted to cylinder coordinates and axially symmetric fields. Of course, one could instead integrate numerically the particles equations of motion with the Lorentz force as the right hand side, although in this case one has to take special care in order to conserve the necessary accuracy even after some 10^5 Larmor revolutions performed by the ion during its life. But the g.c.a. seems to offer advantages in terms of computing time. At the same time the accuracy of the g.c.a. approach adopted here is amply sufficient, as has been demonstrated by comparison with results from the direct integration.

The interaction of the fast ions with the plasma is taken into account by means of the relaxation times τ_b and τ_d for stopping and deflection in a multicomponent plasma including the population of the fast ions themselves.

The only place where random numbers are used is in the description of small angle scattering. But for as long as Coulomb scattering does not play a decisive role, the statistical error in the final results due to this randomness is insignificant (< 5% in the example considered).

2. Remark on the Applied Method

The essence of the guiding centre approximation consists in a transformation from the ion space and velocity coordinates to guiding centre (g.c.) coordinates (those of the 'centre of the Larmor circle'). In contrast to the particle coordinates, describing the fast Larmor rotation, the g.c. coordinates should be smooth functions of time. Therefore the equations of motion expressed in these coordinates are *required* not to contain any trigonometric functions.

There exist several formulations of guiding centre approximations in the literature casting the above verbal requirements into mathematical formulae and differing in certain details. The version of ref.[3] was adopted as the most consistent one. Unfortunately the

straightforward application of the general expressions from [3] (as well as from other sources) to cylinder coordinates leads to essential singularities in the emerging equations. Nevertheless for this special case a transformation could be designed resulting in extremely simple equations of motion. For details it is referred to [1]. There are even two conserved variables among the set of g.c. coordinates: the total energy and a generalized magnetic moment. Nevertheless the conservation of the magnetic moment of the Larmor rotation is *not* presupposed.

The description of the motion in the magnetic field had to be supplemented by a method of accounting for slowing down and small angle scattering in the surrounding plasma. To this end the notion of relaxation times τ_b for slowing down and τ_d for deflection was used. The dependence of τ_b and τ_d on local plasma parameters like electron and ion temperatures, density and plasma composition is stated e.g. by Trubnikov [4]. Expressions relating the changes in total energy and generalized magnetic moment to the two relaxation times could be derived.

Furthermore, if the power of the injected beams of deuterons and tritons approaches the level necessary for an intense source of 14 MeV neutrons, the self-interaction among the population of fast ions cannot be neglected any longer. At present the following four branches of feedback are included:

1. The local densities and energy distributions of previously injected tritons and deuterons are used to calculate relaxation times. Stopping is increased exclusively by the rise in electron density caused by filling in fast ions. Deflection is influenced by the fast ion populations themselves.

2. Inside the plasma the magnetic field induced by the external coils is modified by the magnetic plasma pressure.

3. An ambipolar electric potential is evaluated from the condition of electric neutrality.

4. Last not least the densities of deuterons and tritons in the trap are used for calculating the proper distribution of the injection points of D and T ions originating from the impinging beams of neutrals. Cross-sections σ_{cx} and σ_{ion} for charge exchange and ionization respectively are taken from [6].

The feedback branches enumerated above are included by iterations. The number of iterations necessary for convergence strongly depends on the neutral beam power and the injection angle (see below).

After establishing convergence from the resulting d and t densities the neutron yield is calculated using a semi-empiric formula from [5].

3. An example

As an example a version has been selected corresponding to a predesign of a plasma neutron source based on the gas dynamic trap proposed by the Efremov Institute St. Petersburg [7]. It has been treated by other methods in the Budker Institute Novosibirsk

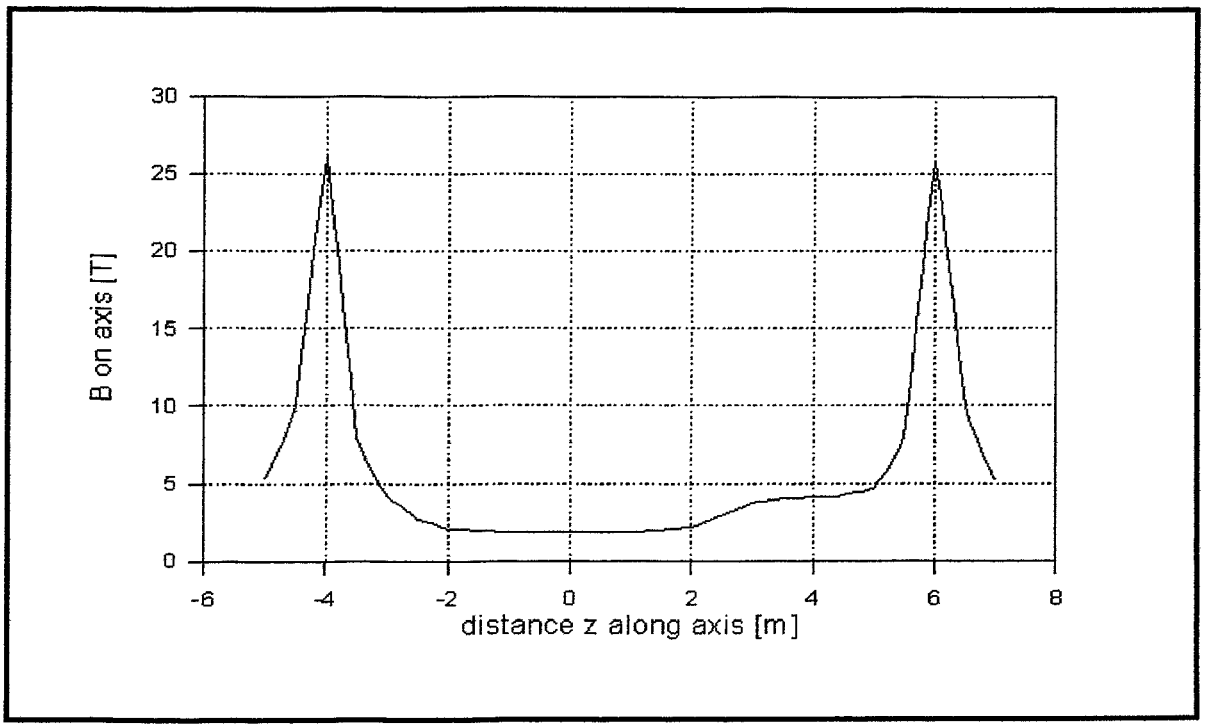

Fig.1: Dependence of the magnetic field on axis in Tesla on the distance z.

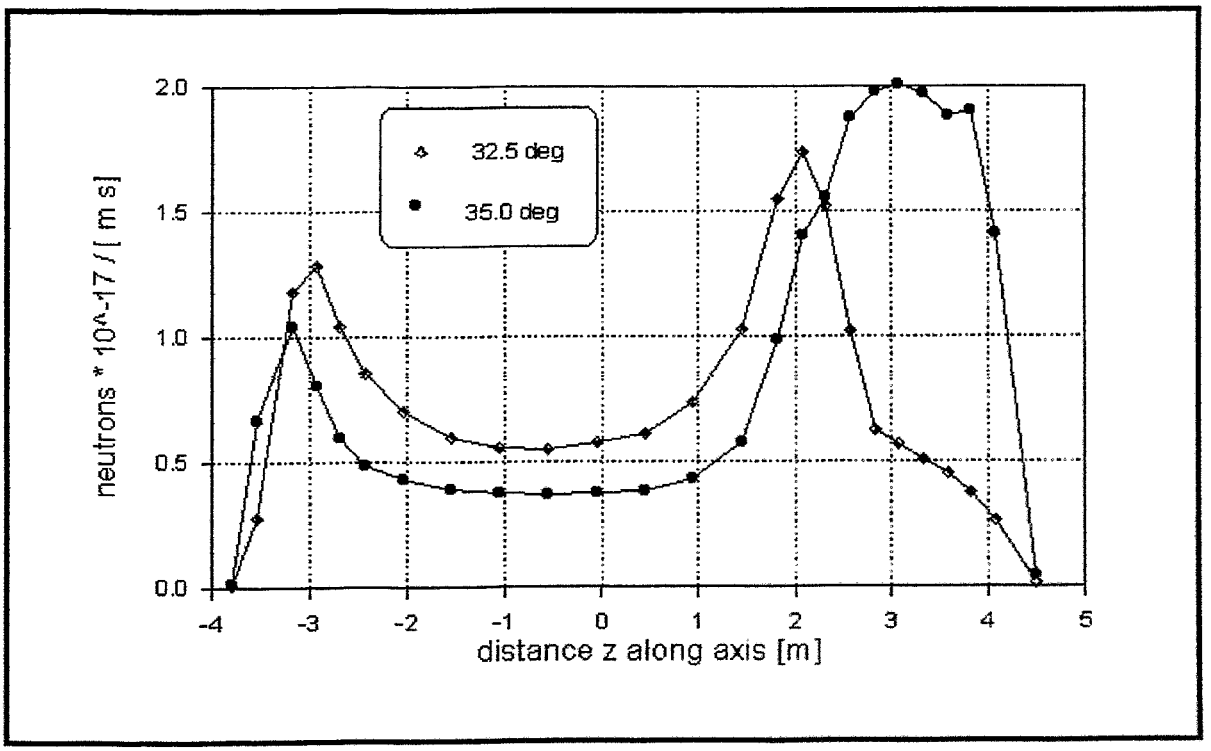

Fig.2: Distribution of neutron source strength [n $s^{-1}m^{-1}$] along the axis of the trap.
Input parameters indicated in the text, but injection angle reduced to 35° resp. 32,5°.

[9]. Its main characteristic feature is the injection of both reacting species deuterons as well as tritons in the form of atomic beams. The intention here is to keep the injection energy so low as to allow the use of positive ion sources with their much better energy efficiency in comparison to that of negative ion sources [8] .

Here the input for the calculation.
The magnetic field on the axis of the configuration is shown in the Fig. 1 .

The injection angle amounts to $\theta = 40°$, for both injected deuterium and tritium beams.

In the right hand part the dependence of the magnetic field in Fig. 1 exhibits a characteristic threshold in front of the mirror, designed for raising the ion densities and therefore the neutron yield in this region. This is achieved by choosing the ratio of the magnetic field B_{th} at the plateau to its value B_0 at the injection point in the centre according to:

$$\sin\theta = \sqrt{\frac{B_0}{B_{th}}}$$

In this case the turning points at least of the freshly injected ions are located in the centre of the hump.

The energies of the beams are W_d = 80 keV and W_t = 94 keV for deuterium and tritium respectively, the corresponding trapped powers P_d = 14 MW and P_t = 12 MW.

The plasma radius is defined by means of a limiter with r_0 = 0.085 m radius, placed at z = 0.

The temperatures for ions and electrons of the thermal component of the target plasma are supposed to be T_i = 6 keV and T_e = 1.1 keV respectively, its density $n_0 = 2.3\ 10^{19}\ m^{-3}$.

If one tries to solve the original task one obtains erratic behaviour of the result, i.e. no convergence. Only after considerable reduction of the input power level of the d and t neutral beams convergence can be established. This demonstrates the essentially nonlinear character of the problem.

An apparent solution is to lower the angle of neutral injection (or if this should be linked with unsurmountable technical difficulties to raise the height of the threshold in the magnetic field). Fig. 2 shows the neutron yield distribution for injection angles 35° resp. 32.5° instead of the designed value of 40°. In the first case the angle appears still too high, in the second one near optimal.

Generally it may be stated, that for the most favourable case cited in the last figure the total neutron yield in the region extended 2m around the peak amounts to about $3.8\ 10^{17}$ neutrons/s or 0.9 MW, corresponding to an efficiency of energy conversion from neutral

beam power to neutron power in the peak of about 3.8 %. The shape of the yield distribution along the axis of the device too is rather favourable, the height of the peak exceeding the value in the center of the trap by a factor of 5.4 and the height of the smaller peak at the left mirror still by a factor of about 3. Thus, the idea of concentrating the neutron output by means of a hump in the magnetic field in front of one of the mirrors has been confirmed. Finally, the observed convergence of the iterations modelling the self-interaction of the plasma (at least at sufficiently low angles of injection!) strengthens confidence in the stability of the version with simultaneous injection of deuterons and tritons.

References

[1] H. Kumpf and K. Noack
"Application of the Guiding Centre Approximation to the Transport of Injected Fast Ions in a Mirror Based Plasma Neutron Source"
Report FZR 121,1996

[2] Int. Conf. "Open Plasma Confinement Systems for Fusion", Novosibirsk, June 1993
Ed. A. A. Kabantsev, World Scientific 1994

[3] B. Weyssow and R. Balescu
J. Plasma Physics 35 (1986) 449-471

[4] B. A. Trubnikov in " Problems of Plasma Theory"
ed. M. A. Leontovich, Vol. 1, Moscow, 1963, p.98 (russ.)

[5] B. N. Kozlov
Atomnaya energiya 12 (1962) 238 (russ.)

[6] R. K. Janev and J. J. Smith
" Atomic and Plasma - Material Interaction Data for Fusion"
Vol.4 (Supplement to Nuclear Fusion), IAEA 1993

[7] V. G. Krasnoperov, V. N. Odinzov, V. N. Skripunov and V. V. Filatov
" Engineering Problems in Designing a Neutron Source Based on a Gas Dynamic Trap Concept"
Plasma Devices and Operations Vol. 3, No 2, 1993

[8] V. V. Mirnov, B. P. Nagorny and D. D. Ryutov
Preprint Budker Inst. Nucl. Phys. Nr. 84-40, Novosibirsk 1984

[9] Yu. Tsidulko
private communication

PARALLEL PARTICLE TRANSPORT SIMULATIONS ON A PowerXplorer™

K. Noack, G. Otto

1. Introduction

Since several years parallel computing has become more and more important as well in fundamental as in applied sciences. This development is pushed by disciplines which demand the application of numerical methods requesting especially high computing perfomances. Monte Carlo transport simulations are of that type. In the department *Particle and Radiation Transport* this method is mainly used for studying neutron/gamma fields in and around fission reactors, high-energetic ion beams used for tumor therapy and ion and neutral particle fields in a mirror based 14 MeV plasma neutron source. It is well-known that the Monte Carlo method does not only demand high computing power but is also well-suited for parallel computing. This situation suggested the decision to do the first step into parallel computing just in the field of Monte Carlo transport simulations.

2. The PowerXplorer™ system

The PowerXplorer™ system is a two-component system consisting of a SUN SPARC-station 5 as the host computer and an 8-nodes computing network. Figure 1 shows the structure of the system. The nodes are arranged in a two-dimensional array. Two links between host and network allow the partitioning into two 4-nodes clusters. These clusters may be independently used by different users. The SUN workstation is controlled by the operating system SOLARIS 2.3. Maintaining compatibility to SOLARIS the Xplorer runs the parallel operating environment PARIX™ - presently the version 1.3.1 - which is a parallel extension to UNIX developed by Parsytec Inc. According to Flynn's classification PARIX realizes the Single Program Multiple Data (SPMD) programming model [1], i. e. each node participating in the calculation executes the same program. Additionally to PARIX the user has the possibility to run parallel applications designed for the PVM message passing system [2]. For that purpose, the powerPVM™ package is available. This package comprises the mostly used PVM routines which have been especially adopted to the Xplorer network. In this context it is worth to note that PARIX runs the same application much more efficiently than PVM [3] what is mainly the consequence of the specific design of PARIX for controlling a homogeneous system of nodes. One node of the PowerXplorer consists of one numerical RISC processor PowerPC™-601 and one transputer T805™ for communication. The PowerPC-601 chip is a result of a collaboration between Apple, IBM

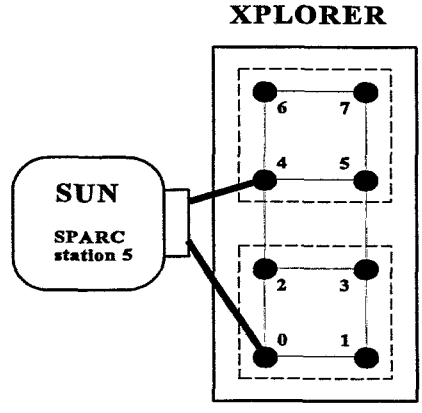

Fig. 1: Parallel computer "parsy"

und Motorola. It is running at 80 MHz, has 32 kByte internal cache and 32 Mbyte of memory. The processor achievs the following performances: 77 SPECint92, 93 SPECfp92, 80 MFLOPS peak (64-bit IEEE), 160 MFLOPS peak (32-bit IEEE). The transputer adds 30 MIPS and 8.8 Mbyte/s intelligent communication bandwidth.

Inside the LAN of the *Research Centre Rossendorf* (RCR) the described parallel computing system is available under the name *"parsy"*. Presently, only the use of a Motorola-FORTRAN 77 compiler is licensed.

3. Parallelization of the FIT code

One of the most computer time consuming applications is the simulation of the ion transport inside the "Gasdynamic Trap" (GDT) experimental facility at the *Budker Institute Novosibirsk* (BIN). This research work is part of the collaboration between RCR and BIN that is directed to the project of a highly intense, 14 MeV plasma neutron source for material research. The subject of the common research work is the development of an Integrated Transport Code System the modules of which are presently under development and validation by comparing with experimental results from the GDT [4]. As modul for simulating the fast ion transport for given target plasma and neutral gas fields the code FIT has been developed. Its mathematical models are basing on the space-dependent Fokker-Planck equation.

Originally the code has been designed for an optimized use of the vector feature of the RCR's computing server CONVEX C3820. In analogy to neutron transport Monte Carlo codes applicable for criticality calculations, e. g. MORSE [5], the ion transport algorithm in FIT is batch-structured, i. e. one simulation cycle comprises the tracking of a user defined multitude of test particles starting from their births up to their deaths. The whole calculation consists of a sequence of such particle batches. This structuring of the transport simulation together with an appropriate allocation of the necessary particle data allow the favourable use of vector routines from a special library and the programming of DO-loops which can be efficiently vectorized by the compiler.

When going to parallelize the code the main question was about the granularity, i. e. what should be the subtask that has to be accomplished by one node. Several of the parallelized particle transport codes use the classical Master-Worker scheme [6]. There, one of the nodes is identified as the master and all the others as workers. The role of the master consists in generating the particle births, distributing them to the workers and collecting the tallies from the workers when they finished the simulation of their particle history. In this scheme the granularity is determined by a test particle history. In the case of FIT it was decided to modify this classical scheme in two regards: on the one hand, the granularity was increased to the maximum extend, namely up to a complete sequence of batches, and on the other hand, after performing some initialization work the master is degraded to a usual worker which also has to simulate a sequence of batches. In this way, the communication is minimized and each of the nodes is maximally employed for numerical work. Figure 2 presents the scheme in a mnemonic description. Step 1 is a call of a PARIX routine which assigns an identification number *id* to the calling node. All nodes carry out this step. In the course of the further code execution this *id* is used as an ordinary FORTRAN-variable. By that, each node can be identified at any time. Step 2

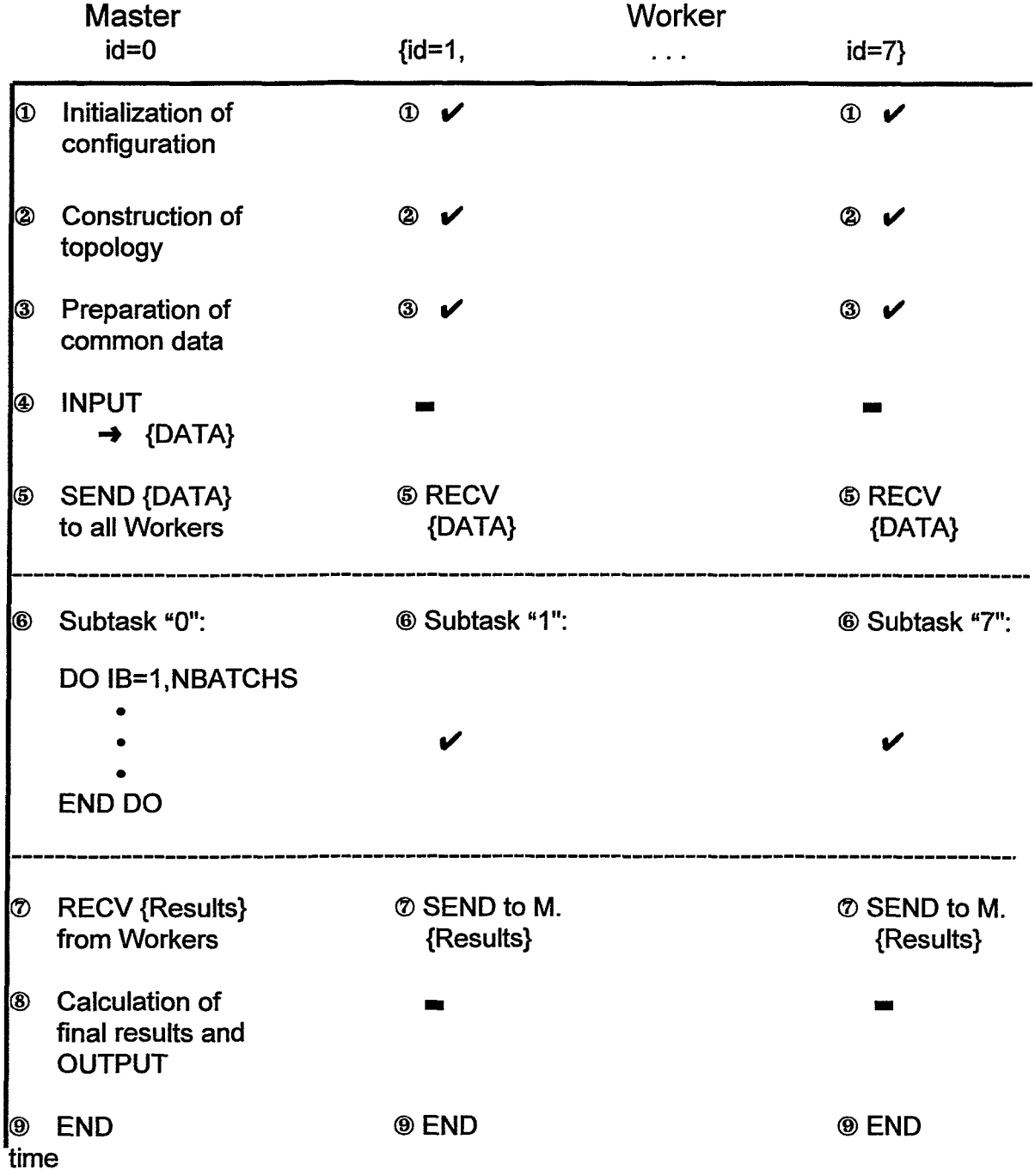

Fig. 2: Modified Master-Worker scheme as used in FIT

performs the construction of the topology with the help of PARIX routines, i. e. the bidirectional links between the master and all the workers are established. In step 3 each node prepares some general data necessary for the particle simulations. After that, the master reads the input data from host files and transforms them into certain data arrays defined inside the code. In step 5 the master sends the data arrays to all workers and the workers receive these data. Step 6 is the actual long-time calculation. Each node, i. e. including the master, performs the same sequence of NBATCHS batches. During their

simulations all nodes write data, e. g. birth points of generated secondary particles (neutrals), on files located at the host. In step 7 all workers send their partial results to the master. Finally, the master calculates the final results and puts them out.

The realized scheme is the most efficient one for the ion transport problems simulated by the FIT code. Communications between the master and the workers take place only during steps 5 and 7. Also, a synchronization of the nodes turned out to be not necessary because the time diffusion of the nodes remains very small - about two or three minutes only in the course of an one-day calculation.

4. Results

Table 1 presents the comparison of the efficiencies of a typical FIT calculation achieved on various computer systems. The calculation on the CONVEX represents the optimum vectorized version of FIT. The "GC (TU-CH.)" is an 128-nodes system of the GC-series of the Parsytec Inc. installed at the Technical University Chemnitz. It is declared as the "Saxonian Parallel Computer" and may be chargeless used by institutions of public law. The implementation of the parallelized FIT code was possible without serious problems. It is now used for FIT applications in the case when particularly high performance is desired. As in case of the Xplorer the nodes of the GC-system are also composed of the PowerPC-601 numeric processor and the T805 transputer.

Tab. 1: Comparison of efficiencies of FIT calculations on various computer systems

Computer	Number of nodes	Rel. efficiency
CONVEX	-	1.0
parsy	4	2.2
parsy	8	4.4
GC (TU-Ch.)	32	18.1
GC (TU-Ch.)	64	33.3

Three important aspects that are expressed by this table are to be pointed out. First, one can see that the use of the "parsy" already gives an essential gain in computing power and consequently a discharge for the RCR's computing server, too. The second aspect concerns the use of the GC-system for potential Monte Carlo users of the RCR. By means of the parallelization of FIT and its implementation on the GC-system it has been demonstrated that a peak perfomance up to about 5 GFLOPS is achievable. The third aspect is of methodical importance for Monte Carlo transport simulations in general. The calculations show a great advantage of the Monte Carlo method in comparison to deterministic transport calculations: their efficiency scales linearly with the number of processors. So, the Monte Carlo method will continue to benefit directly from the further development of parallel computer systems.

References

[1] P. Zanella
"Status of Parallel Computing",
CERN, 1993

[2] A. Beguelin et al.
"A User Guide to PVM",
Report ORNL/TM-11826, Oak Ridge National Laboratory, 1991

[3] A. Hähne
"Zufallsgenerator auf dem PowerXplorer",
Internal Report, Computer Centre, Rossendorf, 1995

[4] H. Kumpf et al.
"Computer Simulation of a Plasma Neutron Source",
Annual Report 1993, IfS, Rossendorf, 1994

[5] M. B. Emmett
"The MORSE Monte Carlo Radiation Transport Code System"
Report ORNL-4972, Oak Ridge National Laboratory, 1977

[6] St. Burkhardt et al.
Parallele Rechnersysteme - Programmierung und Anwendung,
Verlag Technik GmbH, Berlin - München, 1993

The project this report is based on is supported by the STC agreement between Germany and Russia and registered with number X222.72. The authors are responsible for the scientific content of the report.

SIMULATION OF THE TRANSPORT OF HIGH ENERGY IONS AND RESULTING PARTICLES

H.-U. Barz, B.Böhmer

1. Introduction

The main German activities on fast ions use for tumour therapy take place in Darmstadt and are now in a stage shortly before clinical application. The investigations represented here, do not immediately contribute to therapy planning but primarily were to estimate the part of deposited energy in the tissue due to light particles from fragmentation.
First, the tissue was not only described by zones of different electron density. Their elements constituents were taken into account. Second, as the fragmentation processes are not well known up to now, the influence of different fragmentation cross section models have been studied by comparison with experimental data.

2. Calculation Code

A procedure was created to calculate the space dependent energy deposition of the ions and of the particles resulting from fragmentation for given input energy of the primary ions and given material composition of the different layers which constitute the related zones of the human body. As the primary ions undergo fragmentation on their way through the tissue and these fragments can further be fragmented, the energy of the fragments has to be considered. Furthermore, the fluences of different particles must be calculated after the different layers to enable comparison with experiments. The calculation were based on the Bethe equation (1) [1] that describes the energy loss of ions by excitation of ions:

$$\frac{dE}{dx} = -4 * \pi * r_0^2 * m * z^2 * N * Z/\beta^2 * [\ln(2 * m * c^2 * \beta^2/I) - \ln(1-\beta^2) - \beta^2 - \delta/2] \qquad (1)$$

In (1) $m*c^2$ means the rest mass of the electron, r_0 the classical radius of the electron, z the atomic number of the projectile, Z the mean atomic number of the given material composition and N the total nuclear density of all kinds of atoms within the material composition. Z is calculated before together with other constant quantities for the arising material compositions. Further ß stands for v/c and I is the mean ionization potential for the given material composition. The values for I are found in the literatur (e.g. [2]) for the most important materials. However they slightly vary depending on the author.
A charge correction as given in [1] can optionally be used. This correction treats projectile velocities, which are comparable with the classical velocity of electrons in hydrogen. It replaces the charge number z of the projectile by $z^*(1-\exp(-0.95^*v/v_0))$, where v_0 is the mean velocity of the electron in a hydrogen atom.
δ/2 is a density correction introduced by Sternheimer [3]. This correction takes into account a decreasing of slowing down of the ions caused by the electrical field of the ion and the resulting polarization of atoms that are near to the path of the ion. This effect becomes more important for high energies because the interaction range of the electrical field increases for higher energies. Moreover this effect depends on the density of the material and is primarily relevant within fluids and solids. First calculations used this model. It was found that for ion energies and materials typical for ion therapy the contribution to dE/dx is lower than 0.01%. Therefore, in the code this contribution can be considered optionally. Other

possible corrections of formula (1), as e.g. the shell correction that is important for very low energies, have not been considered because no real influence on the dose could be observed.
During the numerical solution of (1) the x-coordinate is divided into small intervals in which dE/dx can be treated constant. This dx-step determines the numerical accuracy and is automatically determined over the change of the derivative. For the representation of results the space step can be arbitrarily chosen.
The statistical fluctuation (straggling) of energy after the transmission of a distance Δx is according to Bohr proportional to Δx and can be better described by a relativistic correction. In the developed code these distances Δx are randomly chosen. The real new energy after Δx is obtained from a Gaussian-distribution using the improved Bohr expression for the standard deviation. The fragmentation is determined by the total cross section of fragmentation. Equation (1) is not sufficient for describing the announced problem but has to be completed. Additionally to (1) equation (2) must be considered:

$$dA/dx=\Sigma(E,x)*x. \qquad (2)$$

A is the number of initial particles depending on the distance x. $\Sigma(E,x)$ is the total fragmentation cross section that depends on E and E depends through equation (1) on x. But there is also a dependence on x by the composition. For the complete problem the Monte Carlo method can be applied very advantageously. Using the Monte Carlo method, equation (1) can be solved simultaneously accomplishing all the necessary corrections as straggling, and e.g. the more accurate treatment of fragmentation by considering the velocity loss of the projectile fragments compared with the projectiles. There are 3 different options to model this effect. The simplest approximation does not take this effect into account. The projectile and fragment nucleons have the same energy. Furthermore, the approximation introduced by Morissey (see e.g. [4]) and byTsao, L.Sihver et al. [5] can alternatively be used. The Tsao, Sihver-approximation is based on a Gaussian distribution of the energy of fragments in the laboratory system.
Several code versions had to be generated according to the different representations of the total and partial fragmentation cross sections. In addition, different energy straggling models were used and the possibility of multifragmentation had to be taken into account. Multifragmentation requires a nonanalogous Monte Carlo treatment. This means that many different fragments can arise from one fragmentation.
The mentioned options were especially important to get a feeling about the influence of the different assumptions and the sensitivity of the results.
The calculations provided the fluences for each layer, the total energy release in each space interval, the energy deposition of the fragments, and the difference of the energy of reacting projectiles and produced fragments. This last mentioned difference might result from target fragments, particles of the "fireball", and the difference of the binding energy of the projectiles and produced fragments.
Concludingly it can be stated that for the one-dimensional transport of ions there are powerful and tested codes with reasonable calculation times (e.g. 1 hour for 1% statistical error and space resolution of .01 cm).

3. Fragmentation Data

Based on the model introduced by Sümmerer, at first a code was developed for the generation of libraries of macroscopic fragmentation cross sections for arbitrary material compositions. For each material composition the total reaction cross section and the probabilities of the generation of different fragments are calculated. For the total cross

section also other empirical formulas can be used, among them one recommended by Sihver [1]. Moreover, many different models by Sihver with energy independent and dependent cross sections were investigated. The main uncertainties of all these models are connected with the portion of light particles among the fragments. Own criteria are developed, regarding which of the shortliving fragments are to be considered. The latest improved models by Sihver take into account multifragmentation and more exact models for reaction kinetics.
For all these different models data libraries were generated. However, the most general model does not ensure conservation of mass and energy for low energies. Moreover, for some cases the sum of the partial cross section is smaller than the calculated total reaction cross section. For these reasons some corrections of this latest model were accomplished. Since the multiplicity cannot be greater than $A_{projectile}$ this value was taken as a limit. In case of $multiplicity_{Sihver}<1$ all partial fragmentation cross sections are increased by the factor $k=1/multiplicity_{Sihver}$. Corrections of this kind are of course not very satisfying because such effects are obviously connected with the insufficiency of the model.
The comparison of all these different models show good correspondence between the different theoretical total reaction cross sections and with experimental values. Concerning the partial fragmentation cross section the situation is worse especially for light fragments.

4. Comparisons with Experiments and Between Different Models

The corrected data library was compared with measured fragment yields obtained by Schardt et al. [6] for 270 MeV ^{12}C-projectiles (effective energy 237 MeV). The curves of angle dependent fragmentation yields taken from [6] were used to obtain the "experimental" partial fragmentation yields for given Z. In Tab. 1 these yields ($SIGMA(Z)_{exp}$) are compared with calculated yields for different energies ($SIGMA(Z)_{calc}$). Additionally the total yield as sum of the partial yields and the total cross section are represented.

Tab. 1: Measured and Calculated Partial Fragmentation Cross Sections in mbarn

Z	$SIGMA(Z)_{exp}$	$SIGMA(Z)_{calc}$				
	237	10.0	50.0	100.0	200.0	300.0 MeV
1	1406.785	2285.359	2616.080	1580.425	1143.115	1106.728
2	1217.986	1742.543	2218.505	1384.765	1006.222	977.380
3	185.952	26.872	135.181	268.101	184.057	161.664
4	126.068	15.239	92.288	182.144	127.075	111.604
5	241.874	250.418	376.913	277.090	253.464	266.160
sum of Z=<6 = 3178.665						
sum of calc.partial c.s. with Z<6 =		4320.431	5438.968	3692.524	2713.933	2623.536
total sum of calc.partial c.s. =		4376.516	5732.914	3903.098	2874.069	2781.059
total cross section =		1164.425	2028.401	1475.635	1275.336	1327.354

Obviously, the heavy fragment yields are in very good agreement with the measured values whereas the calculated lighter fragment yields are about 20-25% smaller. The calculated sum over all fragments is also somewhat smaller than the measured sum. When assessing this comparison one must have in mind the uncertainties of the determination of the "measured values" from a curve of angle dependent fragmentation yields. The comparison between the calculated total cross section and the sum of fragmentation yields shows that in each fragmentation event on average more than two projectile fragments are generated.
For all developed models of cross sections, straggling and different other approximations extensive calculations were performed. Not only homogeneous systems but also inhomoge-

neous ones have been investigated. In Fig. 1 some results for different fragmentation models and a homogeneous system are to be seen.

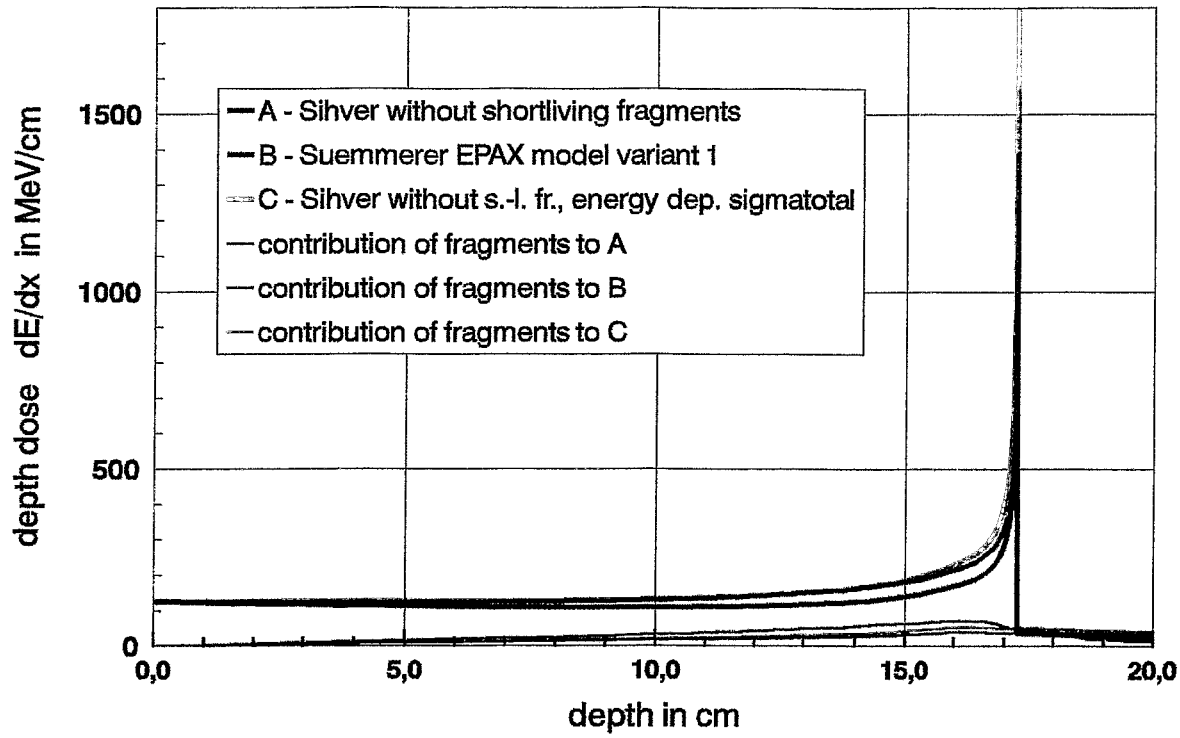

Fig.1: Distributions of Total Doses and Fragment Doses from 3600 MeV C-12 Projectiles in Water for Different Fragmentation Models

A remarkable increase of the energy release near to the Bragg-peak has to be noticed for the Sihver model C without taking into consideration the impulse loss of fragments due to reaction kinetics.

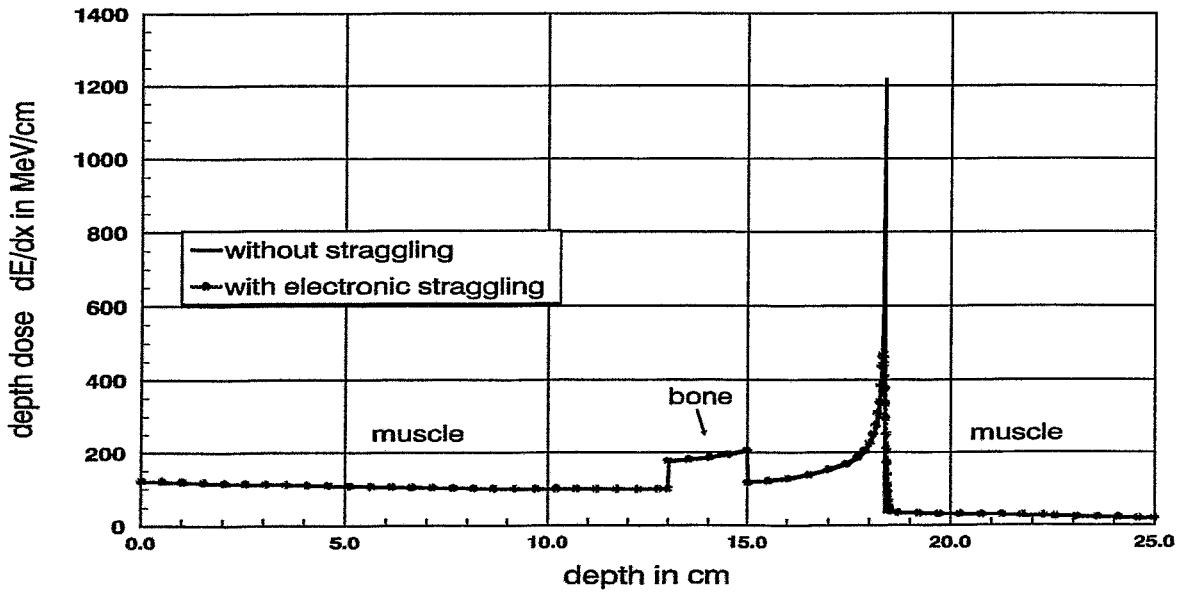

Fig. 2: Distribution of the Total Dose from 4000 MeV C-12 Projectiles in a Heterogeneous Medium (Muscle-Bone-Muscle)

Fig. 2 shows the energy release for a heterogeneous structure and demonstrates the influence of the energy straggling.

In Fig. 3 measured and calculated values of the space dependent energy dose are compared. This picture was taken from [7]. The own calculation results using the latest Sihver cross section model and including all improvements were added. These results agreed so well with the former calculations and the measurements that the differences cannot be distinguished in the picture.

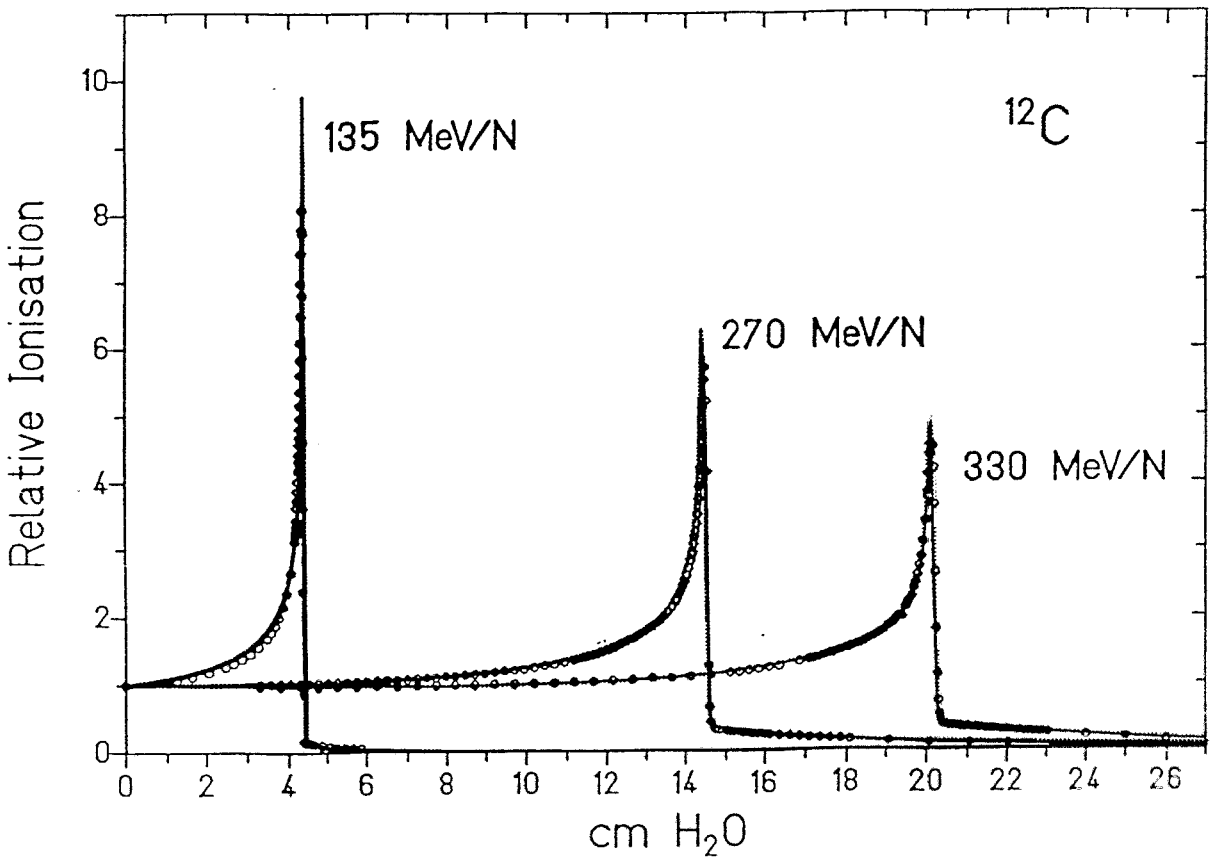

Fig. 3: Measurements (points), Calculations by Sihver et al. and Own Calculations (lines) of the Total Space Dependent Energy Deposition

In the introduction it was announced that even fluence results can be calculated with the developed Monte Carlo code. This opportunity is used to compare with other experiments by Schall [8].
[8] makes available experimental results for 3 different kinds of fragments. Tab. 2 shows these experimental values and our calculations for different fragmentation models. It should be noticed that the measured values are influenced by additional facilities arranged before the measurement arrangement. This effect could not exactly be considered because of missing information.

Table 2 : Space Distribution of Relative Fragment Fluences for ^{12}C Projectiles with Energies of 674 MeV/Nucleon Measured by Schall [7] and Calculated Values Using Two Different Fragmentation Models

Base	fragment	x=4.25 cm	x=8.51 cm	x=17.02 cm	x=25.28 cm
Sihver (M)	Z=6	.847	.7171	.514	.371
"	Z=5	.0315	.0537	.0765	.0812
"	Z<5	.318	.605	1.09	1.47
Sümmerer	Z=6	.841	.705	.497	.355
"	Z=5	.0233	.0394	.0557	.0593
"	Z<5	.136	.255	.447	.581
Schall $_{korr}$	Z=6	.80	.69	.45	.33
"	Z=5	.036	.051	.061	.063
"	Z<5	.21	.32	.52	.63

5. Conclusions

Above all two conclusions can be drawn.
First, the total doses are very insensitive against different fragmentation models. In general a satisfying agreement can be stated between calculation and experiment.
Second, this is not the case for fragment specific fluences. They very sensitively depend on the applied models and corrections.

References

[1] L. Sihver and T. Kanai
Energy Loss, Range and Fluence Distributions, Total Reaction and Projectile Fragmentation Cross Sections in Proton-Nucleus and Nucleus-Nucleus Interactions, NIRS-M-87, HIMAC-002

[2] Stopping Powers for Electrons and Positrons
ICRU-Report 37 (1984), Bethesda, MD. 20814 (U.S.A)

[3] R.M. Sternheimer, S.M. Seltzer and M.J. Berger
Density effect for the ionisation loss of charged particles in various substances
PHYSICAL REVIEW B, Vol. 26, Nr. 11, S.6067

[4] Th. Haberer
Entwicklung eines magnetischen Strahlführungssystems zur tumorkonformen Strahlentherapie mit schweren geladenen Teilchen. GSI-94-09

[5] C.H.Tsao, R.Silberberg, A.F.Bargouty, L.Sihver, Energy Degradation in Cosmic Ray Nuclear Spallation Reactions, Submitted to Astrophys. J., May 1994

[6] D. Schardt, U. Weber, L. Chukov
Physical Characterization of Light-ion Therapy Beams. GSI-07-95

[7] L. Sihver, D. Schardt, and T. Kanai
Depth-Dose and Fluence Distributions when using Heavy Ion Beams. GSI-95-21

[8] I. Schall
Untersuchung der Kernfragmentation leichter Ionen im Hinblick auf die Strahlentherapie
Dissertation, Technische Hochschule Darmstadt 1994, D 17

A THEORETICAL VIBRATION MODEL FOR VVER-440 REACTORS CONSIDERING THE FLUID-STRUCTURE INTERACTION

E. Altstadt, G. Grunwald, M. Scheffler, and F.-P. Weiss

1. Introduction

At many power stations on-line vibration monitoring became a standard procedure of plant surveillance. This development was provoked by abnormal vibrations that happened [1-3]. To detect mechanical faults causing the abnormal vibrations in an early stage a finite element (FE) based vibration model of the whole primary circuit is needed, permitting

- the description of the normal vibrations of the components, especially to assign the measured vibration frequencies in neutron noise, pressure fluctuations or mechanical displacements to vibration modes of the whole coupled mechanical system
- the determination of physical limits for frequency shifts and amplitude changes as alarm thresholds for on-line vibration monitoring
- the assessment of mechanical loads connected with the failure of a certain component.

The correct description of the mechanical vibrations of the reactor pressure vessel and its internals requires the fluid-structure-interaction (FSI) in the downcomer region to be considered in the FE-model using an especially developed fluid-structure-element (FSE).

2. The Finite Element Based Vibration Model

The model comprises the whole primary circuit, including steam generators, loops, coolant pumps, main isolating valves, and the reactor pressure vessel (RPV) with its internals (Fig. 1). It was developed using the FE-code ANSYS® on a Hewlett-Packard workstation platform.

The experimental experience showed the mechanical integrity of the system not to be endangered by shell mode vibrations but by beam mode vibrations in the frequency range up to 30 Hz. Additional FE calculations yielded that all shell modes occur beyond 30 Hz. Thus it is sufficient to assemble the model from 1D pipe elements. Figure 2 shows a topology scheme of the finite-element-model for the RPV and all the internals: core barrel (CB), CB support skirt, core basket, upper core structure. The model of the RPV head considers the upper callotte, the control-element standpipe frame and the standpipes themselfs. Each of the 71 nodes connecting two elastic pipe elements has 6 degrees of freedom. Different reactor components are mutually connected by stiffness matrices (12 x 12) which e.g. represent the CB guide lugs (nodes 20 and 39), or the ring foundation (nodes 43 and 71), or the spring pipe segments between the upper flange of the CB and the RPV head (nodes 31 and 50).

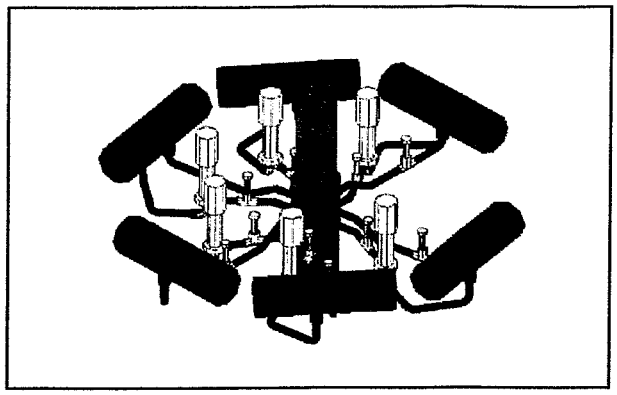

Fig. 1: Element plot of the VVER-440 primary circuit

The parameters of those stiffness matrices were estimated in separate 3D calculations. Extreme stiff connections are modelled by constraints.

The FSEs are located between the RPV and the CB (e.g. between nodes 37 and 16, 38 and 17, 40 and 22, see Fig. 2). Chapter 3 gives an overview about the basic steps of the derivation of the FSE.

In analogy to the RPV with internals, the loop model consists of pipe elements, pipe tee and pipe elbow elements, structural mass elements (which are formulated as 6 by 6 inertia matrices), stiffness matrices and constraints. The loop model includes the steam generator (SG), the hot leg (HL), the cold leg (CL), the main coolant pump (MCP), the hot isolating valve (HV) and the cold isolating valve (CV). Special attention was put on the SG support and on the connection of the SG with the secondary circuit, both modelled by a separately calculated stiffness matrix between the SG center node and the ground. Neglecting these couplings, one would drastically underestimate particularly the first eigenfrequency of the loop. The bearings of the MCP and of the HV are represented by stiffness matrices, too. The parameters of the loop model could be adjusted using results from modal analysis experiments performed at coolant loops in the Greifswald NPP, Germany, and in the Dukovany NPP, Czech, as well.

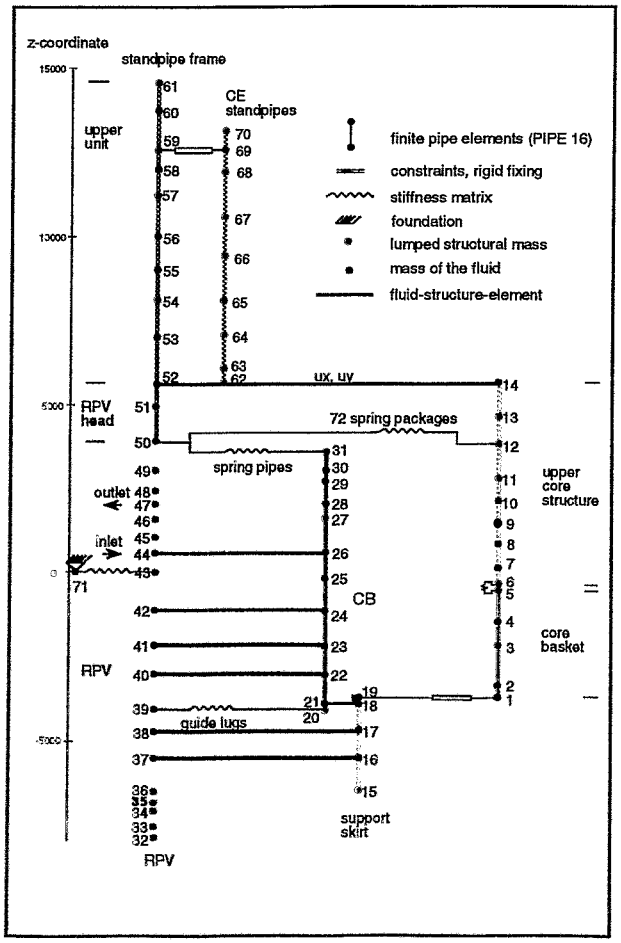

Fig. 2: Topology of the FE-model for the RPV and its internals

The vibration behaviour of the RPV and the six coolant loops cannot strictly be separated. Neither the RPV is a fix clamping for the loops nor is the loop inertia neglectable for RPV motions. So in general it is to be expected that the mode shapes will be coupled. The connection of RPV and coolant loops is realized by rigid area constraint equations between RPV (node 47, Fig. 2) and the first nodes of all six loops and between RPV (node 44) and the last nodes of all six loops respectivly.

3. Modelling the Fluid-Structure Interaction (FSI)

For the consideration of the FSI in the downcomer the coupled system of fluid equations (continuity equation and Navier-Stokes-equation) and of structural equations of motion must be solved. To obtain a fluid-structure-element (FSE) which can be implemented in the FE-model of the reactor, the system of equations must approximately be solved.

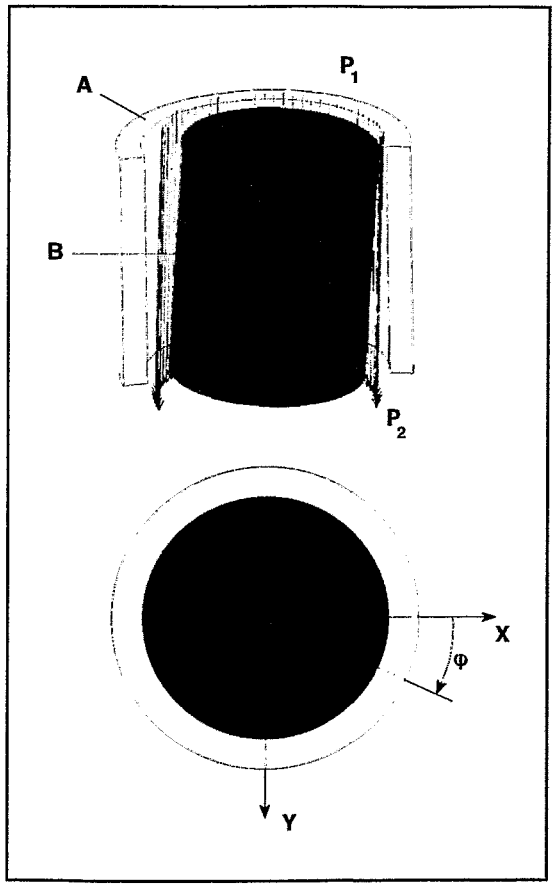

Fig. 3: Fluid-structure-system

The approximation applied to solve the system of fluid equations and equations of motion is specially taylored for incompressible fluids streaming through a narrow annular gap which is formed by two concentric cylinders (Fig. 3). The fluid flow is driven by a pressure gradient $p_1 - p_2$. Each of the cylinders can perform small motions (two displacements and two rotations). Thus the FSE has 8 structural degrees of freedom.

Fluid velocity $\mathbf{v}_F$ and pressure p are described in cylindrical coordinates. Making a linear approach for the radial component of the fluid velocity v_r, and presuming that the components v_φ and v_z do not depend on r but only on φ and z, the continuity equation can be averaged over the gap width [2]. The resulting 2D equation which can be used for narrow gaps and small structural displacements can be solved analytically. The potential solution for the velocity field is applied to calculate the pressure distribution in dependence on the structural motion using the Navier-Stokes-equation [2]. The resulting forces and momenta which act on the structure can in turn be obtained from the pressure field.

After linearizing the pressure distribution with respect to the structural motion (velocity and acceleration) the FSE mass matrix and the FSE damping matrix (both non-symmetric) can be obtained. Experimental investigations at a laboratory set-up were performed to validate the analytical 2D solution [2]. These experiments proved the FSE to be applicable to laminar fluid flow in the annular gap as well as to turbulent fluid flow. In addition to that, the experimental results have shown that the flowing fluid also causes a stiffness reaction, i.e. forces and momenta which are proportional to the relative displacement of the cylinders. This cannot be described by the above approximation. Therefore, the stiffness matrix was obtained by an analytical approximate 3D-solution of the fluid equations for stationary flow through the deformed annular gap.

4. Eigenfrequencies and Mode Shapes

The coupling of all six coolant loops with the RPV results in a great number of eigen-frequencies of the complex system due to the coupling of different degrees of freedom. The whole model then consists of about 450 finite elements with about 2300 active degrees of freedom. In the frequency range up to 30 Hz more than 100 eigen-frequencies are obtained. Many of them are close together but exhibit different mode shapes.

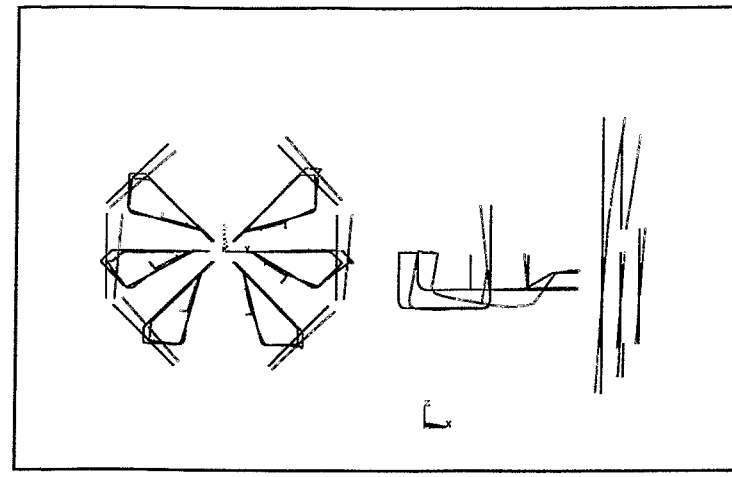

Fig. 4: Coupled mode of the primary circuit at 3.5 Hz

Table 1: Eigenfrequencies and mode shapes of the RPV and its internals

No.	Frequency / Hz		Verbal description
	FSE	no FSE	
1/2	3.5 3.65	3.5 3.65	in-phase pendulum motion of RPV, CB and CB-internals; 1. beam mode of the upper unit in-phase; loops in-phase
3/4	4.6 4.7	4.6 4.7	in-phase pendulum motion of RPV, CB and CB-internals; 1. beam mode of the upper unit in-phase; loops in anti-phase
5/6	8.2 8.3	8.2 8.3	small in-phase pendulum motion of RPV, CB and CB-internals; 1. beam mode of the upper unit in anti-phase; large cold leg displacements (MCP)
7/8	10.3 10.5	10.5 10.7	in-phase pendulum motion of RPV, CB and CB-internals; 1. beam mode of the upper unit in anti-phase; hot leg displacements
9/10	**13.75** **13.75**	**26.0** **26.0**	anti-phase pendulum motion of the RPV with respect to all RPV-internals, elastic deformation of CB and CB-internals, 2. modes of standpipe frame and standpipes
11/12	16.0 16.0	15.8 15.8	2. beam mode of the CE standpipes
13	18.6	18.6	z-vibration of all internals, small z-amplitude of the RPV, in-phase pendulum motion of RPV, CB and CB-internals, 2. beam mode of the upper unit
14/15	**23.6** **23.6**	beyond 30 Hz	anti-phase beam modes of RPV (lower part) and CB; elastic deformation of CB-internals

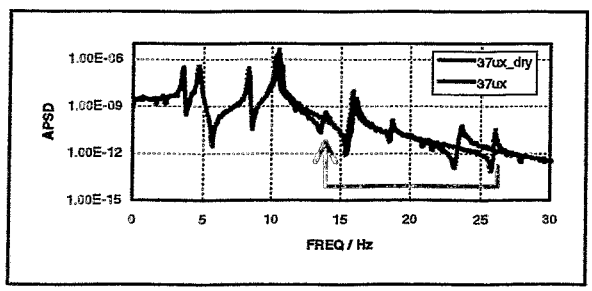

Fig. 5: Forced vibrabtion spectra with and without consideration of FSI

Most of the mode shapes are characterized by various loop displacements in many different phase relations with the RPV being almost in rest position. Some mode shapes only exhibit large displacements of the loops and of the RPV as well. For example Fig. 4 shows the lowest mode shape at 3.5 Hz which has significant displacements of the RPV and of the internals.

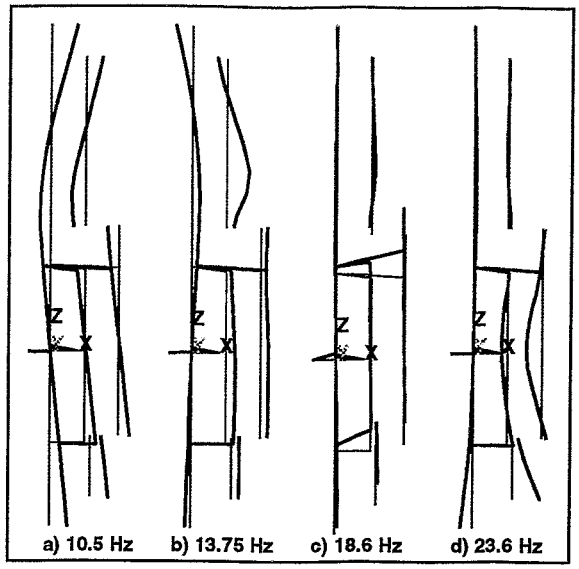

Fig. 6: Modes of RPV and internals

For the investigation of the RPV and its internals it is suitable to reduce the model size by means of the substructure technique to exclude such modes which differ from each other only in the phase relations of the loops. The six coolant loops are represented in the reduced model by a substructure of 12 degrees of freedom. Table 1 gives an overview of the modes of the RPV and its internals up to 30 Hz. To demonstrate how important the consideration of FSI is, the eigen-frequencies are listed for the two cases: with and without FSEs. The first eigenfrequency connected with a significant relative displacement between RPV and CB was calculated to be at 26 Hz without FSI. Consideration of FSI shifts that eingenfrequency down to 13.75 Hz. This effect can also be seen in the forced vibration spectra (Fig. 5)

The eigenmodes 9, 10, 13, 14 and 15 (Fig. 6b-d) are particularly important for the detection of possible degradations of the internal clamping elements like the guide lugs and the spring pipe segments. Mode 13 at 18.6 Hz is above all a z-vibration of all the internals while the vessel amplitude itself is rather small. Even the relative displacements connected with the pendulum component of this mode can be neglected. The modes 9/10 and 14/15 are related to anti-phase motions of the RPV with respect to all internal components. These modes are further characterized by elastic deformations of the internals.

5. Simulation of Mechanical Failures

To reveal how degradations of the safety relevant internal components affect excore vibration spectra, sensitivity studies were performed by varying certain parameters of the FE-model. The calculation of the forced vibration spectra is based on a transient analysis (simulation of time series) followed by a digital signal processing procedure.

Figure 7 indicates how the forced vibration spectra of RPV bottom displacements in all directions would change in case of two broken guide lugs at 0 and 45 degrees azimutal position (in total there are 8 guide lugs with 45 degrees azimutal division). As expected, above all the eigenfrequencies pertaining to anti-phase pendulum motion do respond to that failure. There is almost no effect in the other eigenfrequencies. The change of the spectra can most clearly be observed in the y-direction, because a guide lug mainly acts as a tangential spring. But also the spectrum of the z-vibration provides a significant change though the guide lugs do not have a stiffness in that direction.

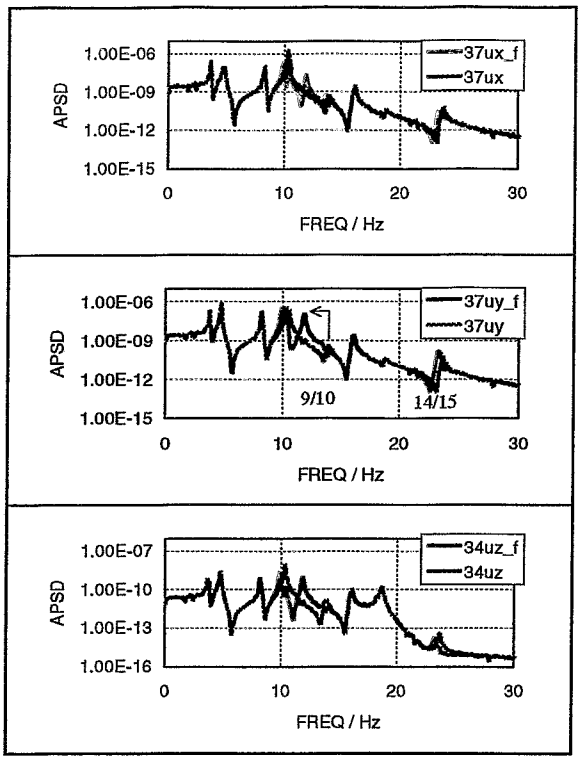

Fig. 7: Change of spectra of RPV bottom displacement (node 37 x and y, node 34 z). Fracture (_f) of two guide lugs at 0 and 45 degrees.

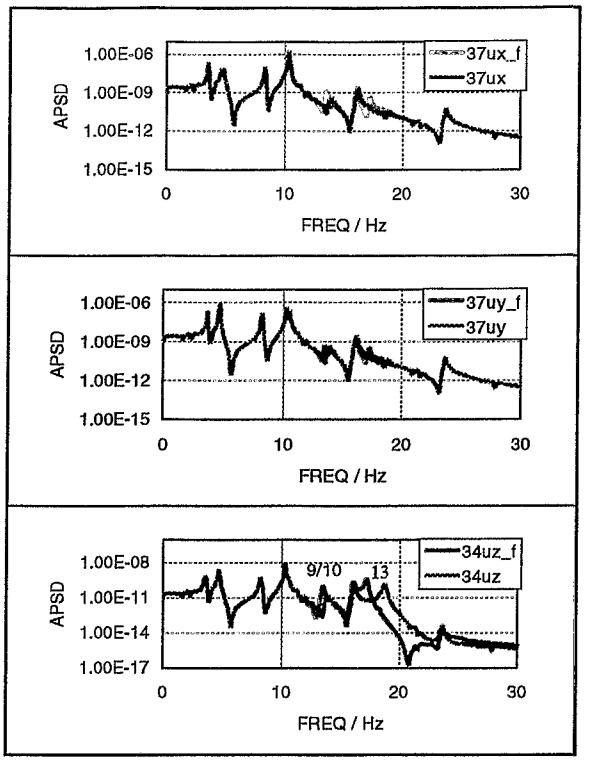

Fig. 8: Change of spectra of RPV bottom displacement (node 37 x and y, node 34 z). Failure (_f) of two hold down spring pipe segments.

Figure 8 shows the change of the spectra of the RPV bottom displacement in all directions in case of the failure of two spring pipes (in total there are six 60 degrees spring pipe segments). A significant effect is observed in a down shift of the eigenfrequency of mode 13 at about 18 Hz and a rather small shift of the modes 9/10. The spectrum change can most clearly be observed in the z-direction, because the pipe segments mainly act as a vertical spring, and mode 13 is a large z-vibration of the RPV internals.

6. Conclusions

The developed model describes the mechanical vibration behaviour of VVER-440 type reactors in the frequency region up to 30 Hz and can be considered to be widely verified.

Modelling the vibrations, the FSI has to be taken into account. It strongly affects vibration modes exhibiting a relative displacement between CB and RPV.

The simulation of mechanical damages of RPV internal components is realized by modification of certain parameters of the FE-model. The modes and the forced vibration spectra of the whole structure with damaged components mostly are clearly different from those of the intact structure. Mode selective shifts of resonance peaks can be considered as unambigious indications of a comoponent failure. The most

important damages are guide lug breaks and hold down spring pipe segment failures.

The forced vibration spectra can be calculated for any location of the structure. Thus, it is possible to give recommendations on a sensitive instrumentation for an early failure detection.

In principle, the model is even suited to estimate the loads of the reactor components which might be imposed by internal or external events (explosion, earthquake, emergency core cooling).

References

[1] Altstadt, E., M. Scheffler, F.-P. Weiß (1995). Component Vibration of VVER-Reactors - Diagnostics and Modelling. *Progress in Nuclear Energy, Vol 29, 1995.*

[2] Grunwald, G. and E. Altstadt (1994). Analytical and Experimental Investigations for Modelling the Fluid-Structure-Interaction in Annular Gaps. *Preprints of the IFAC-Symposium on Fault Detection Supervision and Safety for Technical Processes (SAFEPROCESS '94)*, 147-152.

[3] Liewers, P., W. Schmitt, P. Schumann and F.-P. Weiß (1987). Detection of Core Barrel Motion at WWER-440 Type Reactors. *Progress in Nuclear Energy (SMORN V, Munich 1987)*, 21, 89 - 96.

Nomenclature

CB	Core barrel
CL	Cold leg
CV	Cold isolating valve
FSE	Fluid-structure element
FSI	Fluid-structure interaction
FE	Finite element
HL	Hot leg
HV	Hot isolating valve
NPP	Nuclear power plant
RPV	Reactor pressure vessel
SG	Steam generator

IDENTIFICATION OF DANGEROUS STATES IN CHEMICAL PLANTS USING NEURAL NETWORKS

G. Hessel, W. Schmitt, K. van der Vorst, F.-P. Weiss, J. Neumann [1], S. Schlüter [1], and A. Steiff [1]

1. Introduction

Human errors are one main cause of accidents in complex chemical plants. According to the "Major Accident Reporting System" [1] of the European Research Centre at Ispra (Italy), the vast majority of accidents in chemical plants could have been prevented by properly implementing the experience of the experts regarding the behaviour of the chemical plant on the one hand, and the sequence of incidents during similar situations on the other hand.
For example, the reasons for human errors and uncertainties in making decisions under critical situations could be:

- lack of attention due to the overtiredness
- misinterpretation of the state of the plant under stress
- inappropriate response to unknown situations, and
- overstraining of personnel due to an excessive presentation of information.

Therefore, the objective is to apply pattern recognition procedures such as neural networks or fuzzy pattern classification as an additional supervision system. These self-learning algorithms are expected to detect and assess critical situations unaffected by individual operator errors.
Within the frame of a joint project, this research work will be carried out in cooperation with the Institute for Environmental, Safety and Energy Technology at Oberhausen which is responsible for the development of a process simulator and for the construction of a laboratory reactor. Neural network approaches being developed at Rossendorf shall be trained and tested using experimental and simulated data sets from Oberhausen.

2. Neural Network Approach

The working principle of a supervision method based on neural network is shown in Fig. 1. When applying to the qualitative classification of process states, the neural network first has to be trained by process data from normal conditions and different faulty states as well. In this learning phase, the network is simultaneously confronted with pairs of feature vectors and target vectors at the input and output layer, respectively. To achieve a good classification ability, the input vectors have to consist of symptoms characterizing the respective fault state, while the output vectors contain the expertise knowledge on the specific fault.
During this supervised learning procedure, the connection strengths between the

[1] Institute for Environmental, Safety and Energy Technology Oberhausen

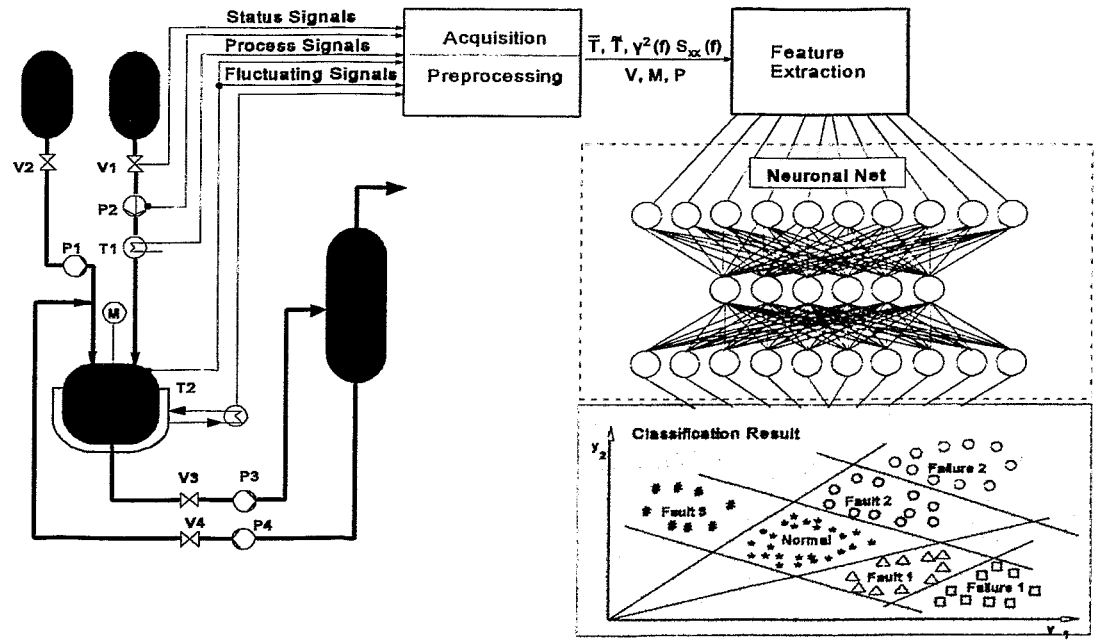

Fig.1: Identification of dangerous operating states in a chemical plant using neural networks

neurons of the different layers are altered by means of a special learning algorithm, and an iterative procedure is used for reducing the error between the actual and desired (target) output vector when the trained network is checked with testing data. Finally, the basic knowledge is stored in the connection strengths as the so-called weight factors. Then, the neural network can also classify unknown pattern vectors correctly when they belong to the trained classes. Beside extracting suitable features of process states, it is important to choose the appropriate type and the optimum topology of the neural network.

3. Experimental Equipment

To teach the neural network, a laboratory reactor has been used at Oberhausen. It consists of a stirred tank reactor (2 l steel vessel) with a jacket heat-exchanger, a distillation column, feed tanks, valves, pumps, measuring and control devices (Fig. 1). As a reference process, the esterification between acetic anhydride and methanol was chosen. This exothermic chemical reaction can be controlled within a certain temperature range. However, it has also enough self-reinforcing potential for heat production to investigate runaway phenomena as a function of temperature and concentration.

To simulate even dangerous process conditions which cannot be carried out in an experimental set-up, the process simulator SIMU was developed. Therefore, the process simulator and the experimental plant were used to train and test the neural network for different normal and faulty conditions. In the present developing phase of the neural network approach, the data sets are transferred from Oberhausen to Rossendorf via "Internet".

For developing a supervision method based on pattern recognition, neural networks and fuzzy pattern classification are available. Earlier, both types of classifiers were successfully tested with another process, namely acoustic leak monitoring in complicated geometric structures [2].

4. Results

To investigate the classification behaviour of the neural networks in different situations, reaction processes with faults of the cooling were simulated. The reactor in which

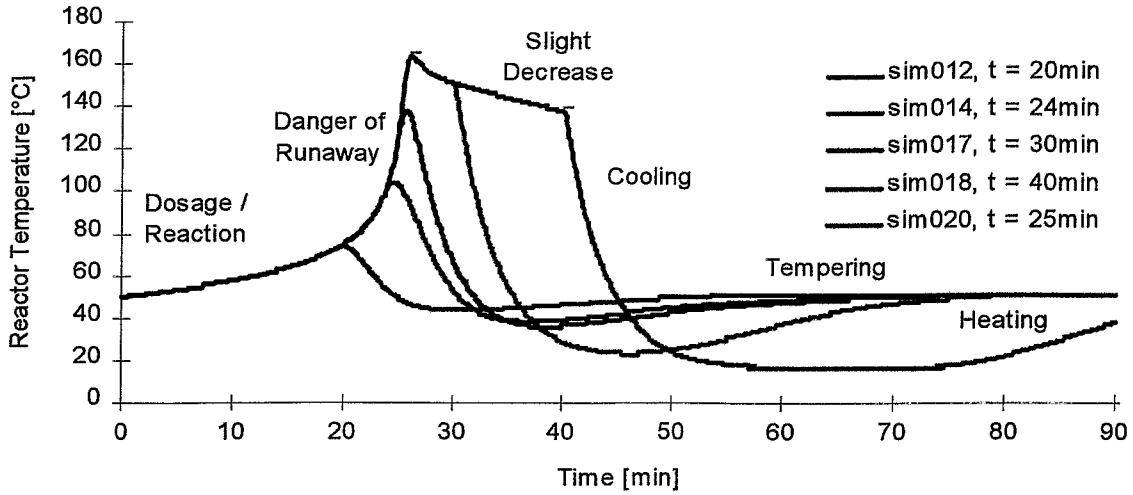

Fig.2: Simulated reactor temperature profiles of a coolant failure at t = 2 min and restart of the jacket cooling after 20, 24, 25, 30, and 40 minutes, respectively

1.5 litres of an equimolar acetic anhydride and methanol with sulfuric acid (catalyst) were reacting at 50°C was continuously charged with acetic anhydride and methanol (molar ratio 7:3). During this semibatch process, the coolant flow was interrupted over differently long periods [3].

Figure 2 shows the profile of the reactor temperature when the coolant flow fails and then later restarts. At the beginning of the coolant failure, the reactor temperature rises gradually due to the released heat of the reaction. This stage is named as the class "dosage/reaction". Then, the temperature of the reaction mass rises steeply because of the exponential acceleration of the reaction rate with increasing temperature. This is defined as the class "danger of runaway" since a thermal explosion might occur.

Only when the reactants are completely consumed, the increase of temperature will cease. In this case, the reactor temperature slowly begins to fall due to heat losses to the surroundings. This state is called "slight decrease of temperature". The steep fall of the reactor temperature is caused by resetting the jacket coolant flow ("cooling"). To bring the reactor temperature to the set point, the reaction mass must be heated ("heating") and tempered ("tempering").

For teaching the neural networks, the simulated data sim017 were used, where the coolant flow restarts only after reaching the maximum temperature (see Fig. 2). In

Fig. 3, the classification capability of a three-layer perceptron network with 10 hidden neurons is depicted. It has been trained using the six above-mentioned process states. The time domains of the trained process states are indicated by different colours as shown at the bottom of Fig. 3. To characterize the criticality of the respective states during interrupting the cooling, the colours of traffic light have been employed. For example, the red colour marks the class "danger of runaway", yellow labels "slight decrease of temperature", and green stands for the process state "dosage/reaction". The colours dark blue, magenta, and light blue indicate the states "cooling", "heating", and "tempering", respectively.
In the upper part of Fig. 3, the classification behaviour of the trained perceptron network regarding the learning data sim017 is represented. As the comparison with

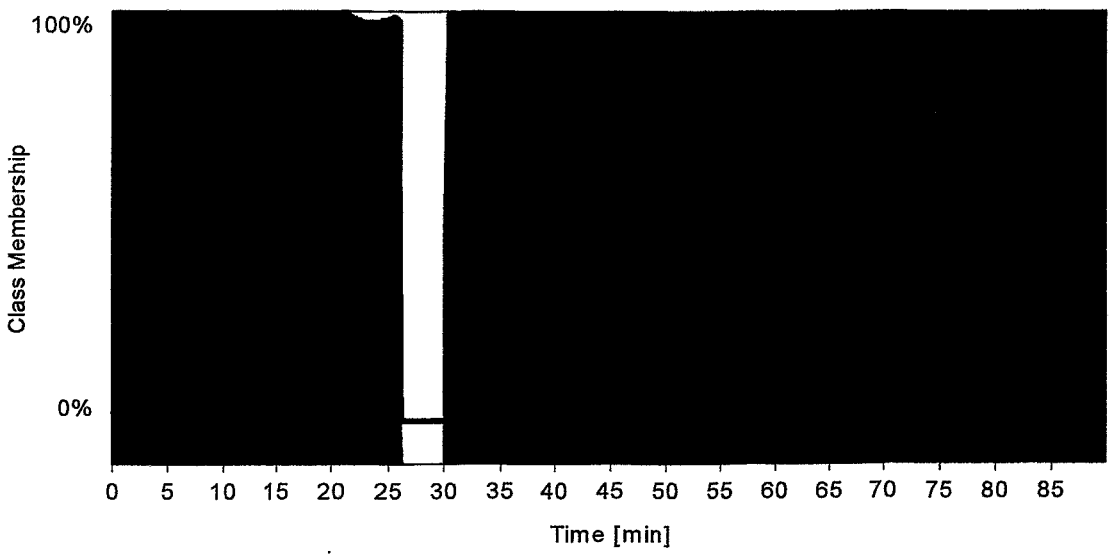

Fig.3: State reclassification of a simulated reaction process using the perceptron network (14/10/6); the sequence of the really simulated process states (sim017) is shown in the reduced diagram at the bottom

the desired results, given by the reduced diagram at the bottom of the same figure, shows, this perceptron network is capable of correctly reclassifying the trained sequences of the defined state classes when a cooling failure occurs. Even if untrained reaction sequences, which are also illustrated in Fig. 2, were offered, the network could correctly assign the different process states. An evidence for that is shown in Fig. 4 where the classification results for the untrained reaction process sim020 are depicted. Although the dominating process states occur in the outputs of the neural network after some delay, all the classes are identified correctly. The reason for the slight delay might be the use of an "1-from-n" classification, which assigns the data for a given time only to a single class. However, this partially contradicts the real process conditions in the reactor where two classes could be simultaneously active, especially in a region of transition, e.g. between the classes "dosage/reaction" (green) and "danger of runaway" (red-marked) in Fig. 4. Moreover, it was found that neural networks can also identify any process states in a laboratory reactor if suitable features for the related class (process state) are available. For example, the process state "calibration" (red-brown coloured) was additionally diagnosed by introducing the

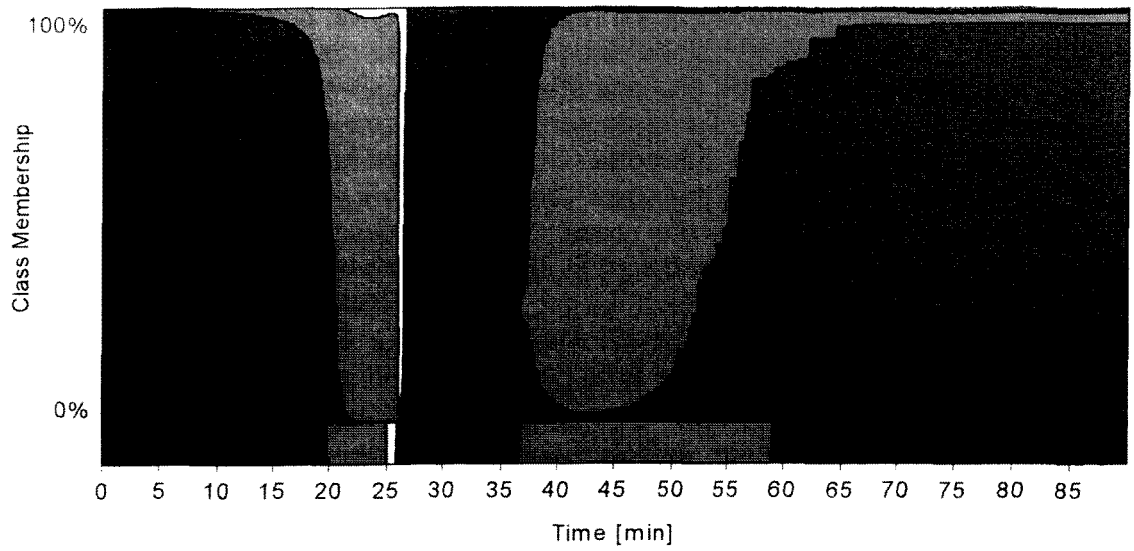

Fig.4: State classification of the untrained reaction process sim020 using the perceptron network (14/10/6) trained with data sim017

calibration power into the feature vector. The feature vector includes among other values the temperatures of the reactor, the jacket and the coolant reservoir, the temperature gradient in the reaction mass, the reactor pressure, the dosing mass rates, and the number of stirrer revolutions. In total, the feature vector comprises 19 elements.

Figure 5 shows the classification results for a semibatch process in a laboratory reactor. Initially, methanol and sulfuric acid (catalyst) are put into the reactor vessel, and then they are heated ("heating", magenta), calibrated ("calibration", red-brown) and

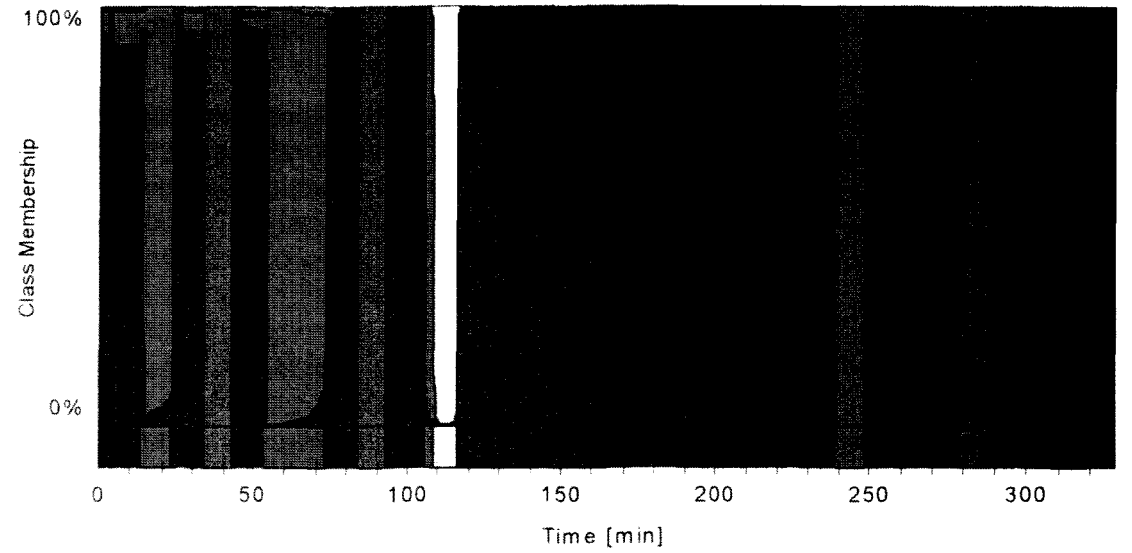

Fig 5. State classification of a reaction process measured in the laboratory reactor (v1708kn) using the perceptron network (19/15/7)

tempered ("tempering", light blue) to keep the reactor temperature at 50°C (set point). At time t = 106 min, acetic anhydride has been charged into the reactor over one hour. Due to the heat production of the beginning reaction, the reactor temperature increases very fast. This is classified by the network as a "danger of runaway". However, a thermal explosion is avoided by intensively cooling the reactor jacket. This suppresses the self-acceleration of the reaction rate (yellow) and a normal reaction process is ensured (green-coloured state "dosage/reaction").

It should be noticed that, before the end of charging (t = 155 min), the neural network already recognizes the process state "cooling" (dark blue), because, due to the consumption of methanol, there is no heat production but there are still heat losses. The following process states characterize different classes in adjusting the set point of the reactor temperature. Again, the correlation between the classified and given conditions, the later are shown at the bottom (Fig. 5), is an evidence for the ability of the neural network to diagnose the true sequence of the process states in a real reactor (e.g. also a state where the reactants of the hold-up were consumed by the reaction). Compared with neural networks, a fuzzy classifier provides a poor classification rate (75-90 %) at least in recognizing the measured process states. As it can be seen from

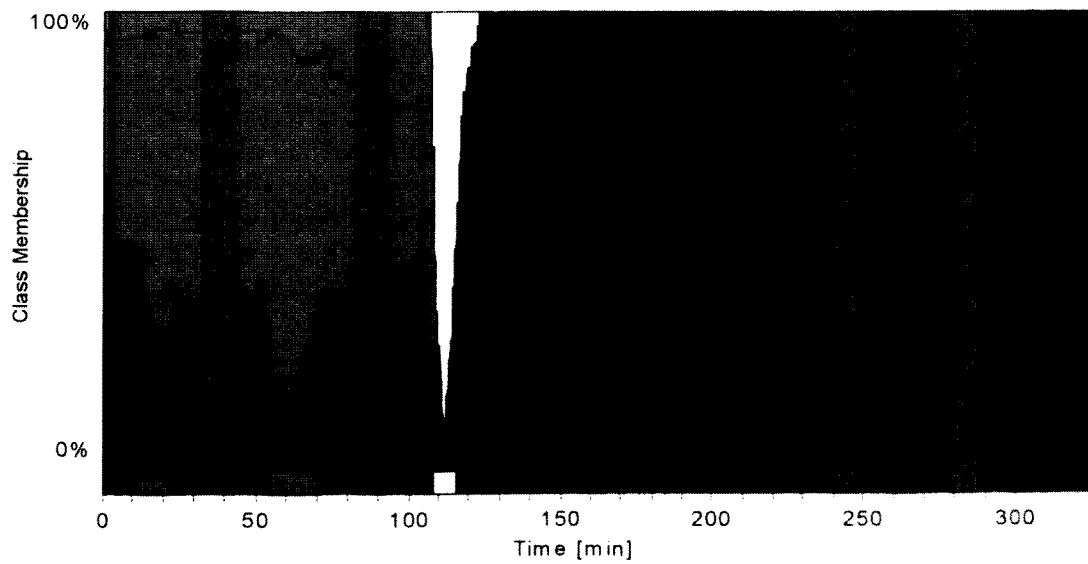

Fig.6: Sequence of the relative membership assigned by fuzzy pattern classification for the measuring data v1708kn

Fig. 6, the fuzzy classifier assigns the states "calibration", "danger of runaway","slight decrease of temperature", and "dosage/reaction". On the other hand, it has difficulties to distinguish between the process states "heating", "cooling", and "tempering" (see also Fig. 5). The error of this classifier is mainly caused by the continuous transitions of some features (e.g. temperature) of the learning data at the boundary of the classes. This contradicts the fuzzy boundaries of the classes when applying the fuzzy pattern recognition which presumes a clustered structure of the features over the different classes.

5. Conclusion

The application of neural networks to identify dangerous process states in chemical reactors has been investigated. The efficiency of the neural network approach could be proved by data sets of a reference process which were delivered both from simulation programmes and measurements in a laboratory reactor. First results show that the three-layer perceptron network provides promising assignments to normal and faulty states of the investigated reference process.

Future work is necessary to investigate all possible fault states and to test the behaviour of the classifiers during simultaneously occurring several faulty states (common-mode faults). Furthermore, it should be examined whether a neural network trained only by simulation data can also be applied to fault detection in experimental plants. Industrial tests of this supervision method are the aim of a following project.

References

[1] A. Benuzzi and J.M. Zaldivar (eds.)
"Safety of Chemical Batch Reactors and Storage Tanks"
Kluwer Academic Publishers, Dordrecht, 1991, pp. 49-77

[2] W. Schmitt, G. Hessel, and F.-P. Weiss
"Acoustic Leak Detection at Complicated Topologies Using Fuzzy Classifiers and Neural Networks"
Proc. of IMEKO XIIIWorld Congress, September 5-9, 1994, Torino, pp. 1259-1264

[3] J. Neumann, S. Schlüter, A. Steiff
"Anwendungsmöglichkeiten neuartiger EDV-gestützter Erkennungsmethoden zur Identifizierung gefährlicher Betriebszustände in Chemieanlagen"
UMSICHT-Zwischenbericht 1995, S. 1-14

The project this report is based on is funded by the BMBF (Bundesministerium für Bildung, Wissenschaft, Forschung und Technologie) and is registered with No. 01RG94234. The authors are responsible for the scientific content of the report.

REMOTE MONITORING OF UKRAINIAN NUCLEAR POWER PLANTS

M. Beyer, H. Carl, K. Nowak[1], P. Schumann, A. Seidel, F.-P. Weiß, J. Zschau

As part of the programme implemented by the German Ministry of Environment, Nature Conservation and Reactor Safety to cooperate with the CENTRAL AND EASTERN EUROPEAN STATES and COMMONWEALTH OF INDEPENDENT STATES in the area of nuclear safety, a technical system to improve operational monitoring has been designed, specified and established since 1992 as a pilot project by the RESEARCH CENTRE ROSSENDORF and the TECHNISCHER ÜBERWACHUNGSVEREIN RHEINLAND with a significant contribution from the state scientific and technical centre of the Ukrainian supervisory authority in the Zaporozh'ye/Ukraine nuclear power plant.

The Zaporozh'ye nuclear power plant is located about 500 km south east of Kiev on the southern bank of the Dnieper River, which is dammed-up to the Kachovska storage lake. It has six uniform units of the type VVER-1000/V-320. With an electric output of 6,000 MW this nuclear power plant is the largest nuclear power generator in Europe at present.

The technical system complements existing operational checking and monitoring facilities by including modern means of information technology. It enables concentration on a continuous monitoring of the state of unit 5 in normal operation and in cases of anomalies or incidents so that when recognisable deviations from the regular plant operation occur, the Ukrainian supervisory authority can immediately inquire and if necessary impose conditions on the operator. The radiological and meteorological parameters at the nuclear power plant location are monitored to the extent necessary to assess the current radiation situation and to implement effective emergency management measures.

The parameters to be monitored were selected on the basis of German and international experience using the criterion of being able to observe and evaluate the adherence to the following four protection aims

- P1 Assurance of reactor shutdown
- P2 Assurance of core cooling
- P3 Assurance of heat removal from the primary circuit and assurance of its integrity
- P4 Assurance of the integrity of the containment

in connection with nine monitoring tasks which refer to certain parts of the plant, mediums, processes and plant conditions.

These monitoring tasks are:

- M1 General plant condition
- M2 Barrier effectiveness
- M3 Radioactivity inventories
- M4 Release of radioactive substances into the air
- M5 Immissions into buildings and surroundings
- M6 Registration of the meteorological conditions
- M7 Release of radioactive substances into water

[1]Technischer Überwachungsverein Rheinland

M8 Operational monitoring threshold values
M9 Plant condition in the event of anomaly or incident/accident.

While the protection aims for the various pressure water reactor types may be generally valid, the monitoring tasks are specially tailored for the Zaporozh'ye nuclear power plant.

The advantage of these procedures is that monitoring the protection aims in connection with control tasks is self-redundant and complements the monitoring of limit values and conditions of safe operation which the operator has to carry out in accordance with the operating instructions.

On the basis of the protection aim and control tasks concept
49 different safety related operational parameters of the core and unit
18 radiological parameters of the unit and the plant site and
6 meteorological parameters
are permanently and automatically recorded, monitored and evaluated.

Fig. 1 shows schematically the parameters which are selected for monitoring. The colors characterize different parts of the unit and the plant. The colors approximately mark the monitoring tasks but not the protection aims. For example the parameters indicated in the red-marked pressure vessel characterize the states of the nuclear process and of the primary circuit (part of the general plant condition M1). Additionally, they enable to observe the assurance of three protection aims: reactor shutdown (P1), core cooling (P2) and heat removal (part of P3). This fact demonstrates the complexity of the monitoring procedures: The actual values of the single parameters are compared with their limit values for various monitoring tasks. After that the results of the comparison are combined to logical information which makes it possible for final conclusions related to the assurance of the protection aims.

The technical system set up in the Zaporozh'ye nuclear power plant is hierarchically structured (fig. 2). The operational parameters are down-loaded by the TRANSFER COMPUTER UNIT 5 and the radiological and meteorological data by the TRANSFER COMPUTER AUXILIARY BUILDING 2. There they are checked, condensed individually or in monitoring-specific links to logical data channels and transferred as data packages at one-minute intervals to the SERVER and to the ON-SITE COMPUTER in the laboratory building. In the ON-SITE COMPUTER the process and plant status is evaluated by comparing the current data with monitoring-specific limit values and by combining the limit value violation of different parameters.

The monitoring-specific limit values generally lie above the operational tolerance values to prevent any restrictions of the operator's room for manoeuvre but necessarily below the approved limit values set by the authorities and below the load limit values specified by the manufacturers, respectively.

If no violation of the protection aims is found, the users receive an information data file every 10 minutes, only. Excess of threshold values causes a report to be sent to the users in the Zaporoge Centre (authority) and in the administration building (On-site-inspector and operator). In view of the importance and possible effects of excess, there are three different information levels called NOTICE 🗀, WARNING ☎ and ALARM 🔔.

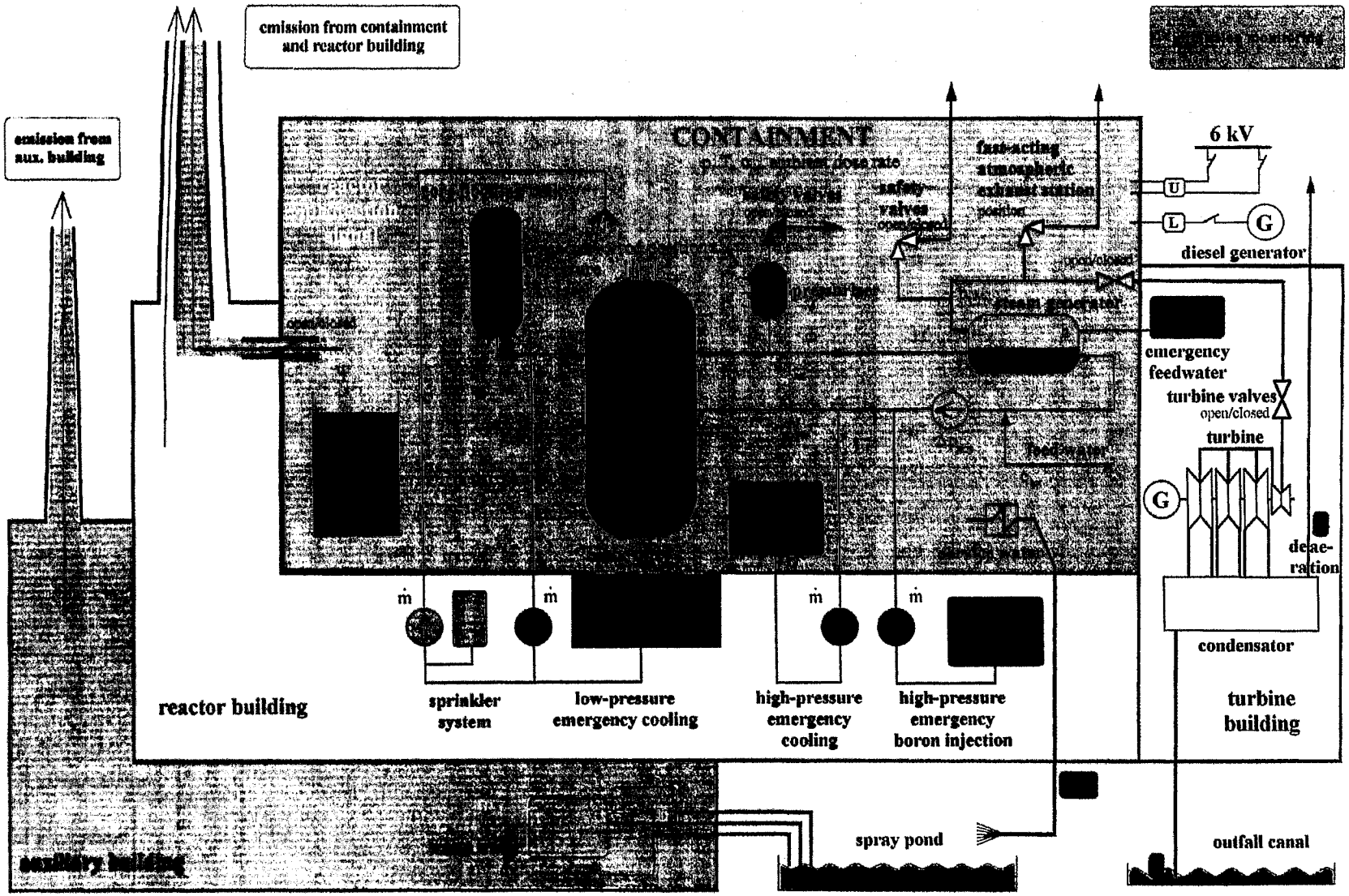

Fig. 1: Parameters selected for the operational monitoring and their assignment to systems and components

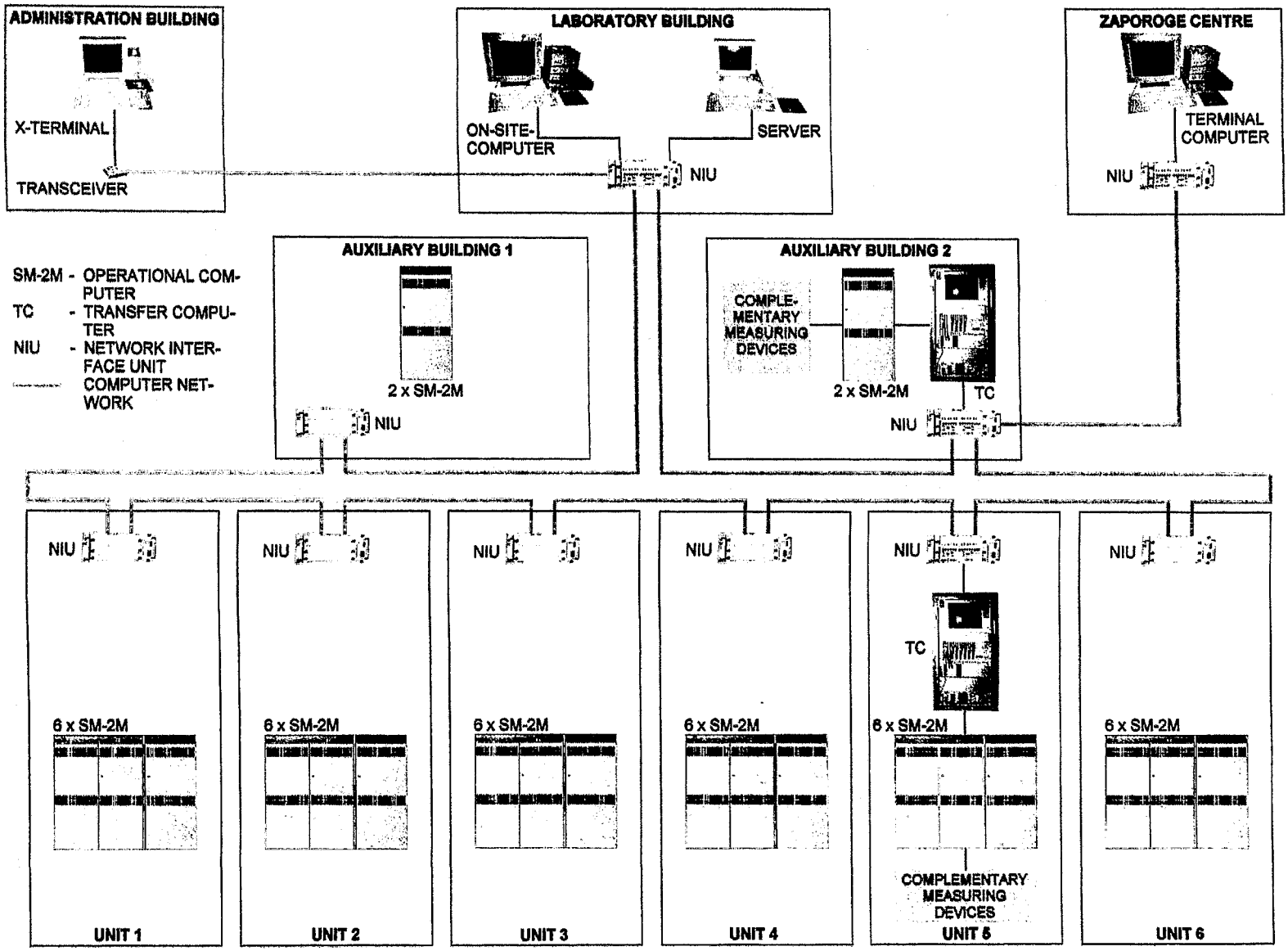

Fig. 2: The structure of the technical system

- A Notice is sent to the authority and the operator in the event of a breakdown in redundant measuring lines or safety systems if it reduces safety margins. The report consists of a short verbal communication on monitor and logging printer, the indication of the measuring point or the system and the repair deadline which must be complied with. The notice is automatically cancelled once the cause has been eliminated.

- A Warning is conveyed to the users in the event of a violation of at least one protection aim. It consists of verbal communication and signalling on the monitor, entry in a warning journal and the output of actual values and limit values for the monitored parameters which can be linked to the protection aim violation. This information should serve to give the trained specialist an overview of the process and plant status which emerged. The receipt of warning must be acknowledged by the users. A state of warning may only be cancelled when the authority gives its consent and no further protection aim violation has occurred for a fairly long period.

- An Alarm in the technical system is triggered if in case of a protection aim violation a process or plant status is reached which for safety reasons requires intensified monitoring. This is always necessary when incidents or accidents occur such as in the International Nuclear Event Scale INES for significant events in nuclear engineering installations. Whereas in all states from normal operation to warning the operational information is transmitted to the users at ten-minute intervals and the radiological-meteorological data at sixty-minute intervals, in the state of Alarm the intervals between two consecutive transmissions is shortened to one and ten minutes, respectively. Moreover, the conditions of the Warning state are valid, too.

Due to the above-mentioned different information levels the algorithms for the automatic evaluation are very complex. Additionally, the algorithms use different threshold values for different purposes to detect limit value violation and they combine the threshold overcrosses of different parameters for different conclusions. Therefore, the algorithms must be based on the actual values of selected parameters and their threshold violations compared with the values one minute before as shown for the parameter emergency flood tank level FTL in fig. 3.

Test operation of the technical system to improve operational monitoring, installed in 1995 with German support in the Zaporozh'ye nuclear power plant, was commenced at the end of 1995.

Following the completion of the user software by the scientific and technical centre of the Ukrainian supervisory authority and the operator, in which the German partners will participate in a consultative capacity, and the establishment of evidence of reliability under nuclear power plant conditions, the industrial testing phase of the system will be started in the middle of 1996.

The technical system is unique in terms of its effective monitoring of nuclear power plants with VVER-1000 reactors in the Central and Eastern European states and in the CIS. The modular and open structure of the system makes it possible to extend the monitoring to all six units and to connect more users.

Fig. 3: **Example of an algorithm of the automatic evaluation**
Parameter T-39, core flooding tank level (FTL), using two different threshold values ltv1 and ltv2 for minimum water level.

A NOTICE 🗀 is given to the users, if the actual value of the parameter FTL crosses the monitor-specific threshold values ltv1 or ltv2, independently of its positive or negative trend. Because of the safety relation of this parameter an information channel failure (ERROR) is equivalent to undercrossing the lowest threshold ltv2.

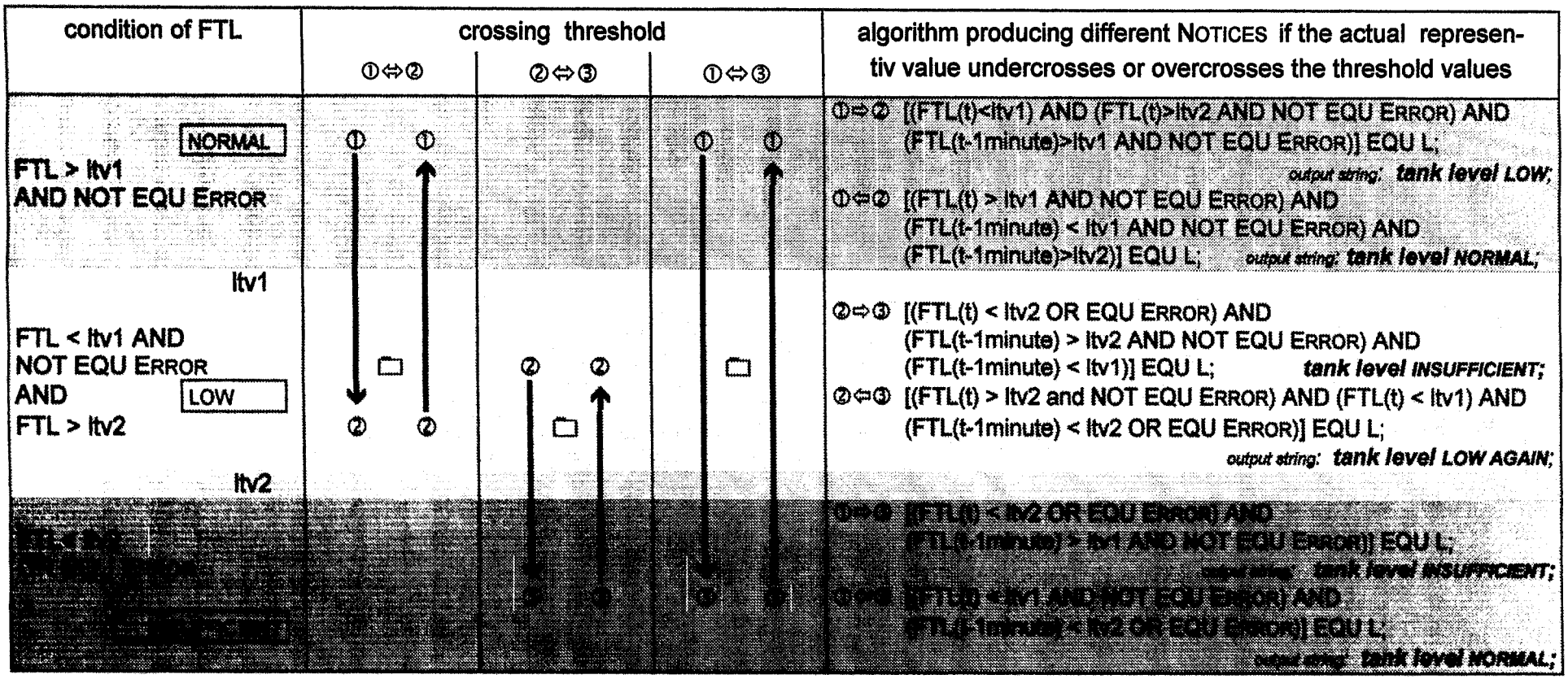

References

[1] M. Beyer, H. Carl, L. Langer, K. Nowak, P. Schumann, A. Seidel, P. Tolksdorf und J. Zschau
Aufbau eines technischen Systems zur Verbesserung der betrieblichen Überwachung der KKW durch die staatlichen Aufsichtsbehörden (Saporoshje).
Abschlußbericht zu den BMU-Vorhaben INT 9210/1und INT 9210/2, bestehend aus Kurzfassung, Anlage A: Textteil, Anlage B: Materialsammlung, Hrsg. Forschungszentrum Rossendorf e.V. und TÜV Rheinland, Köln, Dezember 1993

[2] M. Beyer, H. Carl, B. Schikora, P. Schumann, A. Seidel und J. Zschau
Aufbau eines behördlichen Fernüberwachungssystems zur betrieblichen Überwachung des KKW Saporoshje (Block 5), - 1. Realisierungsstufe -
Abschlußbericht zu dem BMU-Vorhaben INT 9219/2, bestehend aus Textteil und Anhangband, Forschungszentrum Rossendorf e.V., Dezember 1994

[3] M. Beyer, H. Carl, B. Schikora, P. Schumann, A. Seidel und J. Zschau
Lieferung von Investitionsgütern zur Erhöhung der Betriebssicherheit des Kernkraftwerkes Saporoshje, Betriebliche Überwachung, - 2. Realisierungsstufe -
Abschlußbericht zu dem BMU-Vorhaben PTI 6028, bestehend aus TEXTTEIL, Anlage A: FACHBERICHT, Anlage B: MATERIALSAMMLUNG, Forschungszentrum Rossendorf e.V., März 1996

This project is funded by the BMU (Bundesministerium für Umwelt, Naturschutz und Reaktorsicherheit) and is registered with No. PTI 6028.
The authors are responsible for the scientific content of the report.

A COMPUTER SYSTEM FOR THE EVALUATION OF CONTAMINATED SITES

W. Ferse, T. Reitz[1], U. Schneider

1. Introduction

In the last years contaminated sites have become a relevant problem in Germany. In Saxony about 20.600 sites are suspected to be contaminated. About 8.000 of them are old dump sites, 12.000 are former industrial and commercial sites and 600 are former military sites [1]. Additionally, the involved state offices are faced with the problem of radioactively contaminated areas caused by the former uranium mining in Saxony.

Now, intensive efforts are undertaken to start necessary and efficient remediations. Remediation planning has to be based on a systematic registration of suspect sites and on the availability of a uniform evaluation tool for environmental hazards.

2. The Environmental Information-System in Saxony

In order to solve the above described problems Research Centre Rossendorf (FZR - Forschungszentrum Rossendorf) together with the responsible institutions of the State of Saxony have built up a registration and evaluation system for sites which are suspected to be contaminated.

This system is to support the responsible state offices with the uniform evaluation of the hazard potentials of suspected sites or mines and with the preparation of analysis plans. Further, the system is to relieve the staff of their routine work and makes available the experts knowledge to them. Moreover, the system contributes to a standardisation of the evaluation process.

Figure 1 shows the structure of this system. The lines between the objects only represent the data flow. On-line data connections do presently not exist.

2.1 The Knowledge Based System XUMA

The knowledge based system XUMA is installed at the Saxon State Authority for Environment and Geology (LfUG - Landesamt für Umweltgestaltung und Geologie). XUMA is a joint project of the Institute for Applied Information Science (IAI - Institut für Angewandte Informatik) of the Karlsruhe Research Centre (Kernforschungszentrum Karlsruhe) and the State Authority for Environmental Protection of Baden-Württemberg (Landesanstalt für Umweltschutz Baden-Württemberg).

The main component of XUMA is a knowledge base consisting of two parts. The first part includes the criteria, tables and rules for the evaluation of contaminated sites. The second part relates different branches of industry with the corresponding types of

1. Technical University of Dresden

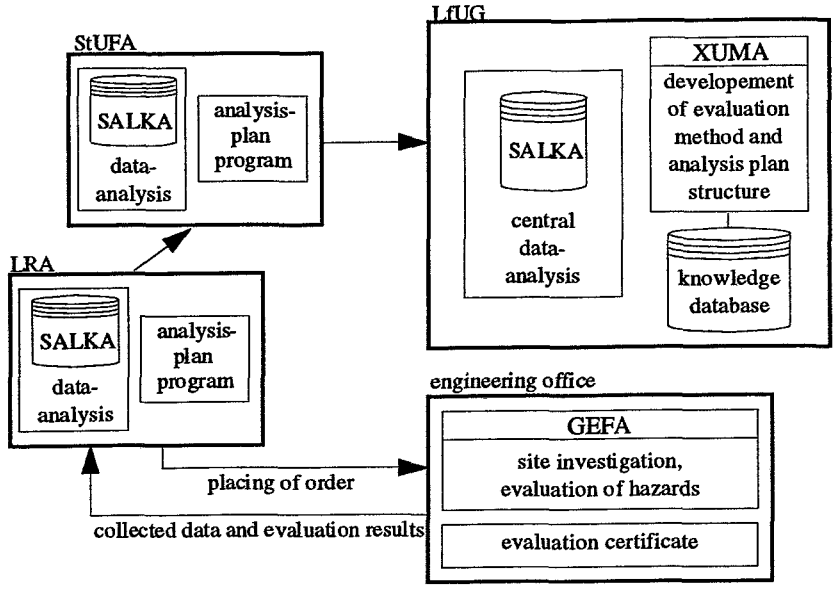

Fig. 1: Structure of the registration and evaluation system in Saxony

waste, toxic substances and analysis parameters. This part is the basis for the preparation of analysis plans.

Additionally XUMA provides a knowledge acquisition module. This module enables the expert user to modify and complete both parts of the knowledge base. The module allows the manipulation (addition, modification, deletion) of objects and rules without any experience in programming. Editable objects are for instance evaluation criteria, evaluation tables, evaluation rules, branches of industry and reference value tables.

The XUMA acquisition module even offers a Graphical User Interface. Rule editing is supported by an editor which represents the editable components in a natural language. So the system allows an easy permanent update of the knowledge base and to implement new parts of the evaluation method.

Now FZR in cooperation with the Technical University of Dresden has developed a program generator which enables to generate two programs from the XUMA knowledge base. These are the site-evaluation program GEFA and the program for analyis planning. That way, these two programs reflect the current state of XUMA's knowledge base. Both programs run under MS-Windows and do not need any additional software-environment or database. So they can be applied through the environmental offices responsible for the district (LRA - Landratsamt) and through any engineering office. Figure 2 shows the process of program generation. As displayed in this figure, also an additional file with the criteria structure is derived from the knowledge base. This file is used to update the data structure of the external database (SALKA) in which site specific investigation data are stored.

This paper only presents the program GEFA. The analysis planning program which is designed to derive an analysis plan for chemical and physical investigations is described in detail in several publications of the IAI [6,7,8]. The generation of analysis plans is based on the knowledge about the wastes comming up from different industries,

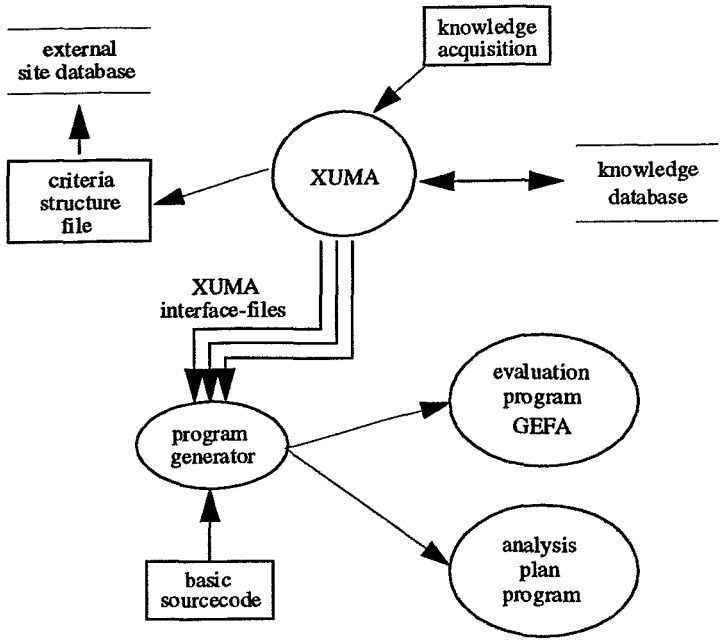

Fig. 2: Process of program generation

about the toxic substances and about appropriate analytical parameters for these substances. This knowledge is stored in the XUMA knowledge base.

2.2 The program GEFA

GEFA is developed for local use in engineering offices and LRAs. GEFA enables a systematic investigation, data acquisition and a uniform evaluation of sites suspected to be contaminated. At present the evaluation methods for the paths groundwater and soil are implemented.

Data acquisition and site evaluation is carried out by the involved engineering offices. GEFA offers a data acquisition tool, checks data consistency and evaluates the chekked data. The evaluation method used in GEFA will be described later. The GEFA output consists of different evaluation protocols and a set of interface-files. These interface-files contain all collected data and the evaluation results in a standard data exchange format. So they can be read into the central database-system SALKA. Figure 3 shows the dataflow around GEFA.

The protocols and the files are transferred to the LRAs. Each LRA of a governmental district stores the data in the database SALKA and transfers a copy to the responsible state office (StUFA - Staatliches Umweltfachamt). The StUFAs also transfer a copy of the received data to the LfUG. At LfUG the complete data of the State of Saxony are available.

2.2.1 The Evaluation Method

The evaluation method supports the first evaluation of sites suspected to be contaminated on the basis of limited informations. With this method it is possible to determine

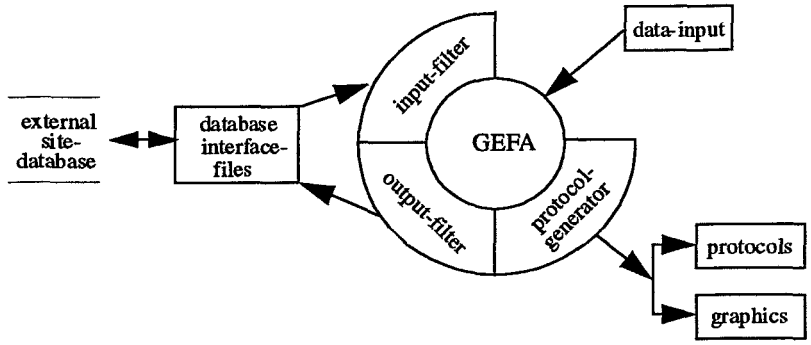

Fig. 3: Dataflow around GEFA

priorities with regard to the environmental hazard and to derive further investigation needs.

In Saxony four levels of evidence are considered during the evaluation of sites. The levels of evidence are characterised by the type of finished investigation. The levels of evidence are:

- BN1 historical investigation is finished (limited information completed with assumptions concerning the substances and the geological situation but without any chemical and physical analyses)
- BN2 orienting investigation is finished (more detailed information with a limited set of samples and chemical or/and physical analyses)
- BN3 detailed investigation is finished (detailed information concerning the substances, the transport of substances etc.)
- BN4 investigation for remediation is finished

The method implemented in GEFA is only useful for the levels BN1 and BN2.

For evaluation purposes, the environment near the site has to be subdivided into four different media to be protected (ground water, surface water, soil and air). For each of these media a separate evaluation has to be carried out. The evaluation method considers the contaminated site as the emission point and the media to be protected as the immission point. Big and nonhomogeneous sites can be separated into smaller areas, huge media to be protected can be separated into different objects. Figure 4 shows the possibilities of separation. GEFA can evaluate each combination of areas and objects. Such a combination is named evaluation object.

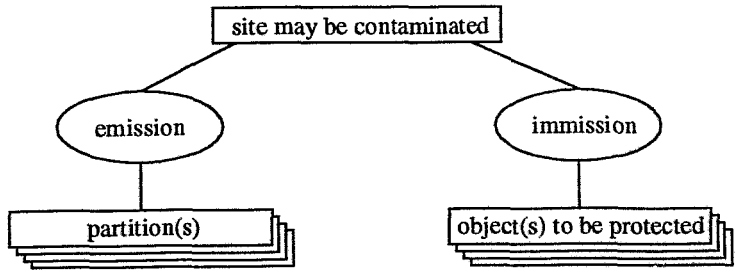

Fig. 4: Local structure of site

The method implemented in GEFA assesses the evaluation object relative to a domestic or industrial reference site. For that a set of evaluation criteria is defined. The GEFA-user can specify each of these criteria for the site he wants to evaluate. After that, GEFA assesses the specified criteria by means of the implemented rules and tables and determines criteria-specific risk values which are hazard-increasing or -decreasing factors relative to the defined reference site. In Saxony these risk values do not consist of single numbers but of a weighted average connected with an evaluation range (best/worst case). If the user is not able to specify a criterion because of the restricted available information about the site, GEFA uses a so called standard risk value with predefined average and range.

The evaluation criteria are categorized into five steps which have to be carried out sequentially. Each of these steps represents a kind of risk. The steps and their meanings are shown in figure 5.

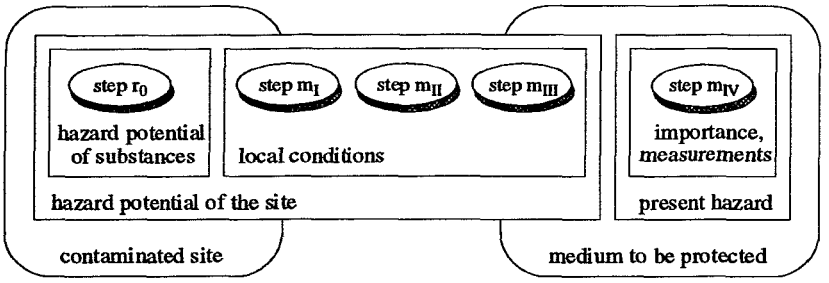

r_0 hazard potential of substances
m_I hazard-increasing by the transport of substances out of the site
m_{II} hazard-increasing by the transport into the medium to be protected
m_{III} hazard-increasing by the transport and effects of substances in the medium to be protected
m_{IV} significance of the medium to be protected, measurements

Fig. 5: Meaning of the evaluation steps

The evaluation steps are separately accomplished. In each step all risk value components (average, range) of all criteria are added. The calculated evaluation results of the steps are named r_0, m_I, m_{II}, m_{III}, m_{IV} corresponding to the step names. These five steps result in a numerical risk value r_{IV} of the site. The calculation of this site risk value r_{IV} is carried out in the following manner.

$$r_I = m_I * r_0$$
$$r_{II} = m_{II} * r_I$$
$$r_{III} = m_{III} * r_{II}$$
$$r_{IV} = m_{IV} * r_{III}$$

The mathematical operations are carried out for each component of the risk values separately. So also r_{IV} consists of a weighted average and a range:

$$r_{IV} = r_{IV,av}\ (r_{IV,best},\ r_{IV\ worst})$$

Depending on the level of evidence this risk value allows the following conclusions.

- The level of evidence and $r_{IV,worst}$ allow to derive the necessary kind of activity. Possible kinds of activities are:
  - A registration of site with no further investigations or inspections
  - B leave out of further investigations with the demand for an inspection after a certain time
  - C leave out of further investigations with the demand for continuous technical control measures
  - E further investigations are required (not enough information for decision)
- The risk value $r_{IV,av}$ determines the priority ranking among the different sites.
- The value of the range between $r_{IV,best}$ and $r_{IV\ worst}$ is a measure for the uncertainty of the result. This uncertainty results from the limited information. If all necessary information for a site were available the value of the range between $r_{IV,best}$ and $r_{IV\ worst}$ will become zero. The use of averages and ranges follows the principle that missing information must not lead to a lower risk value.

Figure 6 shows the dependence of the activities on the evaluation level and the risk value.

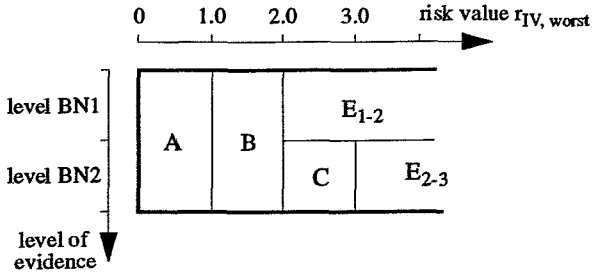

Fig. 6: Activity matrix

Activity E1-2 means that investigations and evaluation on level BN2 has to be executed. Activity E2-3 means that further investigation (level BN3) has to be carried out. These further investigations (level BN3) are not supported by GEFA.

The explanation for this step by step investigation method is that the costs for investigations rapidly increase from one level of evidence to the next one. With the help of this method many costs can be saved if actions A...C can be derived at a lower level of evidence.

3. The Application of the Program GEFA

The program GEFA includes the standard methodology for evaluation of sites suspected to be contaminated at lower levels of evidence (section 2.2.1, "The Evaluation Method"). GEFA was developed on behalf of the Environmental Ministry of Saxony.

The program system GEFA/XUMA is the official site-evaluation program of Environmental Ministries in the states of Saxony and Baden-Württemberg. This has become possible trough the concept of knowledge acquisition and program generation. GEFA uses the same methodology for both states, only the knowledge bases differ concerning the criteria and rules. In this way GEFA could also be applied in other states

provided that the same basic evaluation methodology is used as described in section 2.2.1, "The Evaluation Method".

GEFA 2.1, a first interim version without knowledge acquisition, has been applied in Saxony since the end of 1994. About 1.000 versions of GEFA 2.1 were handed out to LRAs, StUFAs and engineering offices. This version only includes the evaluation method for the medium groundwater. In December 1995 the development of GEFA 3.0 was finished. All user-experiences of version 2.1 have been taken into consideration during the development of version 3.0. This version offers the full functionality described in this paper. GEFA 3.0 will be applied in Saxony and Baden-Württemberg from the beginning of 1996. At this time the saxonian knowledge base will include the evaluation method for groundwater and soil.

References

[1] G. Müller
„Altlasten in den neuen Bundesländern: Horrorszenarium oder Herausforderung und Chance", Vorträge zum V. Sächsischen Altlastenkolloquium, Oktober 1994, Coswig

[2] W. Ferse, Th. Reitz, F. Schröder
Anwenderhandbuch GEFA für Windows Version 2.1 in Handbuch zur Altlastenbehandlung, Teil 3, Anlage 7, Sächsisches Staatsministerium für Umwelt und Landesentwicklung, 1994

[3] W. Ferse, Th. Reitz, F. Schröder
Anwenderhandbuch GEFA für Windows Version 3.0, Forschungszentrum Rossendorf, Institutsbericht, 1995

[4] W. Ferse, Th. Reitz, F. Schröder u.a.
„Spezifikation des Altlastenbewertungsprogramms GEFA", Forschungszentrum Rossendorf, Institutsbericht, 1995

[5] W. Ferse, Th. Reitz, F. Schröder u.a.
Struktur der Bewertung in XUMA und GEFA, Forschungszentrum Rossendorf, Institutsbericht, 1995

[6] R. Weidemann, W. Geiger, M. Reißfelder
XUMA-PC (Analysenplan) - Struktur; Forschungszentrum Karlsruhe, Institut für Angewandte Informatik, Institutsbericht, 1995

[7] R. Weidemann, W. Geiger, M. Reißfelder
XUMA-PC (Analysenplan) - Benutzungsschnittstelle; Forschungszentrum Karlsruhe, Institut für Angewandte Informatik, Institutsbericht, 1995

[8] W. Geiger, G. Osterkamp, R. Weidemann
„Assessment and evaluation of former industrial sites with the aid of the XUMA expert system"; UNPE Industry and Environment, Vol. 14, No. 3, 1991

[9] Gefährdungsabschätzung Pfad und Schutzgut Grundwasser (1994) Handbuch zur Altlastenbehandlung, Teil 3, Sächsisches Staatsministerium für Umwelt und Landesentwicklung, 1994

[10] R. Weidemann, W. Geiger, M. Reißfelder
Die Struktur der XUMA-Wissenserwerbskomponente für den Bewertungsteil, Forschungszentrum Karlsruhe, Institutsbericht, 1995

THERMOCAPILLARY PHENOMENA AT FREE LIQUID SURFACES OR LIQUID-LIQUID INTERFACES

V. Galindo, G. Gerbeth, V. Kolevzon, J. Priede

1. Introduction

Interfacial tensions of any kind can cause considerable fluid flows at liquid-liquid interfaces, besides the usual buoyancy driven convection. Such tensions can be due to temperature or concentration gradients, and via the interface tension dependence on these quantities a fluid flow driving force occurs which, in turn, can lead to serious bulk motions. Flows of this kind are called Marangoni flows, or thermocapillary and solutocapillary flows, respectively. It turned out that Marangoni flows play an important role in many technological processes like crystal growth from the melt, two-phase flows, welding processes, etc. Many fluid flow experiments in Microgravity research programmes are devoted to study these flows since under earth conditions they are difficult to investigate due to the dominating buoyancy convection. In the following we summarize the related research projects performed in the MHD group.

2. Marangoni driven bubble motions

If a liquid drop is placed in another matrix fluid a buoyancy independent drop motion occurs if a temperature gradient is applied to the matrix fluid. This driving mechanism can have a serious, even dominating effect in many materials processing technologies and can be used e.g. in order to prevent sedimentation of a heavier component in various alloy production processes.

The research project briefly described here is focused on basic research of single thermocapillary bubble motions. It is performed in close co-operation with the "Zentrum für angewandte Raumfahrtforschung und Mikrogravitation (ZARM)" Bremen. Gravity free experiments are performed at the Bremen drop tower, numerical simulations at the FZR.

The phenomenon of thermocapillary bubble motion is determined by two independent parameters: the usual Reynolds-number Re and the Marangoni-number Ma (which is proportional to the applied temperature gradient and the coefficient of surface tension temperature dependence). A numerical finite difference code was developed in close cooperation with the Technion Haifa (Israel) for general (Re, Ma) values, but limited to the stationary case. A typical result is shown in figure 1. For increasing Marangoni number an increasing temperature tail occurs after the rising bubble which strongly determines the bubble rise velocity. Good agreement was found between numerical simulation and the drop tower experiments as published in [1]. The project is in continuation, focusing now on the unsteady drop motions and the motion of liquid metal drops.

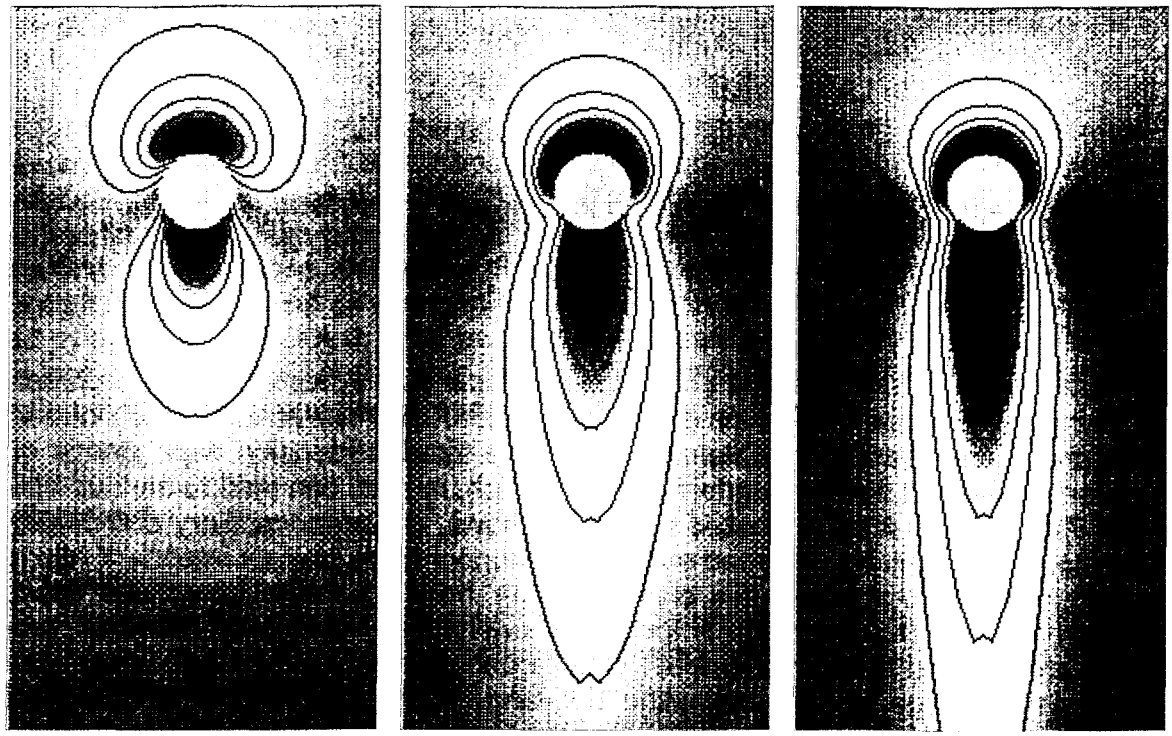

Fig.1: Isolines of the perturbation form uniform temperature gradient for Pr=10 and different Marangoni numbers.

3. Absolute-Convective instabilities

The theoretical analysis of fluid flow instabilities in convectively driven motions in plane fluid layers is usually divided into two approaches:

A) theoretical analysis of the academic problem of an infinitely extended layer,
B) numerical analysis of the real experimental situation with limiting sidewalls.

Case A was up to now limited to the analysis of convective instabilities which are transported with the mean flow, and are likely not the observable ones in a wall bounded real experiment. For a better physical understanding it would be highly desirable to establish some bridge between A and B, i.e. to develop a theoretical description which keeps the 2D modelling of case A but takes into account the limiting and reflecting influence of any real side walls as in case B. Such a bridge is possible using the concept of absolute instabilities where a vanishing group velocity of the critical wave disturbance is required. Here this approach was applied for the first time to a buoyancy-thermocapillary driven flow in a liquid layer heated from the side. First results of this new concept were published in [2]. They lead to a much better agreement between theoretical infinite-layer predictions and experimentally observed instabilities, as shown in figure 2. It is surprising that the usual convective type of instabilities cannot even qualitatively describe the observed instabilities since it does not predict any multicellular convection. Contrary, the absolute instability approach can distinguish between steady and oscillatory instabilities and shows a good agreement with the experiment.

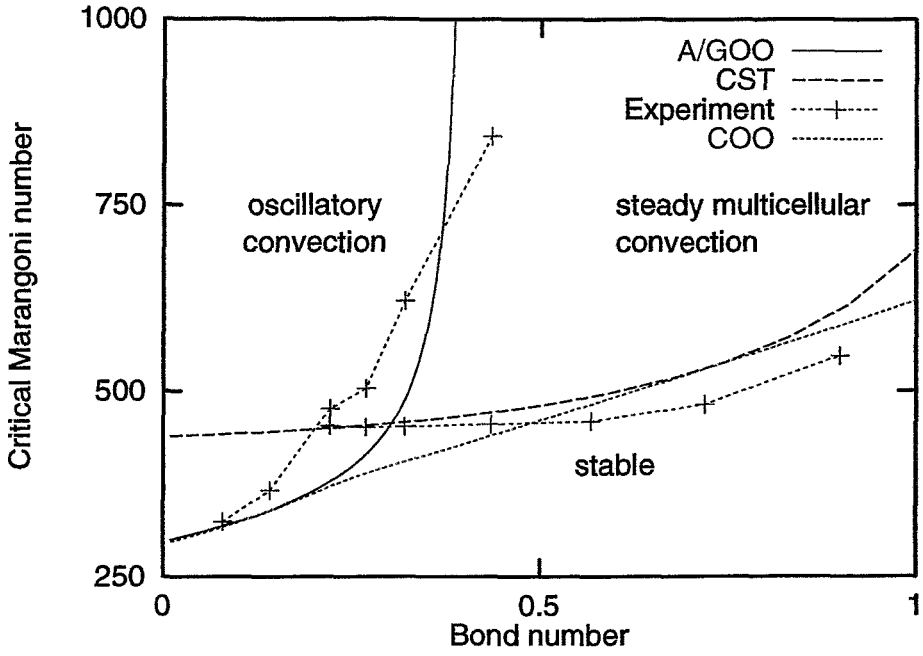

Fig 2: Experimental and theoretical critical Marangoni number for the onset of both steady multicellular (CST) and oscillatory convection (A/GOO) depending on the Bond number for 1 cSt silicon oil (Pr=13.9). Convective Oblique (COO) wave instability threshold is provided by the conventional theory.

4. Marangoni experiments at a free gallium surface

Almost all experiments on thermocapillary motions were performed with "usual" liquids (alcohols, silicon oils, etc.) possessing a Prandtl-number Pr larger than one. However, most of the materials processing problems contain Pr<<1 liquids like liquid metals or semiconductor melts. Nearly no experimental data exist on Marangoni motions for this class of liquids.

Therefore, a research project was initiated in the MHD group to built up special containers, filled with a free surface liquid metal and allowing flow measurements induced by the application of an external temperature gradient. The crucial problem for this task is to prevent oxidation of the liquid metal layer since a free surface is the essential precondition for any Marangoni flow measurements. This project was performed in close cooperation with the Institute of Physics Riga (Latvia). The experts in Riga developed a sophisticated, but clever solution of this problem by the idea of a Finite Volume Vacuum Technique. For details we refer to [3,4]. This technique gives for the first time the possibility to analyse the hierarchy of Marangoni flow phenomena in a Pr<<1 liquid. In fact, an axisymmetric basic flow and an oscillatory regime at higher temperature gradients were found as expected by videorecording tracer motions on the liquid gallium surface. Surprisingly, a second non-axisymmetric stationary flow regime was found in the experiments, too. In addition, the flow direction of the axisymmetric basic flow was not the expected one, which can be explained only by an unusual, positive temperature coefficient of the liquid gallium surface tension.

5. Laser light spectroscopy of liquid surfaces

The precise knowledge of material properties like viscosity or surface tension is crucial for any profound analysis and handling of liquid melts. It is really surprising which lack of data still exists today for liquid metal/liquid alloy melts. For instance, the scatter found in literature for the surface tension temperature derivative of liquid gallium is up to the sign! Therefore, it was decided to built up an own measuring technique in order to determine liquid properties. The Laser Light Scattering (LLS) technique was chosen as it is described in [5]. This relatively precise technique is attractive since it allows not only to measure surface tension and viscosity, but also typical surface quantities (elasticity modulus, surface viscosities) if some layering of any kind (oxide film, melt-vapour layering, lipid monolayers) is present at the liquid surface. This optical system was built up and tested with well-known liquids like ethanol showing exact agreement with the literature data for surface tension and viscosity. First measurements with the gallium containers described above confirm the positive temperature coefficient of the gallium surface tension already to be concluded from the Marangoni flow measurements.

It is worth to emphasize that the LLS experimental stand is not limited to liquid metal measurements, but could serve as unique measuring possibility for a lot of chemical systems as well.

References:

[1] M.Treuner, V.Galindo, G.Gerbeth, D.Langbein, H.J.Rath
Thermocapillary bubble migration at high Reynolds and Marangoni numbers under low gravity.
Accepted at: J.Colloid Interface Science, New York, August 1995

[2] J.Priede, G.Gerbeth
Convective, absolute and global instabilities of thermocapillary-buoyancy driven flows in a horizontal liquid layer. Lecture at: American Physical Society, 48th Annual Meeting of the Division of Fluid Dynamics, Irvine, 20.11.95; Bulletin of the American Physical Society, Series II, Vol.40, No.12, 1995, p. 1955-56

[3] G.Gerbeth
Experimentelle Realisierung einer freien Flüssigmetalloberfläche.
Machbarkeitsstudie. Abschlußbericht für DARA GmbH, September 1995

[4] A.Bojarevics, Yu.Gelfgat, G. Gerbeth
Testing of a new experimental technique to study MHD associated phenomena with free liquid metal surface. Lecture at: MAHYD95, 14th Int. Conference on Magnetohydrodynamics, Riga, August 1995

[5] D. Langevin
"Light scattering by liquid surfaces and complementary technique"
Marcel Dekker, New York, 1992

The projects this report is based on are funded by the German Space Agency under 50 WM 9324, 50 WM 9213, by the Israeli-German Foundation under I 0284-046.10/ 93 , and the Programme "Wissenschaftlich-Technische Zusammenarbeit" of BMBF under X092.3.
The authors are responsible for the scientific content of the report.

1000 ROOFS PHOTOVOLTAIC PROGRAMME - RESULTS IN SAXONY

U. Rindelhardt, G. Teichmann

1. Introduction

More then 2000 small grid coupled PV systems (total power 5.2 MW) were installed in Germany in the frame of the 1000 roof photovoltaic programme between 1991 and 1994. About 10 % of the power are located in Saxony (see Fig. 1). The aims of the programme were to get know-how in design, installation and operation of such systems. This paper summarizes the main results reached in Saxony, for details see [1].

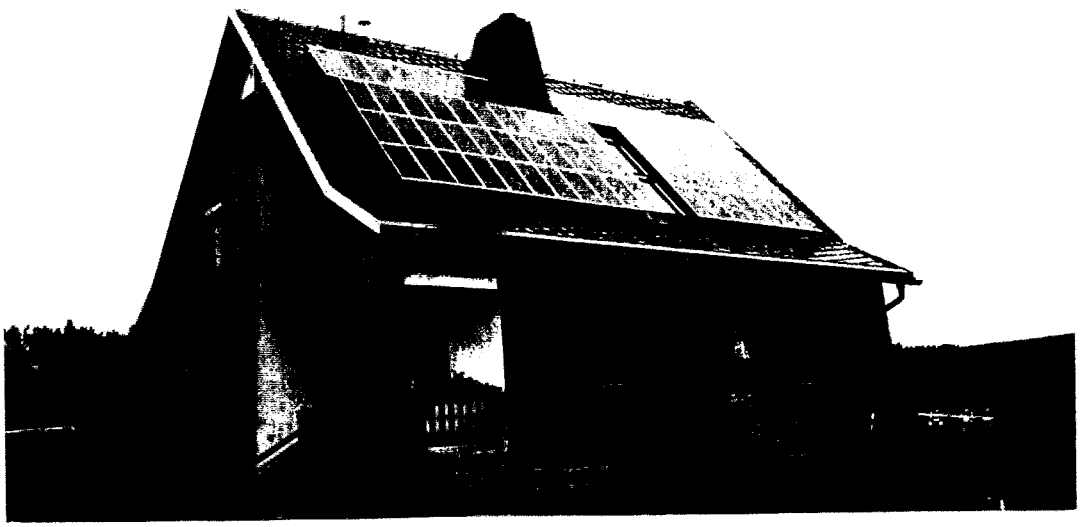

Fig. 1: Grid coupled PV system mounted on the roof of a one family house

2. Irradiation conditions in Saxony

Fig. 2 shows the regional distribution of the annual irradiation measured in the tilted modul planes in the years 1993 and 1994. For the most parts of Saxony typical irradiations between 1000 and 1100 kWh/m² were found. Only in higher regions of the Erzgebirge the irradiation decreases below 1000 kWh/m², and in the north west parts of Saxony the annual irradiation is more than 1100 kWh/m². In contrast to earlier results [2] in the region around Leipzig the highest irradiation was measured. Generally the saxon irradiation values correspond to the mean irradiation values in Germany.

An important problem for large scale use of photovoltaic energy is the synchronity of the insolation in greater areas. A small geometric correlation length can be used for a regional compensation (or stabilization) of photovoltaic energy over a greater area. Fig. 3 shows the daily irradiations measured at 4 different locations in Saxony (locations see

Fig. 1) during a typical summer month in 1994. A large degree of synchronity was found, only during few days a "compensation" between the locations is visible. Remarkable daily compensation effects can therefore be excluded in Saxony (area about 18000 square kilometers). This conclusion holds stronger in the territory of the regional energy suppliers. A possibly increasing use of photovoltaicly generated energy is therefore connected with new demands on the power and load management in the electrical grids and conventional power stations.

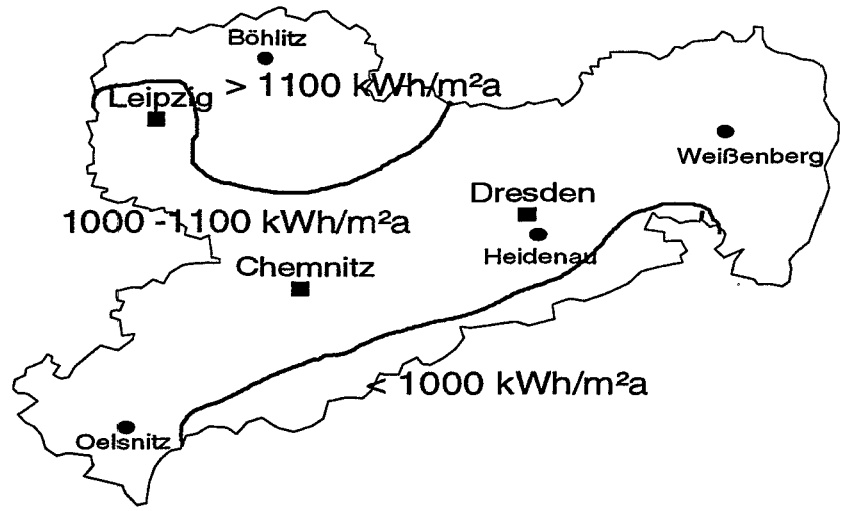

Fig. 2: Distribution of the annual irradiation in Saxony at tilted module planes (measurements in 1994 and 1995)

3. Solar energy generation

For comparing the results of different PV systems the photovoltaic energy EPV is usually rated to the PV generator power PN. The final yield YF is defined by

YF=EPV/PN.

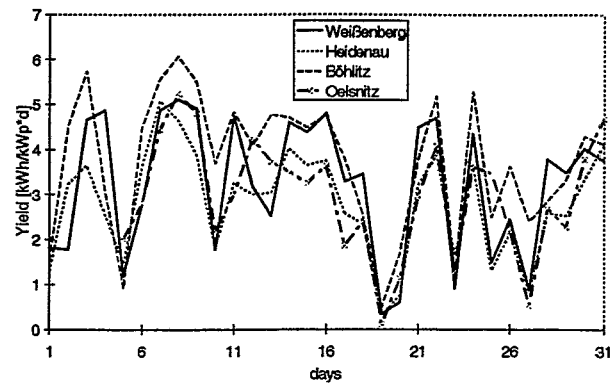

Fig. 3: Synchronity of the daily PV energy produced by 4 PV systems

Fig. 4 shows the mean monthly course of the yield for all investigated systems during the years 1993 to 1995. The saisonal courses follow directly the particular irradiation. The monthly differences between different years reach 30 %. A mean annual yield of nearly 690 Kwh/kWp was found in all the years. The yield differs remarkably (up to 20%) between the investigated systems , which indicates weak points in the used components.
The measurement of the irradiation G in the modul plane allows a deeper analysis of the photovoltaic energy generation. The Performance Ratio PR is defined

PR=EPV*G/PN*HSTC

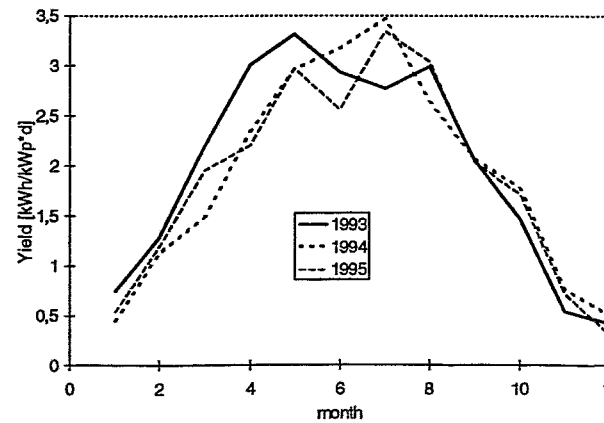

Fig. 4: Saisonal course of the Yield

with the irradiance HSTC=1000 W/m² at standard test conditions. The Performance Ratio is a measure of the energy losses caused by meteorological reasons and by the properties of the system components. The annual mean values of PR measured at 20 systems were found to be 67 % with a weak saisonal dependence. Fig. 5 shows the saisonal course of PR measured at 5 systems equipped with the same module type (M55,Siemens Solar). The annual mean PR of 79 % is clearly higher than the mean value of all monitored systems. However, the conspicuous systematic differences between the systems indicate specific energy losses in the individual systems. The visible decreases of PR in some summer months are connected with system failures (mostly caused by inverters), during the winter months the snow covering of modules results in low PR values. The Performance Ratio is therefore a very sensitive indicator for the efficiency of a PV system. For the interpretation of the differences visible in Fig. 4, the measurement of the PV generator and the inverter efficiencies are needed.That will be done in the next years.

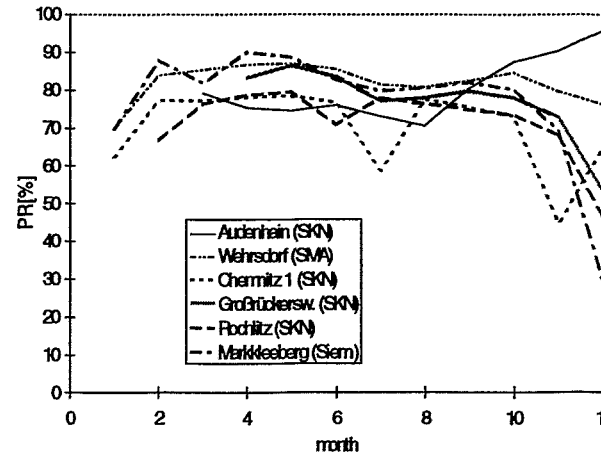

Fig. 5: Saisonal course of the performance Ratio (systems with identical module types)

4. PV energy use in private households

The use of photovoltaic energy by the private owners of the PV systems is described through the solar fraction fs

fs=EPV/EV

with the total annual energy consumption EV and the direct use fraction fd

fd=(EPV-E+)/EPV

with E+ being the energy supplied to the grid (i.e. surplus energy at the moment of generation). At fixed size of the PV system (it determines the energy production EPV) both given parameters depend on the total energy consumption (economic or generous use of energy) and on the synchronity between the private energy demand and the solar energy production.

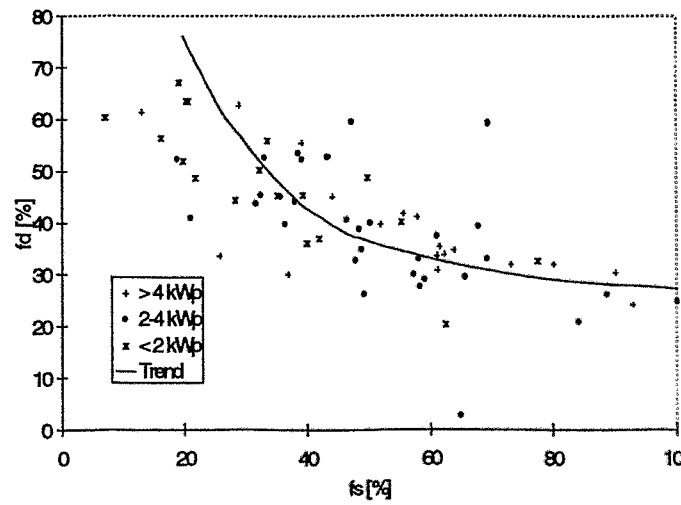

Fig. 6: Direct use fraction as function of solar fraction (90 private households,Saxony 1994)

The investigations showed, that the annual energy demand of private households living in one or two family houses can be covered by PV systems even in Germany (fs=100%). A 5-kWP-system produces 3500 kWh/a, which is clearly above the mean electricity

demand of german households. With contemporary techniques such a PV system needs a roof area of only 50 m².

Fig. 6 shows the dependence of the direct use fraction from the solar fraction measured at more than 90 systems in 1994.The indicated mean curve shows, that only for (energetically minor) solar fractions of lower than 30 % a direct use of about 60 % can be found. Consumers with high solar fractions reach small direct use fracions only. In this case the important role of the public grid as "energy store" is obvious.

5. Conclusions

In the frame of the 1000-roof-photovoltaic-programme in Saxony 150 grid coupled PV systems with different technical designs were installed. The presented results demonstrate the technical potential of such systems for future energy supply. Some identified deviations in the performance of the systems have to be investigated in more detail. The demands on the future grid management caused by the operation of "semistochastically" generating PV systems could be deepely clarified.

References

[1] U. Rindelhardt, G. Teichmann, D. Lang
Projektabwicklung und Ergebnisse des Bund-Länder_1000-Dächer-Photovoltaikprogrammes in Sachsen
FZR-Report 109, Sept.1995

[2] Meteorologischer Dienst der DDR
Klimadaten,Reihe B, Band 3:Strahlung und Bewölkung. 1. Sonnenstrahlung auf horizontale Flächen, Potsdam 1981

The project this report is based on was funded by the BMBF (Bundesministerium für Bildung, Wissenschaft, Technologie und Forschung, number) and by SMWK. The authors are responsible for the scientific content of the report.

Short Contributions

Investigation of thermo-fluiddynamic single effects

E. Krepper
H.-M. Prasser
H. Ringel
W. Zippe

Participation in thermal hydraulic tests

In 1995 natural circulation experiments were carried out at the Russian ISB-VVER test facility. They were initiated and scientifically planned by the Institute of Safety Research. Pre-test calculations were performed with the thermal hydraulic code ATHLET. The experiments aimed at the study of the natural circulation for 100 and 200 kW core power, which corresponds to decay heat removal conditions of VVER-1000 reactors. In addition to the standard instrumentation, needle shaped conductivity probes of RCR were applied to measure the void fraction. The results have shown significant flow instabilities. Their nature was explained by model calculations. Two types of instabilities were found: A periodic loop seal clearing and oscillations caused by density waves.

In cooperation with the Engineering Faculty of the Technical University Dresden natural circulation instabilities were investigated at the DANTON test facility. Again, needle shaped conductivity probes were applied. The possibility of geysering in boiling water reactors was studied in detail.

N. Kossok
H.-M. Prasser
P. Schütz

Development of pattern recognition methods

Pattern recognition methods are used to evaluate the capability of ultrasonic transmission signals for two-phase flow measurements. The work was concentrated on the elaboration of a complex programme environment for the test of pattern recognition methods. Experiments at the new two-phase test loop were started. A linear auto-regressive prediction model was found to be optimal for extracting the components of the pattern vector. This method provided correct identification rates of up to 90%. The results are the basis for the development of an ultrasonic measuring device, which is able to determine the volume flow rates of both the liquid and the gaseous phase simultaneously.

supported by BMBF

F. Hensel

Application of radio tracers

The features of Positron Emission Tomography (PET) were studied concerning their applicability for two-phase flow measurements. The work was focused on the measurement of the density in foams using solid positron sources, and on the observation of mixing phenomena in a bubbly flow by introducing liquid tracer solutions. For the density measurement, experiments with solid foams were performed. It was shown that due to the small mean free path of the positrons densities down to 20 kg/m^3 can be measured without problems even if comparatively massive walls of pipes or vessels have to be penetrated. This is the outstanding advantage of positrons, which generate well penetrating gamma-radiation when they annihilate. Based on the experimental data an optimized sensor configuration for density measurements is under development.

Concerning the use of liquid tracers, experiments on turbulent mixing in the liquid phase of a bubbly flow were carried out. The transient distribution of the tracer concentration was visualized. The measurements are being evaluated. Additionally, preliminary tests on liquid drainage in a cell foam were performed.

A. Böttger
H.-M. Prasser

Development of conductivity probes for two-phase flow measurements

A special kind of a needle shaped conductivity probe for the diversieve water level detection in boiling water reactors was developed. Test pieces of the probes and the related electronics were manufactured and tested under reactor-close conditions (7 MPa, saturated water). The level detector will be installed in a test facility at the site of a German BWR.

contracted with the industry

D. Baldauf
H.-M. Prasser
P. Schütz
G. Tamme
W. Zippe

Two-phase flow lab

The two-phase flow loop for the test and calibration of measuring methods was completed for operation with air-water mixture at atmospheric pressure. It is equipped with flow meters for both phases before mixing. The volume flow densities can be varied in a wide range (air: 0 - 12 m/s, water: 0 - 4 m/s). The profile of the volumetric gas fraction is displayed by an array of 8 needle shaped conductivity probes located at different radial positions. The operation with steam-water mixture is being prepared (heating power 20 kW). The design pressure of the loop is 2.5 MPa.

A small scale facility for the investigation of depressurization processes in chemical reactors was built up and used for pressure relief tests. The runaway reactions were simulated by a simple carbonate decomposition reaction. Emphasis was given to the characterization of the influence of surface active components upon the discharge of the liquid phase due to entrainment effects. It was found that even low-molecular-weight alcohols in a concentration range of 1% can lead to a drastic increase of the entrainment. This has to be considered in the design of pressure relief systems.

Thermalhydraulics and neutronenkinetics for accident analysis

U. Grundmann
D. Lucas
S. Mittag
U. Rohde

Coupling of the thermo-hydraulic code ATHLET with the 3D neutron kinetic core model DYN3D

The reactor core model DYN3D was coupled with the ATHLET thermal hydraulics code in two basically different ways. In the so called internal coupling, the neutron kinetics part of the DYN3D code replaces the 1D kinetics of ATHLET. This requires high software efforts. In the external coupling, the whole core is cut out from the ATHLET plant model and is completely described by DYN3D. The values of pressure, mass flow rate, enthalpy and boron concentration at the bottom and at the top of the core have to be transferred between the codes. This coupling is effectively supported by the

General Control and Simulation Module (GCSM) of ATHLET. Almost no changes of the single programs are necessary. For plausibility testing of the code coupling, comparative calculations between point kinetics, internal and external coupling were performed.

In addition to coupling with ATHLET, further improvement and validation of DYN3D was accomplished including:

- development of a DYN3D option for fuel cycle calculations, improvement of core loading description, and control rod modelling,
- extension of the neutron physical data base by including the KASSETA macroscopic cross section library,
- extension of the coolant mixing model for downcomer and lower plenum for variable mass flow rates,
- participation in the 3rd Benchmark task of the "Atomic Energy Research" association for dynamic code validation,
- comparison of calculated reactor parameters (reactivity coefficients, effectiveness of control rods, critical boron concentration) with measured values from unit 5 of NPP Saporoshje (in the frame of a support project of the BMU for the Nuclear Regulatory Authority of the Ukraine).

supported by BMBF and partially by BMU

U. Grundmann

Development of a DYN3D-version for quadratic fuel assemblies

Based on the computer code DYN3D for transient analyses of reactors with hexagonal fuel assemblies a new neutron kinetic model developed for quadratic fuel assemblies was implemented. The application of parallel processors for the solution of the complex 3-dimensional neutron kinetic equations with the help of a nodal method was taken into account by using a special scheme for inner iteration. Steady state calculation of neutron fields on a 4 processor workstation SUN SPARC 10/514 show a speedup being close to the theoretical value.

An important step of code validation was the participation in the NEACRP rod ejection benchmarks for PWR. A good agreement with the published reference solutions was obtained for different power levels and control rod positions. Calculation of cold water injection and overpressurization transients in a BWR were carried out. Since no reference solutions exist the results were compared with other solutions. The DYN3D results are comparable with the most realistic results provided by the other codes.

E. Krepper
U. Rohde
F. Schäfer

Verification of the thermal hydraulic system code ATHLET

The Institute for Safety Research contributes to the verification of the system code ATHLET. The work is based on the recommendations of the International Working Group on Verification Matrix for Thermal Hydraulic System Codes applied for VVER analysis. A series of post-test calculations of experiments at different integral test facilities was performed. Concerning the Russian type VVER-1000 reactor, the ISB-VVER is the only available test rig up to now. It is located in Elektrogorsk near Moscow. The scaling ratio is 1:3000. During the past, post-test calculations were conducted for

hot and cold leg break tests with small leaks and different injection modes of the high pressure core cooling system. During 1995, the natural circulation test (mentioned under "participation in thermal hydraulic tests") was analyzed. It was shown that ATHLET is able to describe the transient behaviour in satisfying agreement with the experiments.

Further, post-test calculations were made for a 1%-cold leg break test at the Hungarian test facility PMK with primary bleed. The natural circulation instabilities, which occurred during the test were analyzed in detail. The results were compared with RELAP calculations, which were carried out by AEKI Budapest. Finally, the detailed analysis of the IAEA Standard Problem Exercise SPE-4 (7% cold leg break with failure of the high pressure injection system) was completed. Secondary bleed and feed was presumed as an accident management measure. The influence of different nodalization in ATHLET was studied.

A. Aszodi
T. Kern
D. Lucas
H.-M. Prasser
U. Rohde
C. Schneider

Simulation of thermo-fluid dynamic processes in chemical engineering
Investigations on thermo-fluid dynamic processes in chemical reactors and storage tanks were carried out using 1D and 2D fluid flow models developed in the RCR and the 3D computational fluid dynamics code FLOW3D.

Further activities were concentrated on depressurization process simulation and foam behaviour. By means of a 1D thermo-fluid dynamics model, experiments of the University Hamburg-Harburg on depressurization of CO_2 gas-liquid systems were reproduced with good agreement. The development of an advanced theoretical model for the simulation of blow down systems was started (supported by Volkswagenstiftung).

Concerning foam modelling, a partial model for cell foam has been elaborated. This model will be integrated into a 1D thermo-fluid dynamics code for the simulation of blow down processes. Depressurization processes of chemical reactors have to be optimized aiming at fast and effective pressure decrease with minimum mass discharge out of the reactor vessel. Foams can influence the depressurization rate significantly because of liquid entrainment into the discharge line. It is also important for the efficiency of gas removal and natural circulation in electrolytic cells. A two-bubble-class model was developed. It has been tested against experimental data from an experimental mock-up. The work is supported by UHDE GmbH and will be continued.

Another safety relevant problem in chemical technology is the heat-up rate of liquids in storage tanks in case of external fire. An own 2D fluid dynamics code and the code FLOW3D revealed that the process of heat-up is basically different for bottom and side wall heating. The calculations provided a consistent understanding of experimental results obtained in VKTA.

partially supported by VW Foundation and the industry

Materials safety

H.-W. Viehrig
W.-D. Leonhardt

Setting-up of a radioisotope laboratory for mechanical testing

For testing radioactive material specimens from reactor pressure vessels or from internals an appropriately licensed radioisotope laboratory is needed. The rebuilding of such a laboratory which has to meet the requirements of the German licence procedure is going on. Design and building conditions were examined by the TÜV experts. The concept provides the capability to perform Charpy V impact tests, static and dynamic fracture mechanics tests, and tensile tests. The construction of the containment for the testing facilities has been finished. All preparative work to develop the testing techniques has been accomplished, too. Thus, the cold tests can immediately be started after the installation of the containment is completed.

U.Bergmann
J. Böhmert
H.-W. Viehrig

Correlation between mechanical and fracture mechanics parameters

In the framework of a joint project with BAM Berlin, University Magdeburg, and University Bergakdademie Freiberg correlations between mechanical and fracture mechanics parameters were investigated for ductile pressure vessel steels. The contribution of the RCR was the examination of the influence of irradiation. In 1995 preliminary work was performed. It included the takeover of irradiated specimens from the Rheinsberg NPP, decontamination, and deposition of the specimens. Moreover, the neutron fluence monitors were dismantled and prepared for evaluation.

Since on the one hand the establishment of reliable correlations between mechanical and fracture mechanics parameters must be based on a representative number of tested specimens, and on the other hand the amount of irradiated material is very restricted a special reconstitution procedure was developed. This reconstitution technique allows to produce new specimens from already tested half Charpy-V probes and so to triple the number of available tests.

Due to a newly developed short-time welding technology and to electro-erosive machining the reconstituted specimens possess the same mechanical properties as the original Charpy-specimens.

supported by BMBF

U. Bergmann
F. Bergner

Determination of crack resistance curves

In elasto-plastic fracture mechanics several methods for determining stable crack resistance curves are applied. Ultrasound is appropriate for "nondestructive" in-situ measurements of crack propagation and has some well-known advantages over other single-specimen methods (compliance, electric potential method). The basic phenomenon for crack growth monitoring in this technique is the diffraction of ultrasound at the crack tip. Receiving and transmitting angle-beam probes are symmetrically placed on the notched side of the test specimen. The time of flight of the tip-diffracted echo is measured. It is a main disadvantage of the method that the received

US echos are the result of superposition of different modes, mode conversion and wave propagation ways. Therefore, the interpretation of the received signals is not trivial. In order to achieve a better understanding of the sequence of received pulses the experiments were modelled by the elasto-dynamic finite integration technique (EFIT, developed by Langenberg and coworkers at the University of Kassel) taking into account the actual testing geometry. The simulations were capable of reproducing the most important features of the measured echo trains and allow to interpret the individual echoes. The time of flight of the tip-diffracted transverse wave is not only influenced by crack propagation but by bending, too. The results stimulated modifying the technique by applying longitudinal instead of transverse waves.

M. Grosse
J. Böhmert

Microstructural processes during crack initiation

Before ductile crack initiation the microstructure goes through irreversible damages like dislocation pile-ups or jungles, particle fracture or decohesion, and microvoids formation. The extent of the damage depends on the stress state and on the material. Small microstructure defects can be detected by small angle scattering. To investigate the microstructural changes within an inhomogeneous deformation field with a steep stress gradient a finely focussed X-ray beam of high intensity is needed. The beam scans the damaged field step by step. Such experiments were carried out at the MICROFOCUS beam line of ESRF in Grenoble. Beams of 150 μm x 15 μm and 2 μm x 2 μm were used to scan a field of 4 mm x 2mm with a step width of 200 μm and a field of 0.1 mm x 0.08 mm with a step width of 5 μm, respectively. These fields were ahead of the crack tips of bended specimens from pure or alloyed Al. The 2-dimensional small angle scattering pattern was measured in the Q-range of $10^{-2}...10^{-0}$ nm^{-1}. The scattering effects show the influence of the deformation fields near the crack tip. Reduction, processing and interpretation of the large quantity of the obtained data are still problematic.

supported by DFG

M. Grosse
J. Böhmert

Irradiation defects in reactor pressure vessel steels

The nature of the irradiation-induced precipitates in the VVER 440-type 15Kh2MFA steel has been investigated by combination of small angle neutron scattering and anomalous small angle X-ray scattering. Above all, the influence of the thermal annealing was studied. Both techniques show that annealing reduces the volume fraction of the irradiation defects but hardly changes the size of the defects. Even after annealing with 550°C the material state before irradiation could not be reproduced. According to the Russian assessment procedure the state after 550 °C annealing is regarded like the initial reference state. From the point of view of these results, this is only limitedly valid.

supported by SMWK

J. Böhmert

Investigation of wear testing by vibratory cavitation see former

A test equipment was built which consists of a commercially available 20 kHz ultrasonic transducer with velocity transformer and horn, an adjustable power supply, a specimen holder, a double wall vessel containing the test liquid which is thermostatically controlled, and a sound protection box. The test specimen is repeatedly weighed or microscopically examined before testing and during test interrupts. The main results are the cumulative mass loss and the surface damage versus time. The equipment was used to test 4 μm thick layers of TiN on bearing steel. The layers have shown high erosion resistance and high adhesive strength. The pre-treatment of the substrate surface and the deposit conditions influence the sensitivity against cavitation erosion.

Simulation of radiation and particle transport

H.-U.Barz
B.Böhmer
J. Konheiser
I. Stephan

Neutron Dosimetry

The BMBF project on the evaluation of the Rheinsberg irradiation program was succesfully completed. Nevertheless the program was continued outside the BMBF project with the extraction of additional monitors, gamma-spectrometric analysis of the detectors, evaluation of measurements, transport calculations of fluences and spectrum adjustment.

The irradiation of fluence monitors which were manufactured by the Research Center Rossendorf at Russian WWER-1000 reactors could be finished.

Preparing the new BMBF-project (WWER-1000) which was announced for 1996 some important generalizations of the Monte Carlo code TRAMO were accomplished. The main activities were the implementation of the international code NJOY on the CONVEX-computer and the development of codes packages for generating the needed TRAMO-input format on the basis of the results of NJOY. Now, it is possible to use different numbers of groups and all modern data libraries as input data for TRAMO.

Moreover, the possibility was prepared to take into account the distribution of the source neutrons over the fuel assemblies and the pins for WWER-1000 reactors. New generalized codes for generating time integrated sources considering the WWER-1000 specialities have beeen developed. The Monte Carlo code for the generation of optimal weights has also been improved. Now the optimal sequence of regions within the recursive calculation procedure can be calculated.

H.-U. Barz
B. Böhmer
J. Konheiser

Evaluation of the neutron activition originating from the 20 MeV electron accelerator ELBE

The activation of the soil below a 20 MeV electron accelerator foundations by photoneutrons has been assessed. This assessment contributes to the safety design of the 20 MeV electron accelerator ELBE. The neutron transport problem was solved by means of a special version of the Monte Carlo code TRAMO assuming a neutron source of 10^{12} n/sec and an energy distribution similiar to the fission

spectrum of uranium. The resulting volume integrated energy dependent fluxes (40 energy groups) were used to calculate activities produced in the soil. For the isotopic composition of the soil all constituents which could contribute to the activation, were assumed to have the highest reasonably possible concentration.
It was shown that the produced activities from all possibly generated nuclides were far below the permitted limits.

H. Kumpf
St. Krahl
K. Noack
G. Otto
S. Collatz[1]

[1] *Visitor to the Institute for Safety Research*

Physics database of a plasma neutron source

The Monte Carlo simulation codes TUBE for the neutral particle transport and FIT for the fast ion transport have been applied to study the particle fields inside the "Gasdynamic Trap" facility (GDT) at the Budker Institute Novosibirsk during nonstationary experiments. The codes have been specifically prepared so that their mathematical models correspond with the physical conditions to maximum degree. A special series of experiments was devoted to the investigation of the interaction between neutral gas and fast ion population. To take this interaction into account a first approximation was achieved: the energetic neutrals that have been generated in a FIT simulation assuming a constant neutral gas distribution were considered as source for the TUBE calculation. The comparison of numerical and experimental results for the neutral gas still shows considerable discrepancies.

The guiding centre simulation code that has been developed for the nonlinear fast ion transport in the proposed neutron generator has been applied for checking some important assumptions of the project. The calculated neutron yield shows the feasibility of such a neutron source for material research.

The FIT code has been parallelized and implemented on an 8-node Parsytec PowerXplorer™ and on an 128-node system of the Parsytec GC-series installed at the Technical University Chemnitz. In comparison to the code application on the RCR's computing server CONVEX C3820 a remarkable gain in efficiency could be achieved.

supported by SMWK and BMBF

H.-U. Barz
B. Böhmer

Ion tumor therapy

A one dimensional Monte Carlo code was developed and succesfully tested for the investigation of the space dependent energy deposition of the ion projectiles and projectile fragments depending on the energy and type of the incidenting ion and the material composition of the medium which can consist of an arbitrary sequence of material layers of different compositions. Moreover, the fluences of different particles are given for each layer.

Different usually applied corrections and the energy straggling are taken into account. Various models of the reaction kinetics can be used.
The projectile fragmentation is treated by a number of different models mainly using results obtained by Sihver. Codes are developed for the representation of fragmentation cross sections and fragmen-

tation yields which give these quantities for a grid of energy points and for different material compositions. So the resulting libraries can be easely used by the Monte Carlo code.
A number of one dimensional arrangements of materials was evaluated to estimate the influence of different models and data libraries and especially the influence of different fragmentation models. Furthermore, some calculations were performed to compare the results with available experimental data.
It can be stated that the fragmentation models give rather large differences especially for the yields of fragments but the influence on the results of the energy yield is small. All available experimental Bragg-curves are reproduced with good accuracy even with different fragmentation models. The influence on the fluences of the single fragments is in general greater.

Mechanical integrity of technical systems and process monitoring

E. Altstadt
G. Grunwald
M. Scheffler
F.-P. Weiß

Analytical modelling of mechanical vibrations of VVER-440 primary circuit components using finite elements

The project contributes to the improved evaluation of the mechanical integrity of the soviet-type VVER-440 reactors especially, to a sensitive early failure detection and to the localization of mechanical damages of reactor components by means of vibration monitoring. For that purpose the mechanical vibration of all primary circuit components was modelled by finite elements. Modeling was built on the finite element code ANSYS®.
The interaction between the coolant flowing in the downcomer and the vibrating components has been considered by a fluid-structure element, which describes additional mode selective damping and intertia due to the coolant displacement when the downcomer geometry changes.
The calculation model was adjusted using results from experimental vibration investigations. To some extent data from earlier measurements were available. But additionally dedicated experiments had to be performed at original VVERs. Now, the model can be regarded to be widely verified.
Mainly it was applied to clarify how hypothetical damages of reactor internals influence the vibration signature of the primary circuit. Such kind of damage simulation is an appropriate means to find sensitive measuring positiones for on-line monitoring and to define physically based threshold values.
In principle, the model is even suited to estimate the loads of reactor components which might be imposed by external events (explosion, earthquake).

supported by BMBF

The project was finished in December 1995.

G. Grunwald
W. Zimmermann
J. Zoller

Fluid-structure-interaction

The flow between a cylindrical pendulum and fixed outer tube was investigated experimentally and numerically. Near a pendulum in air, pressure measurements were performed to verify - at first - an analytical formula describing the added stiffness caused by the streaming air and - at second - the assumed boundary condition at the outlet of the annular gap. A computer code being able to calculate the laminar velocity field of the fluid was developed.

G.Hessel
W.Schmitt
K.van der Vorst
F.-P.Weiß

Leak localization and estimating leak rates

A neural-network approach has been developed for localizing leaks and estimating the leak rate in pressurized plants with complicated three-dimensional structures. The capabilities of the method were demonstrated with simulated leaks at a VVER-440 reactor vessel head. Features for characterizing a leak were extracted from RMS values of acoustic emission sensors, coherence values, and from power spectra of microphone signals. Three-layer perceptron networks were found to be best suited for leak localization and for estimation of leak rates. However, the estimation of leak rates required an additional neural network because a different normalization procedure was necessary for extracting features from the RMS values of the acoustic emission sensors. Perceptron networks with continuously valued outputs corresponding to the coordinates of the leak positions were useful for classifying even positions which had not been offered during training.

supported by SWMK

G. Hessel
W. Schmitt
K. von der Vorst
F.-P. Weiß

Early detection of dangerous states in chemical plants

Within the framework of a joint project with the Institute for Environmental, Safety and Energy Technology Oberhausen (UMSICHT), a supervision method for dangerous process states in chemical batch reactors is being developed. In this project, UMSICHT is responsible for developing a process simulator and for setting-up a laboratory reactor, while the RCR develops a supervision approach based on pattern recognition. The efficiency of neural networks and fuzzy pattern classification has been proven when monitoring an exothermic chemical process, i.e. the esterification between acetic anhydride and methanol. Data sets delivered by both a process simulator and measurements in a laboratory reactor were used for training and testing the state classifiers. First results show that perceptron networks provide promising classification results and that they might be successfully applied as an additional supervision method to support the operator in decisions making under critical situations in chemical plants.

supported by BMBF

M. Beyer
H. Carl
B. Schikora
A. Seidel
P. Schumann
J. Zschau

Realization of a remote monitoring system for the improved operational monitoring of the Ukrainian nuclear power plant Zaporozh'ye - Second level of realization -

A technical system to improve operational monitoring of the Zaporozh'ye NPP was established as a pilot project by Research Centre Rossendorf and Technischer Überwachungsverein Rheinland with a significant contribution from the State Scientific and Technical Centre of the Ukrainian Supervisory Authority. The technical system complements existing operational checking and monitoring facilities by including modern means of information technology. It enables continuous monitoring of the state of unit 5 in normal operation and in case of anomalies or incidents so that when recognisable deviations from the regular plant operation occur, the Ukrainian supervisory authority can immediately inquire and if necessary impose conditions on the operator. The radiological and meteorological parameters at the nuclear power plant location are monitored to the extent necessary to assess the current radiation situation and to implement effective emergency management measures. Trial operation of this technical system was commenced at the end of 1995. Thus, supervisory authority and operator have been able to fulfil their monitoring duties more efficiently than before.

supported by BMU

Hazard ranking and risk management for waste deposits

W. Ferse
T. Reitz
U. Schneider

An expert system for the evaluation of contaminated sites

The expert system XUMA-GEFA is a tool for the systematic registration of sites suspected to be contaminated, for the uniform evaluation of the environmental hazard and for the determination of priorities for further investigation. XUMA-GEFA is used in Saxony and Baden-Württemberg and was developed in cooperation with the Research Centre Karlsruhe.

The main component of XUMA is a knowledge base. Its scientific content can be modified and completed by the expert user of the state-agency by means of a knowledge acquisition module without having experience in programming.

The site-evaluation program GEFA was developed for the external data acquisition, the check of the data consistency and a uniform evaluation of suspect sites.

An additional program deriving analysis plans for chemical and physical investigations and GEFA are generated automatically from the XUMA knowledge base, so that the whole program system works consistently. Together with the database systems used in the two federal states a closed cycle of information is achieved.

supported by SMU

S. Kruber
W. Ferse

Applied decision analysis for remedial decisions at contaminated sites

In 1995 the work on the case study for a waste disposal site in Saxony was continued in collaboration with the Saxonian Ministry of the Environment and the Saxon State Institute for Environmental Protection . This test case is a large waste disposal site located near Hoyerswerda. The open cast coal mining in this region created large

holes and lowered the groundwater level about 50m. Such a hole was filled with municipal waste between 1970 and 1990. After the closure of the coal mines, the groundwater level raised again, so large parts of the waste disposal site are now under the water level. This results in a large emission of pollutants into the groundwater.
With the support of the decision-makers at this site a set of criteria for evaluating different remediation concepts was established. According to the criteria, the results of all concepts were estimated. For this purpose many simulation models and algorithms had to be constructed and the input data necessary for these models were extracted from knowledge-bases and by comparing the situation at the test site with similar, better investigated remediation cases. Additionally, many facts could be derived by consulting remediation companies.
Additionally, a case study was initiated which evaluates the possibilities of prescriptive decision analysis for emergency management at technical-urban complexes.

supported by SMU

Magneto-hydrodynamics of conductive fluids

S.Eckert
G.Gerbeth
H.Langenbrunner
W.Witke

Heat and mass transport measurements
The bubble transport measurements at the sodium facility have been finished. A new test section for MHD-turbulence and heat transfer measurements has been installed. Main feature of this new test section is its flexibility regarding different inserts like honeycombs, turbulence promoters or electrical isolations, respectively. The performed turbulence measurements show very distinctly the typical properties of two-dimensional MHD turbulence: Strongly increased turbulence intensities transverse to the magnetic field without increase of the overall pressure drop. These results are important for the design of liquid metal cooling circuits. The measurements are based on own developed potential probes.

supported by DFG

G. Mutschke
V. Shatrov
G. Gerbeth

Numerical simulation of MHD flow around a cylinder
The calculations have been finished for the 2d-case. The 3d stability analysis was developed and implemented numerically. The 2d results are in contradiction to the literature but give for the first time correct results for a broad range of parameters. In the 3d case the results are in good agreement with the recently found hierarchy of flow transitions in the standard Karman vortex street. First calculations with magnetic fields reproduce the experimentally observed tendency to longwave instabilities. They show also a non-expected destabilizing influence of the steady magnetic field.

supported by DFG

J.Priede
G.Gerbeth

Marangoni flows at free liquid metal surfaces
The theoretical investigations on the stability of thermocapillary flows and its control by means of external magnetic fields have been finished for a coplanar magnetic field. They show that the travelling wave-fronts are more and more elongated parallel to the field

direction for an increasing magnetic field strength. Surprisingly, there is a critical Prandtl number of Pr = 0.018 above which the elongation is not continuous but connected with a sudden jump. This effect is not experimentally verified up to now.

supported by German Space Agency

V. Kolevzon
A. Cramer
G. Gerbeth

Experiments at free fluid surfaces

Several measuring cycles have been performed with the special vacuum box for free liquid metal surfaces. For an increasing temperatur gradient a hierarchy of flow transitions was observed ranging from the laminar thermocapillary flow to turbulence. For the first time thermoelectrically driven flows were clearly detected, also oscillating melting fronts. The experimental setup for the laser light scattering was put into operation. First measurements with water or ethylen gave very good agreement with the known data of surface tension and viscosity.

supported by German Space Agency and German-Israeli Foundation

A. Gailitis
G.Gerbeth

Dynamo experiment for magnetic field selfexcitation

The existing stability analysis for a planned dynamo experiment was extended to a sensitivity analysis. Variation of experimentally relevant radii, wall thickness or wall conductivities defines optimal values for the experiment planning. A cooperation with hydraulics experts of Dresden University was started in order to prepare the pump design for the dynamo experiment.

supported by DFG

Renewable energies

H. Futterschneider
Götze
Th. Ihle
U. Rindelhardt
G. Teichmann

Investigations on photovoltaic (PV) systems

In the frame of the project "long term monitoring of PV systems" total 50 grid coupled PV systems operated in Saxony have been investigated in detail. A special equipment for analysing the energy flow in such systems was developed. This PV system analyser allows as well the estimation of the module and inverter efficencies as I-U-characteristic measurements of the generator at operation conditions. First measurements provided relatively strong deviations of the rated generator power from the design values. A real photovoltaic energy production of about 800 kWh/kWp seems to be possible with grid coupled PV systems in middle Europe.

A second PV project started in 1995, concerns stand alone PV systems. A traffic density counter at a motorway is supplied by a PV generator and a new type of Ni-Cd battery. By monitoring the energy flow during the winter 1995/96 the design criteria of the system will be verified and compared with other results.

supported by BMBF

D. Brünig
F. Naehring
U. Rindelhardt
W. Voitus

Solar heat supply

A pilot solar system for feeding solar heat into a small district heating network was investigated in Freital near Dresden. A remote control and measuring system was used for continuously monitoring the system operation. In 1995, a specific energy of 322 kWh per squaremeter collector area was generated. Primarily due to the relatively high temperature level of the district heating network (55°C - 58°C) this earn is somewhat lower than expected. The optimum solar fraction rate in future solar aided heat networks was estimated to be about 10 %.

In another project the possibilities for integration of saisonal heat storages into solar aided heat networks were studied. The particular conditions for the installation of such storages at different, but typical heat supply structures in East Germany were examined. It could be shown that in most cases such an integration makes sense from the technical point of view. A realizable project was not found mainly because of financial problems.

Additionally the possible use of old mines as saisonal heat storages were investigated using the simulation programme TRYNSYS. Due to the bad surface/volume relation such caverns were found not to be suitable for this application.

supported by SMU and BMBF

W. Hirsch
U. Rindelhardt

Wind energy ressources in Saxony

In continuation of an earlier project the saxon wind energy ressources were more precisely estimated.By comparison with long term speed measurements of the geostrophic wind over Dresden, representative time series were seperated from the wind records of 12 measuring stations in Saxony. Using the programme system WASP the wind energy potential was estimated in selected saxon areas. Taking into account the latest technology developments of wind energy converters (i.e. hub height, gearless generator, variable - speed) an important increase of the usable wind ressources was found. Many sites could be identified which allow an operation of wind converters with more than 2000 full power hours per year. Under the conditions of the German electricity feed law an economic operation is achievable.

supported by SMU

Publications

Publications in scientific and technical journals and in conference proceedings

Altstadt, E., G. Grunwald, M. Scheffler, F.-P. Weiß
A Finite Element Based Vibration Model for VVER-440 Type Reactors Considering the Fluid-Structure-Interaction
Proc. Jahrestagung Kerntechnik '95, Nürnberg, 16. - 18. Mai 1995, S.227-230

Altstadt, E., M. Scheffler, F.-P. Weiß
Component Vibration of VVER-Reactors - Diagnostic and Modelling
IMORN-25, 1995
Progress in Nuclear Energy, Vol. 29, Number 3/4, pp. 129 - 138

Altstadt, E., G. Grunwald, M. Scheffler, F.-P. Weiß
Theoretical Vibration Model of VVER Reactors Considering Fluid-Structure Interaction
Proc. SMORN VII, Avignon, France, 19-23 June, 1995, Vol. 2, 9.7

Altstadt, E., M. Scheffler, F.-P. Weiß
A Vibration Model for the Primary Circuit of VVER-440 type Reactors Based on Finite Elements
SMIRT 13, Porto Alegre, Brasil, August 13-18, 1995, Vol. 2, pp. 323-328

Bergner, F., U. Bergmann
Punktquelle-Punktempfänger-Modell zur Rißfortschrittsmessung mit Ultraschall
DVM-Arbeitsgemeinschaft Werkstoffe, Tagung "Werkstoffprüfung"
Bad Nauheim, 5. - 6. Dezember 1995, Proc. S. 419

Bergmann, U., J. Böhmert, F. Bergner
Ultraschallverfahren zur Messung des duktilen Rißfortschritts bei quasistatischer Dreipunktbiegung
27. Vortragsveranstaltung des DVM-Arbeitskreises Bruchvorgänge
Köln, 14. - 15. Feburar 1995, Proc. S.177

Bergmann, U., F. Bergner, K. J. Langenberg, Ch. Hofmann
Investigation of Crack Growth Processes of Surface-Breaking by Ultrasound - Comparison of Simulation and Experiments
Proc. 1995 World Congress of Ultrasonics, Berlin 3. - 7. Sept. 1995,
Part 2, p. 601

Beyer, M., H. Carl, L. Langer, K. Nowak, A. Seidel, P. Schumann, P. Tolksdorf, J. Zschau
Aufbau eines technischen Systems zur Verbesserung der betrieblichen Überwachung des KKW Saporoshje durch die staatliche Aufsichtsbehörde der Ukraine (in Russisch)
Atomnaja Technika sa Rubeschon, Heft 3 (1995) S. 3

Beyer, M., H. Carl, L. Langer, P. Schumann, A. Seidel, J. Zschau, K. Nowak, P. Tolksdorf
Specification of a Technical System to Improve the Operational Monitoring of the Zaporsh'ye NPP by the State Supervisory Authority of the Ukraine
SMORN VII, 7th Symposium on Nuclear Reactor Surveillance and Diagnostics, Avignon, France 19-23 June 1995, Vol. 2, 14.3

Böhmert, J., F. Bergner, M. Große, H.-W. Viehrig
Influence of the Depth Position on the Neutron Embrittlement of the VVER Reactor Pressure Vessel Steel 15CrMoV (A) - Consequences for the Assessment of Reactor Safety
Nucl. Engn. Design 159 (1995) 131 - 141

Böhmert, J.; M. Große
Nachweis von Bestrahlungsdefekten in WWER-RDB-Stählen durch Kleinwinkelstreuexperimente
Proc. Jahrestagung Kerntechnik '95
Nürnberg, Mai 1995, S. 379 - 381

Böhmert, J., M. Große
Detection of Irradiation-Induced Microstructures Changes of VVER-Type RPV Steel by Small Angle Scattering Methods
Proc. International Topical Meeting on VVER-Safety, Prague, Sept. 1995
Session III, paper 7

Brünig, D.; U. Rindelhardt
Solare Trinkwasserbereitung und Einspeisung in ein Fernwärmenetz
- Demonstrationsanlage Waldblickschule Freital
Terratec'95, 4. Fachmesse und Kongreß für Umweltinnovationen,
Leipzig, 01.-03. März 1995, Tagungsband S. 156

Brünig, D., U. Rindelhardt
Betriebserfahrungen mit einer 100m²-Solaranlage zur Trinkwarmwasserbereitung und Fernwärmeeinspeisung - Waldblickschule Freital
5. Symposium Thermische Solarenergie , Staffelstein, 21. - 23.6.1995
Tagungsband S. 133

Brünig, D., U. Rindelhardt
Solaranlage Waldblickschule Freital - Solare Warmwasserbereitung und Fernwärmeeinspeisung
Tagung "Energie und Umwelt '95", Freiberg, 22.-23.03.1995
Tagungsband S. 95

Gaschenko, M.P. u.a.; H.-M. Prasser, W. Zippe
Hot Leg Break Tests at the ISB-VVER Integral Test Facility
Proc. Jahrestagung Kerntechnik, Nürnberg, 16.-18. Mai 1995, p. 123

Gaschenko, M.P., H.-M. Prasser, W. Zippe, et. al.
Experimental Investigation of Accidental Thermohydraulic Processes under Circuit Depressurization at ISB-VVER Safety Integral Test Facility
Int. Symposium on Two-Phase Flow Modelling and Experimentation,
Rom, Italy, October 09 -11, 1995, p. 537

Große, M.; J. Böhmert, G. Brauer, F. Eichhorn
ASAXS-Investigations of Irradiation - Induced Precipitates in VVER-440-Type Reactor Pressure Vessel Steel with High Cu Content
HASYLAB-Jahresbericht 1994, Hamburg, Januar 1995, S. 535

Große, M., F. Eichhorn, J. Böhmert, H.-G. Heubold, G. Goerigk
ASAXS and SANS Investigations of the Chemical Composition of Irradiation-Induced Precipitates in Nuclear Pressure Vessel Steels
Nucl. Instruments and Methods in Physics Research B97 (1995) 487 - 490

Grundmann, U.; D. Lucas, U. Rohde
Coupling of the Thermohydraulic Code ATHLET with the Neutron Kinetic Core Model DYN3D
Int. Conference on Mathematics and Computations, Reactor Physics and Environmental Analysis
Portland, Oregon, USA, April 30 - May 5, 1995
Proc., Vol. 1, pp. 257 - 263

Grundmann, U., D. Lucas, U. Rohde
Coupling the Advanced Thermohydraulic Code ATHLET with the 3D-Core Model DYN3D
International Topical Meeting on VVER Safety
Prague, September 21 - 23. 1995, Proc. pp. 197 - 200

Grundmann, U., U. Rohde
Comparative Analysis of the Third Three-Dimensional Dynamic AER-Benchmark Problem with the Help of the Code DYN3D
Fifth Symposium of AER, Dobogokö, Hungary, 15 - 19 October, 1995
Proc. pp. 329 - 343

Grundmann, U.; D. Lucas, U. Rohde
Coupling of the Thermohydraulic Code ATHLET with the Neutron Kinetic Core Model DYN3D
Int. Conf. "Thermophysical Aspects of WWER-Type Reactor Safety"
Obninsk, Rußland, 21. - 24. November 1995, Proc. Vol. 2, pp. 155 - 164

Hessel, G., W. Schmitt, F.-P. Weiß
Acoustic Leak Monotoring Using Neural Networks
Proc. Annual Meeting on Nuclear Technology '95, Nürnberg, May 16 -18th 1995
pp. 231 - 234

Hessel, G., W. Schmitt, F.-P. Weiß
Akustische Lecküberwachung mit Neuronalen Netzen an Druckanlagen komplizierter Topologie
DECHEMA-Jahrestagungen '95, Wiesbaden, 30.05. - 01.06. 1995
Band 3, S. 227 - 228

Hessel, G., W. Schmitt, F.-P. Weiß
A Neural Network Approach for Acoustic Leak Monitoring at Pressurized Plants with Complicated Topology
Preprints of the IFAC Workshop on On-line Fault Detection and Supervision in the Chemical Process Industries
Newcastle (England), June 12 - 13th 1995, pp. 98 - 102

Hessel, G.; W. Schmitt, F.-P. Weiß
Acoustic Leak Monitoring with Neural Networks at Complicated Structures
Proc. SMORN VII, Avignon, France, 19 - 23 June, 1995, 4.11

Hessel, G., W. Schmitt, F.-P. Weiß
Fuzzy-based Acoustic Leak Localization at Complicated Structures
Third European Congress on Intelligent Techniques and Soft Computing
EUFIT'95, Aachen, August 28 - 31, 1995, pp. 1165 - 1169

Hollstein, F., K. Meyer
Calculation of Neutron Noise Due to Control Rod Vibrations Using Nodal Methods for Hexagonal-Z-Geometry
Proc. Specialists Meeting on Reactor Noise, SMORN VII, Vol. 2, 12.1
Avignon, France, 19 - 23 June, 1995

Jahn, U., D. Tegtmeyer, U. Rindelhardt, G. Teichmann
PV Covers Electricity Demand
13th European Photovoltaic Solar Energy Conference, Nizza, 23-27th October 1995, Vol. II, p. 2247

Knight, M. P., P. Brohan, U. Grundman, U. Rohde, H. Finnemann, H. Hüsken
Comparison of Rod-Ejection Transient Calculations in Hexagonal-Z Geometry
Int. Conference on Mathematics and Computations, Reactor Physics and Environmental Analysis
Portland, Oregon/USA, April 30 - May 5, 1995, Proc. Vol. 2, pp. 1248 - 1258

Krepper, E.
Post Test Calculations to 11% Break LOCA Experiments in the Integral Test Facility ISB-VVER Using the Thermalhydraulic Code ATHLET
Proc. Jahrestagung Kerntechnik, Nürnberg, 16. - 18. Mai 1995, pp. 83 - 87

Krepper, E.
Post Test Calculations to 11% Break LOCA Experiments in the Integral Test Facility ISB-VVER Using the Thermalhydraulic Code ATHLET
Conference "Thermophysical Aspects of WWER-Type Reactor Safety
Obninsk, Russia, Nov. 1995, Proc. Vol. 2, pp. 150 - 154

Maletti, R., M. Ulrich
105 Mio. DM Zuschüsse - Energie-Förderung durch das SMWA
IHK Wirtschaftsdienst 6 (1995), H. 6, S. 20

Maletti, R., M. Ulrich
Energie-Förderung durch das Sächsische Staatsministerium für Wirtschaft und Arbeit im Jahre 1994
Energieanwendung 44 (1995), H. 4, S. 50

Maletti, R.
Solaranlagen in Sachsen: eine Zwischenbilanz
Sonnenenergie & Wärmetechnik 1995, H. 5, S. 21

Prasser, H.-M., F. Schäfer, G. Eszöl. A. Guba
Small Cold Leg Break Experiment on PMK-2
Proc. Jahrestagung Kerntechnik, Nürnberg, 16.-18. Mai 1995, p. 119

Priede, J., G. Gerbeth
Convective, Absolute and Global Instabilities of Thermocapillary-Buoyancy Driven Flows in a Horizontal Liquid Layer
Bulletin of the American Physical Society, Series II, Vol. 40, No. 12, 1995, pp. 1955-56

Rindelhardt, U.
Solar Heat Feeding into a District Heating Network
Deutsch-Italienische Konferenz "Erneuerbare Energien",
Brescia, 14. - 16. Juni 1995, Tagungsband S. 241

Rindelhardt, U.
Stand und Wirtschaftlichkeit von Sonnen- und Windenergienutzung zur Stromerzeugung in Sachsen
XXVII. Kraftwerkstechnisches Kolloquium TU Dresden, 24./25.10.1995,
Tagungsband Teil I, S. 45

Rohde, U., I. Elkin, V. Kalinenko
Analysis of a Boron Dilution Accident for WWER-440 Combining the Use of the codes DYN3D and SiTAP
Proc. Jahrestagung Kerntechnik, Nürnberg, 16. - 18. Mai 1995, pp. 111 - 114

Schäfer, F., E. Krepper
Rechnungen zum 1%-Leck an der Versuchsanlage PMK-2 mit dem Code AHTLET
Proc. Jahrestagung Kerntechnik, Nürnberg, 16. - 18. Mai 1995, S. 79 - 82

Schmitt, W., A. Steiff
Anwendungsmöglichkeiten neuartiger EDV-gestützter Erkennungsmethoden zur Identifikation gefährlicher Betriebszustände in Chemieanlagen
Preprints des Workshops "Reaktionsführung bei chemischen Synthesen im technischen Maßstab mit Unterstützung durch moderne Methoden elektronischer Datenverarbeitung"
Bonn, 24.05.1995, S. 67 - 75

Teichmann, G., D. Schubert, R. Götze, U. Rindelhardt
Ein neues PV-Kennlinien-Meßgerät
10. Symposium Photovoltaische Solarenergie, Staffelstein, 15.-17.03.1995
Tagungsband S. 461

Valo, M., J. Böhmert, U. v. Estorff, K. Törrönen
Proposed Post Service Investigation on Decommissioned Greifswald Units
Mol, Belgium, 27 - 28 June, 1995
Proc. OCDE/GD (96)10, pp. 131 - 146

Viehrig, H.-W., H. Böhmert, M. Große
Through-Thickness Characterization of Mechanical Properties of Russian VVER-Type Reactor Pressure Vessel Steel Forgings
IAEA Specialists Meeting "Neutron Embrittlement and Mitigation"
Espoo, Finland, 23 - 26 Oct., 1995
Proc. IWG-LMNPP-95/5, Vol. II, Session 4, paper 3

Viehrig, H.-W., J. Böhmert
Anwendung der Verbundprobentechnik zur Mehrfachprüfung von Proben mit Charpy-Geometry
Vortrags- und Diskussionstagung "Werkstoffprüfung '95", Bad Nauheim
Proc. S. 447 - 456

Weiß, F.-P.
Nutzung von Fluktuationssignalen und deren Auswertung mit Fuzzy-Logik / neuronalen Netzen zur Früherkennung von unerwünschten Betriebszuständen in chemischen Reaktoren
Workshop "Reaktionsführung bei chemischen Synthesen in techn. Maßstab mit Unterstützung durch moderne Methoden elektronischer Datenverarbeitung"
Bonn, 24.05.1995, Proc. S. 76 - 84

Weiß, F.-P., J. Valko
Identification of Topics for Cooperation between the European Community and Eastern European Countries in the Field of Nuclear Reactor Safety, Radioactive Waste and Site Restoration
Study accomplished by order of EU DG XII, Rossendorf, 1995

Conference contributions

Altstadt, E., K. Richter, R. Weiß, W. Zimmermann
Experimentelle Modalanalyse an einer Kühlschleife eines Druckwasserreaktors
TUD-Sonderdruck, Fakultätsseminar Identifikation 1995 der TU Dresden
(Fakultät Maschinenwesen), Schmochtitz, 2. - 3. 5. 1995

Anikeev, A. V., et. al. K. Noack, H. Kumpf, G. Otto, St. Krahl
Energy balance and stability of GDT plasma under intense neutral beam heating,
22nd EPS Conf. on Controlled Fusion and Plasma Physics
Bournemouth, July 1995

Bagryansky, P. A., et. al. St. Krahl, K. Noack
Neutral Particle Balance in GDT with Fast Titanium Coating of the First Wall
Int. Conf. on Plasma Science, Madison, July 1995

Böhmert, J., M. Große, A. Hempel, C. Riekel, P. Engstroem
SAXS Investigation of Structural Changes in the Plastic Zone Ahead of the Crack Tip in Ductile Metals
ESRF-User Meeting 1995, Grenoble, 20. - 21. Nov. 1995

Bojarevics, A., Yu. Gelfgat, G. Gerbeth
Testing of a New Experimental Technology to Study MHD-Associated Phenomena with Free Liquid Metal Surface
MAHYD-95 - Conference on MHD, Riga, Lettland, August 1995

Brünig, D., U. Rindelhardt, A. Dittmann, T. Doltze, A. Gassel
Betriebserfahrungen mit großen solarthermischen Anlagen in Sachsen
Tagungsserie Klimagipfel der Fördergesellschaft Erneuerbare Energien Berlin/Brandenburg e. V., Wildau, 20.01.1995

Bucenieks, I., O. Lielausis, G. Gerbeth, G. Falk
Stabilisation of Thin Liquid Metal Jets by Magnetic Field
MAHYD-95 - Conference on MHD, Riga, Lettland, August 1995

Buhrig, E., U. Wunderwald, G. Gerbeth, Y. Gelfgat, L. Gorbunov
Gradient Freeze Crystal Growth with Optimized Convection Induced by a Rotating Magnetic Field
MAHYD-95 - Conference on MHD, Riga, Lettland, August 1995

Eckert, S., G. Gerbeth, H. Langenbrunner, W. Witke
Measurements of Longitudinal Velocity Fluctuations in Liquid Sodium at High Interaction Parameters in a Channel with Conducting Walls
MAHYD-95 - Conference on MHD, Riga, Lettland, August 1995

Eckert, S., G. Gerbeth, H. Langenbrunner, W. Witke
Heat Transfer Experiments in a Turbulent Sodium MHD Channel Flow
MAHYD-95 - Conference on MHD, Riga, Lettland, August 1995

Erbacher, F. J., J. Böhmert
High-Temperature Deformation and Burst Behaviour of Zirconium-Niobium Cladding Tubes Compared to Zircaloy
11th ASTM Symposium on Zirconium in the Nuclear Industry
Garmisch-Patenkirchen, Sept. 11-14, 1995

Gailitis, A., G. Gerbeth
Generation Properties of a Laboratory MHD Dynamo Model
MAHYD-95 - Conference on MHD, Riga, Lettland, August 1995

Gerbeth, G., Yu. Gelfgat, L. Gorbunov, E. Buhrig, U. Wunderwald
Use of a rotating magnetic field in vertical Bridgeman crystal growth - magnet design and model experiments
11th Int. Conference on Crystal Growth, The Hague (Netherlands)
June 18-23, 1995

Große, M., A. Hempel, J. Böhmert, F. Eichhorn, L. Riekel, P. Engström
SAXS Investigation of the Structural Changes in the Plastic Zone Ahead of a Crack Tip in Ductile Metals
Topical Meeting on Horizonts in Small Angle Scattering from Mesoscopic Systems
Stromboli, Italy, Sept. 1995

Grundmann, U., U. Rohde
DYN3D-Results of 3rd Kinetic Benchmark of AER
Meeting of AER Working Group D "VVER-Reactor Safety Analysis"
VTT Energy, Espoo, Finland, 17 - 19 May, 1995

Grundmann, U., U. Rohde
Comparisons of Different Options for Coupling DYN3D-ATHLET
Meeting of AER Working Group D "VVER-Reactor Safety Analysis"
VTT Energy, Espoo, Finland, 17 - 19 May, 1995

Ivanov, K., U. Grundmann, S. Mittag, U.Rohde
Comparative Study of a Boron Dilution Scenario in VVER Reactors
Specialist Meeting on Boron Dilution Reactivity Transients
State College, PA, USA, 18 - 20 October, 1995

Maletti, R.
Fördermöglichkeiten für Energieprojekte in Sachsen
Vortrag ILK-Symposium, Dresden, 12.01.1995

Kljukin, A., Yu. Kolesnikov, O. Lielausis, E. Platacis, M. Skopis, S. Eckert, G. Gerbeth
Local Properties of a Hg/N_2 Bubbly Flow injected by a Single Orifice in a Longitudinal Magnetic Field
MAHYD-95 - Conference on MHD, Riga, Lettland, August 1995

Kolevzon, V., G. Gerbeth
Light scattering by different liquid surfaces
Lecture at: Fachtagung "Lasermethoden in der Strömungsmeßtechnik"
Rostock, September 1995

Prasser, H.-M., H. Ringel
Gasgehaltsprofile in einer Blasenströmung bei erzwungener Konvektion
Sitzung des GVC-Fachausschusses "Mehrphasenströmung"
Magdeburg, 16.-17.2.1995

Prasser, H.-M., C. Schlenkrich
Void Fraction Measurements in Transient Bubble Columns by Needle-Shaped Conductivity Probes
33rd European Two Phase Flow Group Meeting
Hertogenbosch, The Netherlands, 30 May - 02 June 1995

Prasser, H.-M., H. Steinkamp, U. Rohde
Aufwallen und Austragen von zweiphasigen Gemischen
DECHEMA-Jahrestagung, Wiesbaden, 30.05. - 01.06.1995

Priede, J., A. Thess, G. Gerbeth
Oblique hydrothermal wave instability of thermocapillary driven convection in a coplanar magnetic field
9th European Symposium "Gravity Dependent Phenomena", Riga, Lettland May 1995
MAHYD-95 - Conference on MHD, Riga, Lettland August 1995

Priede, J., G. Gerbeth
Convective, absolute and global instabilities of thermocapillary-buoyancy driven flows in a horizontal liquid layer.
Lecture at: American Physical Society, 48th Annual Meeting of the Division of Fluid Dynamics, Irvine, 20.11.1995

Treuner, M., D. Langbein, V. Galindo, G. Gerbeth
Thermocapillary bubble and drop migration in a drop tower experiment
9th European Symposium "Gravity Dependent Phenomena", Berlin, May 1995

Weiß, F.-P.
Übersicht zu Arbeiten des Institutes für Sicherheitsforschung des FZR
Seminarvortrag, Institut für Reaktorsicherheit im FZK
Karlsruhe, 23. Februar 1995

FZR-reports and other publications

Altstadt, E., G. Grunwald, F.-P. Weiß
Theoretical Vibration Model of VVER Reactors Considering
Fluid-Structure-Interaction
FZR, März 1995, Preprint of SMORN VII

Altstadt, E., H. Carl, G. Hessel, W. Schmitt, P. Schumann, F.-P. Weiß
Prozeß- und Anlagendiagnostik
Ein Überblick über die Arbeiten des Institutes für Sicherheitsforschung
FZR, März 1995

Altstadt, E., F.-P. Weiß, R. Weiß
Vibration Experiments at a Coolant Loop of the Dukovany NPP
FZR-86, April 1995

Altstadt, E., M. Scheffler, F.-P. Weiß
Theoretische Modellierung des Druckbehälters und der Druckbehältereinbauten eines Siedewasserreaktors (SWR)
FZR, Laborbericht, September 1995

Barz, H.-U., B. Böhmer, J. Konheiser, I. Stephan
Ermittlung der Neutronendosis von bestrahlten WWER-Reaktordruckbehältermaterialien
FZR-87, Juni 1995

Bergmann, U., J. Böhmert, H.-W. Viehrig
Bestimmung bruchmechanischer Kennwerte an Reaktordruckbehälterstählen mit der Einproben-Compliance-Methode und Korrelationen zur Kerbschlagarbeit
FZR-81, März 1995

Beyer, M., H. Carl, B. Schikora, A. Seidel, P. Schumann, J. Zschau
Aufbau eines behördlichen Fernüberwachungssystems zur betrieblichen Überwachung des KKW Saporoshje (Block 5), 1. Realisierungsstufe
FZR-88, Mai 1995

Böhmert, J., M. Große, H.-W. Viehrig
Abhängigkeit der mechanischen Eigenschaften, des Bestrahlungs- und des Ausheilverhaltens von der Tiefenlage in Schmiedestücken des WWER-Reaktordruckbehälterstahles 15Ch2MFA
FZR-93, April 1995

Eckert, S., G. Gerbeth, H. Langenbrunner, W. Witke
MHD Turbulence: Use of Gas Bubbles as Local Tracers in Liquid Metal MHD Flows
FZR-80, March 1995

Ezsöl, Gy., A. Guba, L. Perneczky, H.-M. Prasser, F. Schäfer, E. Krepper
1% Cold Leg Break Experiment on PMK-2 Test Results and Computer Code Analysis
FZR-76, March 1995

Freund, T.
Einfluß von Orographie und Rauhigkeit auf das Windenergiepotential in ausgewählten Gebieten Sachsens
Diplomarbeit Technische Universität Dresden, Fakultät Maschinenwesen
Nr. 1549, 28.09.1995

Gerbeth, G.
Experimentelle Realisierung einer freien Flüssigmetalloberfläche
Machbarkeitsstudie / Abschlußbericht für DARA GmbH, September 1995

Gorbovsky, A. I., et. al. (INP),
Kumpf, H., K. Noack, G. Otto, St. Krahl (FZR)
Robouch, V. (ENEA Frascati, Italy)
Hydrogen Prototype of a Plasma Neutron Source
Novosibirsk 1995, Budker INP 95-90

Grundmann, U., D. Lucas, S. Mittag, U. Rohde
Weiterentwicklung und Verifikation eines dreidimensionalen Kernmodells für Reaktoren vom Typ WWER und seine Ankopplung an den Störfallcode ATHLET
FZR-84, März 1995

Grundmann, U.
The Code DYN3DR for Stead-State and Transient Analyses of Light Water Reactor Cores with Cartesian Geometry
FZR-114, November 1995

Hessel, G.; W. Schmitt, F.-P. Weiß
Leckdetektion an komplizierten dreidimensionalen Topologien
FZR-67, Januar 1995

Hollstein, F.
Berechnung von Neutronenflußdichteschwankungen in WWER-Druckwasserreaktoren infolge strömungsinduzierter Schwingungen
FZR-110, September 1995

Ihle, T.
Entwicklung und Erprobung eines Photovoltaik-Generator-Kennlinienmeßgerätes
Diplomarbeit Technische Universität Dresden, Fakultät Elektrotechnik
Nr. 22/94, 01.12.94 - 31.05.95

Kern, T.
Modellierung der axialen Gasgehaltsverteilung bei transienten Vorgängen in einer Zweiphasenströmung
Diplomarbeit Technische Universität Dresden, Institut für Verfahrens- und Umwelttechnik, Nov. 1995

Noack, M.
Entwurf eines solar unterstützten Nahwärmesystems in einer zu sanierenden Wohnsiedlung
Diplomarbeit Nr. 708 Technische Universität Dresden, Institut für Thermodynamik und Technische Gebäudeausrüstung 1995

Nollau, M.
Solarwärmeeinspeisung in ein Nahwärmenetz durch dachintegrierte Kollektorfelder und einen saisonalen Speicher
Diplomarbeit Nr. 1542 Technische Universität Dresden, Institut für Energietechnik 1995

Rindelhardt, U., G. Teichmann, D. Lang
Projektabwicklung und Ergebnisse des Bund-Länder-1000-Dächer-Photovoltaik-Programmes in Sachsen
FZR-109, September 1995

Szabados, L., Gy. Ezsöl, L. Perneczky, E. Krepper, H.-M. Prasser, F. Schäfer,
Two-Phase Flow Behaviour During a Medium Size Cold Leg LOCA Test on PMK-2 (IAEA-SPE-4)
FZR-101, August 1995

Meetings and Workshops

MEETINGS AND WORKSHOPS

1. 3. Internationaler Workshop zum BMU-Vorhaben
   Fernüberwachung KKW Saporoshje
   Rossendorf, 27.03. - 07.04.1995
   17 participants from Ukraine and Germany

2. 4. Internationaler Workshop zum BMU-Vorhaben
   Fernüberwachung KKW Saporoshje
   Rossendorf, 20. - 27.04.1995
   16 participants from Ukraine and Germany

3. Workshop "Entscheidungsanalyse"
   Rossendorf. 03.05.1995
   18 participants from Germany

4. Sitzung des GMA-Arbeitskreises
   Rossendorf, 11. und 12.05.1995
   13 German participants

5. 5. Internationaler Workshop zum BMU-Vorhaben
   Fernüberwachung KKW Saporoshje
   Rossendorf, 28.08 - 08.09.1995
   14 participants from Ukraine and Germany

6. Workshop: Harmonisierung von Codes und Standards
   "On-line monitoring of NPPs components"
   Rossendorf, 30.08. - 04.09.1995

7. Work Meeting
   "Vibration modeling of VVER-reactors"
   Rossendorf, 01.-03.11.1995
   6 participants from GUS and 7 German participants

8. Workshop "1000-Dächer"
   Rossendorf, 08.11.1995
   25 German participants

Seminars

SEMINARS 1995

01. Jahresrückblick 1994 und Ausblick 1995
Ref.: Prof. F.-P. Weiß
T.: 11.01.95

02. Monte-Carlo-Simulation des Ionentransportes im menschlichen Gewebe bei der Tumortherapie
Ref.: Dr. K. Noack
T.: 20.01.95

03. Ultraschallverfahren zur Erfassung von Rißfortschritt bei quasistatischer Dreipunktbiegung
Ref.: Dipl.-Ing. U. Bergmann
T.: 27.01.95

04. Experimente zum Einsatz von Radiotracern - Stand und Vorbereitung -
Ref.: F. Hensel
T.: 31.01.95

05. Anwendung neuronaler Netze zur akustischen Leckdetektion
Ref.: Dr. W. Schmitt
T.: 14.02.95

06. Windenergienutzung in Sachsen - Potentials und Realisierungschancen -
Ref.: Dr. U. Rindelhardt, Dr. W. Hirsch
T.: 28.02.95

07. Gleitlagerdiagnose mittels Magnetfeldmessung
Ref.: Dr. Bittner, HTWS Zittau/Görlitz
T.: 14.03.95

08. Zweiphasenmeßtechnik
Ref.: Dr. H.-M. Prasser
T.: 11.04.95

09. Gittergasautomaten in der Hydrodynamik
Ref.: Dr. W. Miller, Berlin
T.: 21.04.95

10. Bestrahlungsinduzierte Änderung der Mikrostruktur in CrMoV-legierten Druckbehälterstählen
Ref.: Dr. J. Böhmert, M. Große
T.: 25.04.95

11. Experimentelle und analytische Untersuchungen des thermohydraulischen Verhaltens der Heizrohre liegender Dampferzeuger von WWER-Anlagen unter Störfallbedingungen
Ref.: S. Alt, B. Kraus, A. Fjodorow, HTWS Zittau/Görlitz
T.: 23.05.95

12. Bewertung von Altlasten mit dem Programmsystem GEFA - XUMA
Ref.: Dr. W. Ferse
T.: 29.05.95

13. Die Arbeiten des IRI Delft
Ref.: Dr. J. Valko, Universität Delft
T.: 01.06.95

14 Marangoni-Konvektion bei überlagerten horizontalen und vertikalen Temperaturgradienten
Ref.: Dr. A. Cramer, Prof. Dr. D. Schwabe, Universität Gießen
T.: 07.06.95

15. Depth-Dose and Fluence Distributions when using Heavy Beams
Ref.: Dr. Lembit Sihver, GSI Darmstadt
T.: 08.06.95

16. Ergebnisse der Fluenzbestimmungen am Rheinsberg Reaktor
Ref.: Dr. Barz, B. Böhmer
T.: 13.06.95

17. Modelling of Direct Evaporation in Columns
Ref.: Prof. Ming Song, Umsicht Oberhausen
T.: 16.06.95

18. Photovoltaikanlagen der EU
Ausgewählte Ergebnisse der Demonstrationsprogramme
Ref.: Dr. G. Blässer
T.: 29.06.95

19. Fusion Plasma Based Neutron Source Project in Japan
Ref.: Prof. Dr. Takaya Kawabe
T.: 30.06.95

20. The Novosibirsk Project of High-Gradient Wake-Field Electron Accelerator
Ref.: Dr. Andrey Koudryavtsev, Budker Institut Novosibirsk
T.: 03.08.95

21. Overview on nuclear safety research activities at Pennsylvania State University
- Capabilities of the TRAC-Code -
Ref.: Prof. Baratta (USA)
T.: 27.09.95

22. Berechnung von Neutronenflußdichteschwankungen in WWER-DWR infolge strömungsinduzierter Schwingungen
Ref.: Dr. F. Hollstein
T.: 12.10.95

23. Modell zur Berechnung des Temperaturfeldes in der Spaltzonen-eintrittsebene von DWR bei Berücksichtigung der makroskopischen Kühlmittelvermischung
Ref.: Dr. F. Hollstein
T.: 12.10.95

24. Modellierung des reaktiven Transportes von Radionukliden im Grundwasser
Ref.: Dipl.-Phys. O. Nitzsche, TU Freiberg
T.: 03.11.95

25. Ergebnisse des 1000-Dächer-Photovoltaik-Programms in Sachsen
Ref.: U. Rindelhardt, G. Teichmann
T.: 16.11.95

26. Information on Structure and Tasks of the Scientific and Engineering Center for Nuclear and Radiation Safety of Russian GOSATOMNADZOR
Pressure Vessel Neutron Dosimetry of VVER Nuclear Power Plants
Ref.: Herr Borodkin
T.: 17.11.95

27. Die Kopplung der Computercodes DYN3D und ATHLET - ein fortgeschrittene Werkzeug für die Störfallanalyse in WWER
Ref.: U. Grundmann, D. Lucas, S. Mittag, U. Rohde
T.: 07.12.95

28. Aufprall der Kernschmelze auf den Deckel eines Druckwasserreaktors infolge einer Dampfexplosion
Ref.: Dr. Ch. Laible
T.: 14.12.95

29. Information on current Investigations in the Reactor Calculation and Design Department of the Institute of Physics and Power Engineering Obninsk with Special Attention to the Nuclear Data Laboratory
Ref.: Dr. G. N. Manturov
T.: 15.12.95

Programmseminar mit FWR, 24.10.95

Schadstofftranport im Bergbaubetrieb Königstein
Ref.: B. Heinzelmann (VKTA)

Schadstofftransport in ungesättigter Zone
Ref.: E. Franke (VKTA)

Anwendung von chemischen Modellen und Datenbanken zur Bestimmung von Speziationen
Ref.: V. Brendler (FWR)

Doktorandenseminar, 09.11.95

Untersuchungen des Wachstums von Oberflächenrissen mit Ultraschall - Vergleich zwischen Simulation und Experiment
Ref.: Bergmann, Ute - Abt. FWSN

Schallemissionsuntersuchungen an zähen Stählen unter dynamischer Dreipunktbiegebeanspruchung
Ref.: Richter, Holger - Abt. FWSN

Geschwindigkeitsfluktuationen in einer Natrium-MHD-Strömung
Ref: Eckert, Sven - Abt. FWSS - MHD

Numerische Untersuchungen eines axial angeströmten Zylinderpendels
Ref.: Zoller, Jürgen - Abt. FWSM

Anwendung der Entscheidungsanalyse bei der Sanierung von Altlasten
Ref.: Kruber, Stefan - VKTA / Gruppe FWSA

Einsatz von Positronenemittern zur Bestimmung von Parametern zweiphasiger Systeme - Erste Ergebnisse von Experimenten -
Ref.: Hensel, Frank - Abt. FWSS

Untersuchungen zu Naturumlaufinstabilitäten bei Leckstörfällen in Reaktoren vom Typ WWER
Ref.: Schäfer, Frank - Abt. FWSS

Lectures

1. U. Rindelhardt: Renewable Energies
   Lectures at Universität Leipzig,
   Fakultät für Physik und Geowissenschaften

2. U. Rindelhardt: Photovoltaic/Wind Energy
   Lectures at TU Dresden, Fakultät für Maschinenwesen

3. F.-P. Weiß: Reliability and Safety of Technical Systems
   Lectures at TU Dresden, Fakultät für Maschinenwesen

4. U. Rindelhardt; G. Teichmann: Photovoltaic
   Practicum held for the TU Dresden, Fakultät für Maschinenwesen

5. Schmitt, W.; Hessel, G.; Weiß, F.-P.:
   Reactor Neutron Noise
   Practicum held for the TU Dresden, Fakultät für Maschinenwesen

Departments of the Institute

Research Center Rossendorf, Inc. Organigram

Institute for Safety Research
01314 Dresden, PF 510119

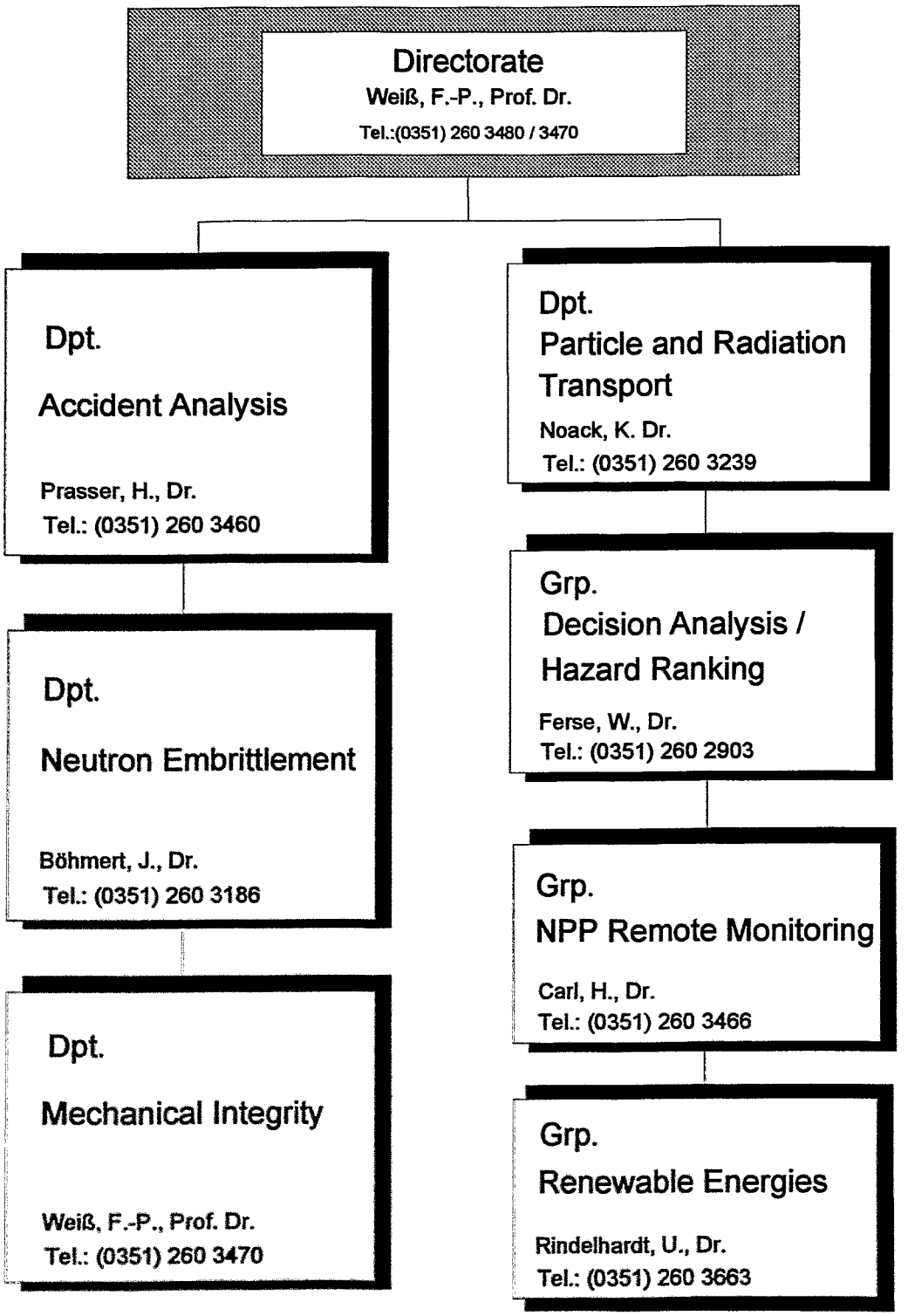

Personnel

Director: Prof. Dr. F.-P. Weiß

Scientific Staff

Altstadt, Eberhard Dr.
Barz, Hansulrich Dr.
Barz, Ralph-Uwe Dr.
Bergmann, Ute
Beyer, Matthias
Brünig, Dietlinde Dr.
Böhmer, Bertram
Böhmert, Jürgen Dr.
Carl, Helmar Dr.
Cramer, Andreas
Erlebach, Stephan
Ferse, Wolfgang Dr.
Galindo, Vladimir Dr.
Gerbeth, Günter Dr.
Große, Mirco
Grundmann, Ulrich Dr.
Grunwald, Gerhard Dr.
Hessel, Günter
Hirsch, Werner Dr.
Hollstein, Frank Dr.
Ihle, Tilo
Jüttner, Bernhard
Kliem, Sören
Kolevzon, Vladimir
Konheiser, Jörg
Krahl, Steffen
Krepper, Eckhard Dr.
Kumpf, Hermann Dr.
Laible, Christoph Dr.
Langer, Lutz
Lielausis, Olgerts Prof.
Lucas, Dirk Dr.
Maletti, Rainer Dr.
Mittag, Siegfried Dr.
Mutschke, Gerd
Naehring, Friedrich Dr.
Nitzsche, Petra
Noack, Klaus Dr.
Prasser, Hans-Michael Dr.
Priede, Janis Dr.
Rindelhardt, Udo Dr.
Rohde, Ulrich Dr.
Scheffler, Michael
Schikora, Bernd
Schmitt, Wilfried Dr.
Schröder, Frank
Schütz, Peter
Schumann, Peter Dr.
Seidel, Andre
Stephan, Ingrid Dr.
Teichmann, Günther
Tefera, Nurelegne Dr.
Utke, Holger
van der Vorst, Klaus
Viehrig, Hans-Werner Dr.
Weiß, Frank-Peter Prof. Dr.
Witke, Willy
Zschau, Jochen Dr.
Zippe, Winfried Dr.

Post Doc

Steinkamp, Helmut Dr.

PhD Students:

Bergmann, Ute
Eckert, Sven
Grahn, Alexander
Hensel, Frank
Nitschke, Kerstin
Richter, Holger
Schäfer, Frank
Schneider, Carola
Schulze, Lars
Weier, Tom
Zoller, Jürgen

Technical Staff

Baldauf, Dieter
Behrens, Sieglinde
Blumentritt, Thea
Böttger, Arnd
Borchardt, Steffen
Dietze, Anke
Eichhorn, Christine
Enkelmann, Wolfgang Dr.
Elert, Edith
Fischer, Manfred
Futterschneider, Hein
Gebel, Margitta
Götze, Rainer
Heinze, Gerda
John, Annett
Kaule, Christian
Kunadt, Heiko
Lang, Dorothea
Leonhardt, Wolf-Dietrich
Leuner, Bernd
Leuschke, Grit
Losinski, Claudia
Lotzmann, Roland
Otto, Gerlind
Pietzsch, Jens
Richter, Annett
Richter, Henry
Richter, Joachim
Richter, Karl-Heinz
Richter, Petra
Rott, Sonja
Russig, Heiko
Schmidt, Johannes
Schuster, Elke
Seidler, Christa
Skorupa, Ulrich
Tamme, Marko
Tamme, Günter
Webersinke, Wolfgang
Weichelt, Steffen
Weiß, Rainer
Werner, Matthias Dr.
Willkomm, Heike
Zimmermann, Wilfried